Agilent
Fundamentals of RF and Microwave Power Measurements

Application Note 64-1C

Classic application note on power measurements

Newly revised and updated

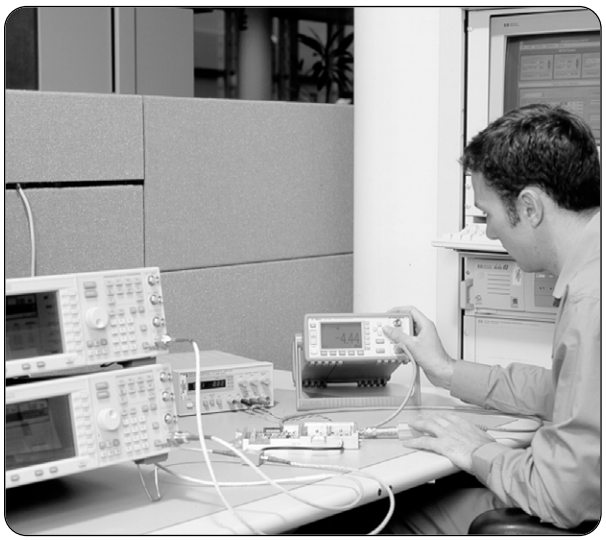

Agilent Technologies

Table of Contents

VI. Peak and Average Diode Sensors and Instrumentation

VII. Measurement Uncertainty

VIII. Power Measurement Instrumentation Compared

Introduction

This application note, AN64-1C, is a major revision of several editions of AN64-1, (and the original AN64, circa 1965) which served for many years as a key reference for RF and microwave power measurement. AN64-1C was written for two purposes:

1) to retain some of the original text of the fundamentals of RF and microwave power measurements, which tend to be timeless, and
2) to present the latest modern power measurement techniques and test equipment that represents the current state-of-the-art.

This note reviews the popular techniques and instruments used for measuring power, discusses error mechanisms, and gives principles for calculating overall measurement uncertainty. It describes metrology-oriented issues, such as the basic national power standards, round robin intercomparisons, and traceability processes. These will help users to establish an unbroken chain of calibration actions from the U.S. National Institute of Standards and Technology (NIST) or other national standards organizations, down to the final measurement setup on a production test line or a communication tower at a remote mountaintop.

This note also discusses new measurement uncertainty processes such as the ISO "Guide to the Expression of Uncertainty in Measurement," and the USA version, ANSI/NCSL Z540-2-1996, "U.S. Guide to the Expression of Uncertainty in Measurement," which define new approaches to handling uncertainty calculations. Reference is also made to ISO Guide 25, ISO/IEC 17025, and ANSI/NCSL Z540-1-1994, which cover, "General Requirements for the Competence of Testing and Calibration Laboratories." All are described further in Chapter VII.

This introductory chapter reviews the importance of power quantities and presents a brief history of power measurements. Chapter II discusses units, defines terms such as average and pulse power, reviews key sensors and their parameters, and overviews the hierarchy of power standards and the path of traceability to the United States National Reference Standard. Chapters III, IV, and V detail instrumentation for measuring power with the three most popular power sensing devices: thermistors, thermocouples, and diode detectors. Peak and average power sensors and measurement of signals with complex modulations are discussed in Chapter VI. Chapter VII covers power transfer principles, signal flowgraph analysis and mismatch uncertainty, along with the remaining uncertainties of power instrumentation and the calculation of overall uncertainty. Chapter VIII compares the various technologies and provides a summary of applications charts and Agilent's product family.

The importance of power

The output power level of a system or component is frequently the critical factor in the design, and ultimately the purchase and performance of almost all radio frequency and microwave equipment. The first key factor is the concept of equity in trade. When a customer purchases a product with specified power performance for a negotiated price, the final production-line test results need to agree with the customer's incoming inspection data. These shipping, receiving, installation or commissioning phases often occur at different locations, and sometimes across national borders. The various measurements must be consistent within acceptable uncertainties.

Secondly, measurement uncertainties cause ambiguities in the realizable performance of a transmitter. For example, a ten-watt transmitter costs more than a five-watt transmitter. Twice the power output means twice the geographical area is covered or 40 percent more radial range for a communication system. Yet, if the overall measurement uncertainty of the final product test is on the order of ±0.5 dB, the unit actually shipped could have output power as much as 10% lower than the customer expects, with resulting lower operating margins.

Because signal power level is so important to the overall system performance, it is also critical when specifying the components that build up the system. Each component of a signal chain must receive the proper signal level from the previous component and pass the proper level to the succeeding component. Power is so important that it is frequently measured twice at each level, once by the vendor and again at the incoming inspection stations before beginning the next assembly level. It is at the higher operating power levels where each decibel increase in power level becomes more costly in terms of complexity of design, expense of active devices, skill in manufacture, difficulty of testing, and degree of reliability.

The increased cost per dB of power level is especially true at microwave frequencies, where the high-power solid state devices are inherently more costly and the guard-bands designed into the circuits to avoid maximum device stress are also quite costly. Many systems are continuously monitored for output power during ordinary operation. This large number of power measurements and their importance dictates that the measurement equipment and techniques be accurate, repeatable, traceable, and convenient.

The goal of this application note, and others, is to guide the reader in making those measurement qualities routine. Because many of the examples cited above used the term "signal level," the natural tendency might be to suggest measuring voltage instead of power. At low frequencies, below about 100 kHz, power is usually calculated from voltage measurements across an assumed impedance. As the frequency increases, the impedance has large variations, so power measurements become more popular, and voltage or current are the calculated parameters. At frequencies from about 30 MHz on up through the optical spectrum, the direct measurement of power is more accurate and easier. Another example of decreased usefulness is in waveguide transmission configurations where voltage and current conditions are more difficult to define.

A brief history of power measurement

From the earliest design and application of RF and microwave systems, it was necessary to determine the level of power output. Some of the techniques were quite primitive by today's standards. For example, when Sigurd and Russell Varian, the inventors of the klystron microwave power tube in the late 1930s, were in the early experimental stages of their klystron cavity, the detection diodes of the day were not adequate for those microwave frequencies. The story is told that Russell cleverly drilled a small hole at the appropriate position in the klystron cavity wall, and positioned a fluorescent screen alongside. This technique was adequate to reveal whether the cavity was in oscillation and to give a gross indication of power level changes as various drive conditions were adjusted.

Some early measurements of high power system signals were accomplished by arranging to absorb the bulk of the system power into some sort of termination and measuring the heat buildup versus time. A simple example used for high power radar systems was the water-flow calorimeter. These were made by fabricating a glass or low-dielectric-loss tube through the sidewall of the waveguide at a shallow angle. Since the water was an excellent absorber of the microwave energy, the power measurement required only a measurement of the heat rise of the water from input to output and a measure of the volumetric flow versus time. The useful part of that technique was that the water flow also carried off the considerable heat from the source under test at the same time it was measuring the desired parameter. This was especially important for measurements on kilowatt and megawatt microwave sources.

Going into World War II, as detection crystal technology grew from the early galena cat-whiskers, detectors became more rugged and performed at higher RF and microwave frequencies. They were better matched to transmission lines, and by using comparison techniques with sensitive detectors, unknown microwave power could be measured against known values of power generated by calibrated signal generators.

Power substitution methods emerged with the advent of sensing elements which were designed to couple transmission line power into the tiny sensing element.[1] Barretters were positive-temperature-coefficient elements, typically metallic fuses, but they were frustratingly fragile and easy to burn out. Thermistor sensors exhibited a negative temperature coefficient and were much more rugged. By including such sensing elements as one arm of a 4-arm balanced bridge, DC or low-frequency AC power could be withdrawn as RF/MW power was applied, maintaining the bridge balance and yielding a substitution value of power.[2]

Through the 1950's and 60's, coaxial and waveguide thermistor sensors were the workhorse technology. Agilent was a leading innovator in sensors and power meters with recognizable model numbers such as 430, 431 and 432. As the thermocouple sensor technology entered in the early 1970's, it was accompanied by digital instrumentation. This led to a family of power meters that were exceptionally long-lived, with model numbers such as 435, 436, 437, and 438.

Commercial calorimeters also had a place in early measurements. Dry calorimeters absorbed system power and by measurement of heat rise versus time, were able to determine system power. Agilent's 434A power meter (circa, 1960) was an oil-flow calorimeter, with a 10 watt top range, which also used a heat comparison between the RF load and another identical load driven by DC power.[3] Water-flow calorimeters were offered by several vendors for medium to high power levels.

A history of peak power measurements

Historically, the development of radar and navigation systems in the late 1930s led to the application of pulsed RF and microwave power. Magnetrons and klystrons were invented to provide the pulsed power, and, therefore, peak power measurement methods developed concurrently. Since the basic performance of those systems depended primarily on the peak power radiated, it was important to have reliable measurements.[4]

Early approaches to pulse power measurement have included the following techniques: 1) calculation from average power and duty cycle data; 2) notch wattmeter; 3) DC-pulse power comparison; 4) barretter integration. Most straightforward is the method of measuring power with a typical averaging sensor, and dividing the result by the duty cycle measured with a video detector and an oscilloscope.

The notch wattmeter method arranged to combine the unknown pulsed signal with another comparison signal usually from a calibrated signal generator, into a single detector. By appropriate video synchronization, the generator signal was "notched out" to zero power at the precise time the unknown RF pulse occurred. A microwave detector responded to the combined power, which allowed the user to set the two power levels to be equal on an oscilloscope trace. The unknown microwave pulse was equal to the known signal generator level, corrected for the signal attenuation in the two paths.

The DC-power comparison method involved calibrating a stable microwave detector with known power levels across its dynamic range, up into its linear detection region. Then, unknown pulsed power could be related to the calibration chart. Agilent's early 8900A peak power meter (acquired as part of the Boonton Radio acquisition in the early 1960's) was an example of that method. It used a biased detector technique to improve stability, and measured in the 50 to 2000 MHz range, which made it ideal for the emerging navigation pulsed applications of the 1960's.

Finally, barretter integration instrumentation was an innovative solution which depended on measuring the fast temperature rise in a tiny metal wire sensor (barretter) which absorbed the unknown peak power.[5] By determining the slope of the temperature rise in the sensor, the peak power could be measured, the higher the peak, the faster the heat rise and greater the heat slope. The measurement was quite valid and independent of pulse width, but unfortunately, barretters were fragile and lacked great dynamic range. Other peak power meters were offered to industry in the intervening years.

In 1990, Agilent introduced a major advance in peak power instrumentation, the 8990A peak power analyzer. This instrument and its associated dual peak power sensors provided complete analysis of the envelope of pulsed RF and microwave power to 40 GHz. The analyzer was able to measure or compute 13 different parameters of a pulse waveform: 8 time values such as pulse width and duty cycle, and 5 amplitude parameters such as peak power and pulse top amplitude.

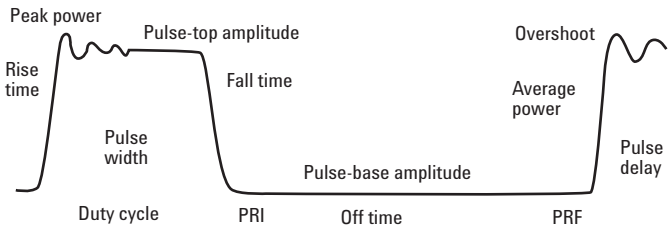

Figure 1-1. Typical envelope of pulsed system with overshoot and pulse ringing, shown with 13 pulse parameters which the Agilent 8990A characterized for time and amplitude.

Because it was really the first peak power analyzer which measured so many pulse parameters, Agilent chose that point to define for the industry certain pulse features in statistical terms, extending older IEEE definitions of video pulse characteristics. One reason was that the digital signal processes inside the instrument were themselves based on statistical methods. These pulsed power definitions are fully elaborated in Chapter II on definitions.

However, as the new wireless communications revolution of the 1990's took over, the need for instruments to characterize complex digital modulation formats led to the introduction of the Agilent E4416/17A peak and average power meters, and to the retirement of the 8990 meter. Complete descriptions of the new peak and average sensors, and meters and envelope characterization processes known as "time-gated" measurements are given in Chapter VI.

This application note allocates most of its space to the more modern, convenient, and wider dynamic range sensor technologies that have developed since those early days of RF and microwave. Yet, it is hoped that the reader will reserve some appreciation for those early developers in this field for having endured the inconvenience and primitive equipment of those times.

---

1. B.P. Hand, "Direct Reading UHF Power Measurement," Hewlett-Packard Journal, Vol. 1, No. 59 (May, 1950).
2. E.L. Ginzton, "Microwave Measurements," McGraw-Hill, Inc., 1957.
3. B.P. Hand, "An Automatic DC to X-Band Power Meter for the Medium Power Range," Hewlett-Packard Journal, Vol. 9, No. 12 (Aug., 1958).
4. M. Skolnik, "Introduction to Radar Systems," McGraw-Hill, Inc., (1962).
5. R.E. Henning, "Peak Power Measurement Technique," Sperry Engineering Review, (May-June 1955).

II. Power Measurement

Units and definitions

Watt

The International System of Units (SI) has established the watt (W) as the unit of power; one watt is one joule per second. Interestingly, electrical quantities do not even enter into this definition of power. In fact, other electrical units are derived from the watt. A volt is one watt per ampere. By the use of appropriate standard prefixes the watt becomes the kilowatt (1 kW = 10^3W), milliwatt (1 mW = 10^{-3}W), microwatt (1 μW = 10^{-6}W), nanowatt (1 nW = 10^{-9}W), etc.

dB

In many cases, such as when measuring gain or attenuation, the ratio of two powers, or relative power, is frequently the desired quantity rather than absolute power. Relative power is the ratio of one power level, P, to some other level or reference level, P_{ref}. The ratio is dimensionless because the units of both the numerator and denominator are watts. Relative power is usually expressed in decibels (dB).

The dB is defined by

$$dB = 10 \log_{10} \left(\frac{P}{P_{ref}} \right) \quad (2\text{-}1)$$

The use of dB has two advantages. First, the range of numbers commonly used is more compact; for example +63 dB to –153 dB is more concise than 2 x 10^6 to 0.5 x 10^{-15}. The second advantage is apparent when it is necessary to find the gain of several cascaded devices. Multiplication of numeric gain is then replaced by the addition of the power gain in dB for each device.

dBm

Popular usage has added another convenient unit, dBm. The formula for dBm is similar to the dB formula except that the denominator, P_{ref}, is always one milliwatt:

$$dBm = 10 \log_{10} \left(\frac{P}{1\ mW} \right) \quad (2\text{-}2)$$

In this expression, P is expressed in milliwatts and is the only variable, so dBm is used as a measure of absolute power. An oscillator, for example, may be said to have a power output of 13 dBm. By solving for P using the dBm equation, the power output can also be expressed as 20 mW. So dBm means “dB above one milliwatt” (no sign is assumed positive) but a negative dBm is to be interpreted as “dB below one milliwatt.” The advantages of the term dBm parallel those for dB; it uses compact numbers and allows the use of addition instead of multiplication when cascading gains or losses in a transmission system.

Power

The term “average power” is very popular and is used in specifying almost all RF and microwave systems. The terms “pulse power” and “peak envelope power” are more pertinent to radar and navigation systems, and recently, TDMA signals in wireless communication systems.

In elementary theory, power is said to be the product of voltage (v) and current (I). But for an AC voltage cycle, this product V x I varies during the cycle as shown by curve P in figure 2-1, according to a 2f relationship. From that example, a sinusoidal generator produces a sinusoidal current as expected, but the product of voltage and current has a DC term as well as a component at twice the generator frequency. The word “power” as most commonly used, refers to that DC component of the power product.

All the methods of measuring power to be discussed (except for one chapter on peak power measurement) use power sensors which, by averaging, respond to the DC component. Peak power instruments and sensors have time constants in the sub-microsecond region, allowing measurement of pulsed power modulation envelopes.

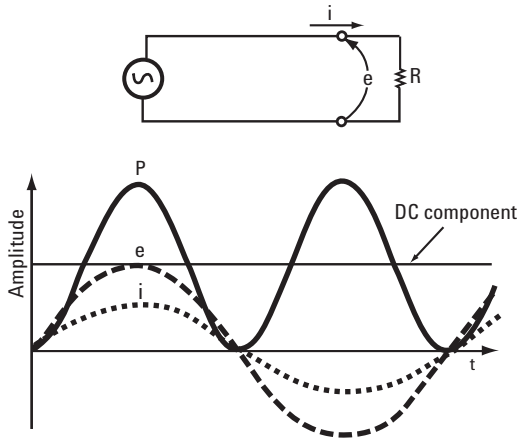

Figure 2-1. The product of voltage and current, P, varies during the sinusoidal cycle.

The fundamental definition of power is energy per unit time. This corresponds with the definition of a watt as energy transfer at the rate of one joule per second. The important question to resolve is over what time is the energy transfer rate to be averaged when measuring or computing power? From figure 2-1 it is clear that if a narrow time interval is shifted around within one cycle, varying answers for energy transfer rate are found. But at radio and microwave frequencies, such microscopic views of the voltage-current product are not common. For this application note, power is defined as the energy transfer per unit time averaged over many periods of the lowest frequency (RF or microwave) involved.

A more mathematical approach to power for a continuous wave (CW) is to find the average height under the curve of P in figure 2-1. Averaging is done by finding the area under the curve, that is by integrating, and then dividing by the length of time over which that area is taken. The length of time should be an exact number of AC periods. The power of a CW signal at frequency ($1/T_0$) is:

$$P = \frac{1}{nT_0}\int_0^{nT_0} e_p \sin\left(\frac{2\pi}{T_0}t\right) \cdot i_p \sin\left(\frac{2\pi}{T_0}+\phi\right) \quad (2\text{-}3)$$

where T_0 is the AC period, e_p and i_p represent peak values of e and i, ϕ is the phase angle between e and i, and n is the number of AC periods. This yields (for n = 1, 2, 3 . . .):

$$P = \frac{e_p i_p}{2} \cos\phi \quad (2\text{-}4)$$

If the integration time is many AC periods long, then, whether or not n is a precise integer makes a vanishingly small difference. This result for large n is the basis of power measurement.

For sinusoidal signals, circuit theory shows the relationship between peak and rms values as:

$$e_p = \sqrt{2}\, E_{rms} \text{ and } i_p = \sqrt{2}\, I_{rms} \quad (2\text{-}5)$$

Using these in (2-4) yields the familiar expression for power:

$$P = E_{rms} \cdot I_{rms} \cos\phi \quad (2\text{-}6)$$

Average power

Average power, like the other power terms to be defined, places further restrictions on the averaging time than just "many periods of the highest frequency." Average power means that the energy transfer rate is to be averaged over many periods of the lowest frequency involved. For a CW signal, the lowest frequency and highest frequency are the same, so average power and power are the same. For an amplitude modulated wave, the power must be averaged over many periods of the modulation component of the signal as well.

In a more mathematical sense, average power can be written as:

$$P_{avg} = \frac{1}{nT} \int_{0}^{nT_{\ell}} e(t) \bullet i(t)dt \qquad (2\text{-}7)$$

where T is the period of the lowest frequency component of e(t) and i(t). The averaging time for average power sensors and meters is typically from several hundredths of a second to several seconds and therefore this process obtains the average of most common forms of amplitude modulation.

Pulse power

For pulse power, the energy transfer rate is averaged over the pulse width, τ. Pulse width τ is considered to be the time between the 50 percent risetime/fall-time amplitude points.

Mathematically, pulse power is given by

$$P_p = \frac{1}{\tau} \int_{0}^{\tau} e(t) \bullet i(t)dt \qquad (2\text{-}8)$$

By its very definition, pulse power averages out any aberrations in the pulse envelope such as overshoot or ringing. For this reason it is called pulse power and not peak power or peak pulse power as is done in many radar references. The terms peak power and peak pulse power are not used here for that reason. Building on IEEE video pulse definitions, pulse-top amplitude also describes the pulse-top power averaged over its pulse width. Peak power refers to the highest power point of the pulse top, usually the risetime overshoot. See IEEE definitions below.

The definition of pulse power has been extended since the early days of microwave to be:

$$P_p = \frac{P_{avg}}{\text{Duty Cycle}} \qquad (2\text{-}9)$$

where duty cycle is the pulse width times the repetition frequency. See figure 2-2. This extended definition, which can be derived from (2-7) and (2-8) for rectangular pulses, allows calculation of pulse power from an average power measurement and the duty cycle.

For microwave systems which are designed for a fixed duty cycle, peak power is often calculated by use of the duty cycle calculation along with an average power sensor. See figure 2-2. One reason is that the instrumentation is less expensive, and in a technical sense, the averaging technique integrates all the pulse imperfections into the average.

The evolution of highly sophisticated radar, electronic warfare and navigation systems, which is often based on complex pulsed and spread spectrum technology, has led to more sophisticated instrumentation for characterizing pulsed RF power. Chapter VI presents the theory and practice of peak and average sensors and instrumentation.

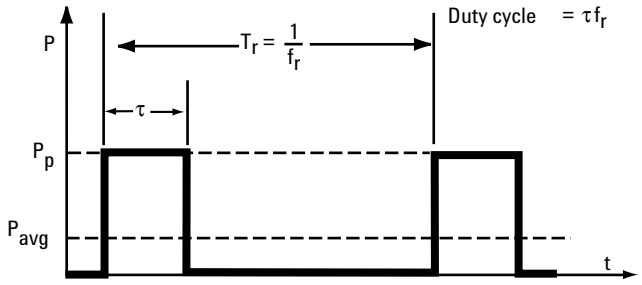

Figure 2-2. Pulse power Pp is averaged over the pulse width.

Peak envelope power

For certain more sophisticated, microwave applications and because of the need for greater accuracy, the concept of pulse power is not totally satisfactory. Difficulties arise when the pulse is intentionally non-rectangular or when aberrations do not allow an accurate determination of pulse width *τ*. Figure 2-3 shows an example of a Gaussian pulse shape used in certain navigation systems, where pulse power, by either (2-8) or (2-9), does not give a true picture of power in the pulse. Peak envelope power is a term for describing the maximum power. Envelope power will first be discussed.

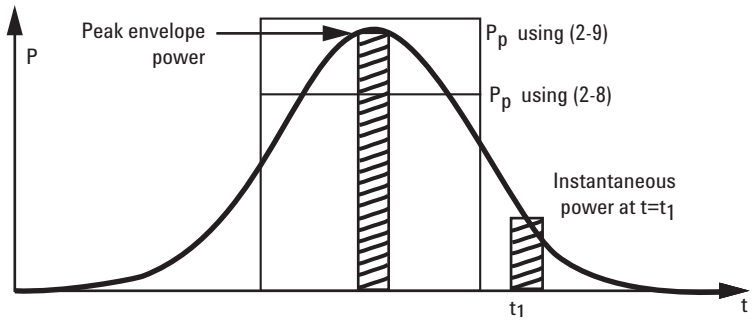

Figure 2-3. A Gaussian pulse and the different kinds of power.

Envelope power is measured by making the averaging time greater than $1/f_m$ where f_m is the maximum frequency component of the modulation waveform. The averaging time is therefore limited on both ends: (1) it must be large compared to the period of the highest modulation frequency, and (2) it must be small compared to the carrier.

By continuously displaying the envelope power on an oscilloscope (using a detector operating in its square-law range), the oscilloscope trace will show the power profile of the pulse shape. (Square law means the detected output voltage is proportional to the input RF power, that is the square of the input voltage.) Peak envelope power, then, is the maximum value of the envelope power.

Average power, pulse power, and peak envelope power all yield the same answer for a CW signal. Of all power measurements, average power is the most frequently measured because of convenient measurement equipment with highly accurate and traceable specifications.

IEEE video pulse standards adapted for microwave pulses

As mentioned in Chapter I, the 1990 introduction of the Agilent 8990 peak power analyzer (now discontinued) resulted in the promulgation of some new terminology for pulsed power, intended to define pulsed RF/microwave waveforms more precisely. For industry consistency, Agilent chose to extend older IEEE definitions of video pulse characteristics into the RF/microwave domain.

One reason that pulsed power is more difficult to measure is that user-waveform envelopes under test may need many different parameters to characterize the power flow as shown in figure 2-4.

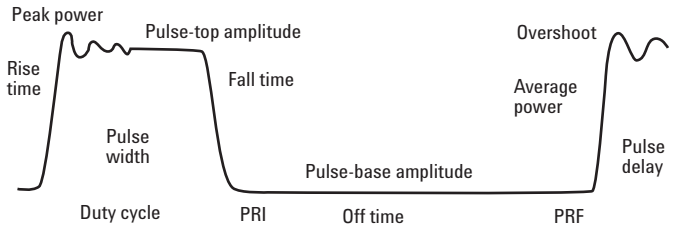

Figure 2-4. Typical envelope of pulsed system with overshoot and pulse ringing, shown with 13 pulse parameters which characterize time and amplitude.

Two IEEE video standards were used to implement the RF/microwave definitions:

1) IEEE STD 194-1977, "IEEE Standard Pulse Terms and Definitions," July 26, 1977.[1]

2) ANSI/IEEE STD 181-1977, "IEEE Standard on Pulse Measurement and Analysis by Objective Techniques," July 22, 1977. (Revised from 181-1955, *Methods of Measurement of Pulse Qualities*.[2]

IEEE STD 194-1977 was the primary source for definitions. ANSI/IEEE STD 181 is included here for reference only, since the 8990 used statistical techniques to determine pulse top characteristics as recommended by IEEE STD 181 histogram process.

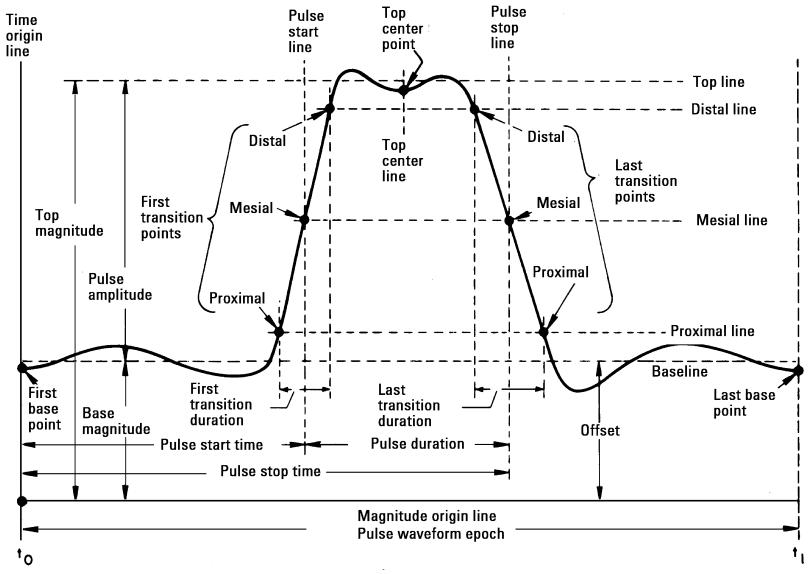

Figure 2-5. IEEE pulse definitions and standards for video parameters applied to microwave pulse envelopes. ANSI/IEEE Std 194-1977, Copyright © 1977, IEEE all rights reserved.

It was recognized that while terms and graphics from both those standards were written for video pulse characteristics, most of the measurement theory and intent of the definitions can be applied to the waveform envelopes of pulse-modulated RF and microwave carriers. Several obvious exceptions would be parameters such as pre-shoot, which is the negative-going undershoot that precedes a pulse risetime. Negative power would be meaningless. The same reasoning would apply to the undershoot following the fall time of a pulse.

For measurements of pulse parameters such as risetime or overshoot to be meaningful, the points on the waveform that are used in the measurement must be defined unambiguously. Since all the time parameters are measured between specific amplitude points on the pulse, and since all the amplitude points are referenced to the two levels named “top” and “base,” figure 2-5 shows how they are defined.

Peak power waveform definitions

The following are definitions for thirteen RF pulse parameters as adapted from IEEE video definitions:

Rise time — The time difference between the proximal and distal first transition points, usually 10 and 90 percent of pulse-top amplitude (vertical display is linear power).

Fall time — Same as risetime measured on the last transition.

Pulse width — The pulse duration measured at the mesial level; normally taken as the 50 percent power level.

Off time — Measured on the mesial (50%) power line; pulse separation, the interval between the pulse stop time of a first pulse waveform and the pulse start time of the immediately following pulse waveform in a pulse train.

Duty cycle — The previously measured pulse duration divided by the pulse repetition interval.

PRI — (Pulse Repetition Interval) The interval between the pulse start time of a first pulse waveform and the pulse start time of the immediately following pulse waveform in a periodic pulse train.

PRF	(Pulse Repetition Frequency) The reciprocal of PRI.
Pulse delay	The occurance in time of one pulse waveform before (after) another pulse waveform; usually the reference time would be a video system timing or clock pulse.
Pulse-top	Pulse amplitude, defined as the algebraic amplitude difference between the top magnitude and the base magnitude; calls for a specific procedure or algorithm, such as the histogram method.*
Pulse-base	The pulse waveform baseline specified to be obtained by the histogram algorithm.
Peak power	The highest point of power in the waveform, usually at the first overshoot; it might also occur elsewhere across the pulse top if parasitic oscillations or large amplitude ringing occurs; peak power is not the pulse-top amplitude which is the primary measurement of pulse amplitude.
Overshoot	A distortion that follows a major transition; the difference between the peak power point and the pulse-top amplitude computed as a percentage of the pulse-top amplitude.
Average power	Computed by using the statistical data from pulse-top amplitude power and time measurements.

New power sensors and meters for pulsed and complex modulation

As the new wireless communications revolution of the 1990's took over, the need for instruments to characterize the power envelope of complex digital modulation formats led to the introduction of the Agilent E4416/17A peak and average power meters, and to the retirement of the 8990 meter. Complete descriptions of the new peak and average sensors and meters along with envelope characterization processes known as "time-gated" measurements are given in Chapter VI. "Time-gated" is a term that emerged from spectrum analyzer applications. It means adding a time selective control to the power measurement.

The E4416/17A peak and average meters also led to some new definitions of pulsed parameters, suitable for the communications industry. For example, burst average power is that pulsed power averaged across a TDMA pulse width. Burst average power is functionally equivalent to the earlier pulse-top amplitude of figure 2-4. One term serves the radar applications arena and the other, the wireless arena.

Three methods of sensing power

There are three popular devices for sensing and measuring average power at RF and microwave frequencies. Each of the methods uses a different kind of device to convert the RF power to a measurable DC or low frequency signal. The devices are the thermistor, the thermocouple, and the diode detector. Each of the next three chapters discusses in detail one of those devices and its associated instrumentation. Chapter VI discusses diode detectors used to measure pulsed and complex modulation envelopes.

Each method has some advantages and disadvantages over the others. After the individual measurement sensors are studied, the overall measurement errors are discussed in Chapter VII.

The general measurement technique for average power is to attach a properly calibrated sensor to the transmission line port at which the unknown power is to be measured. The output from the sensor is connected to an appropriate power meter. The RF power to the sensor is turned off and the power meter zeroed. This operation is often referred to as "zero setting" or "zeroing." Power is then turned on. The sensor, reacting to the new input level, sends a signal to the power meter and the new meter reading is observed.

* In such a method, the probability histogram of power samples is computed. This is split in two around the mesial line and yields a peak in each segment. Either the mode or the mean of these histograms gives the pulse top and pulse bottom power.

Key power sensor parameters

In the ideal measurement case above, the power sensor absorbs all the power incident upon the sensor. There are two categories of non-ideal behavior that are discussed in detail in Chapter VII, but will be introduced here.

First, there is likely an impedance mismatch between the characteristic impedance of the RF source or transmission line and the RF input impedance of the sensor. Thus, some of the power that is incident on the sensor is reflected back toward the generator rather than dissipated in the sensor. The relationship between incident power P_i , reflected power P_r , and dissipated power P_d , is:

$$P_i = P_r + P_d \tag{2-10}$$

The relationship between P_i and P_r for a particular sensor is given by the sensor reflection coefficient magnitude ρ_ℓ.

$$P_r = \rho_\ell^{\,2} P_i \tag{2-11}$$

Reflection coefficient magnitude is a very important specification for a power sensor because it contributes to the most prevalent source of error, mismatch uncertainty, which is discussed in Chapter VII. An ideal power sensor has a reflection coefficient of zero, no mismatch. While a ρ_ℓ of 0.05 or 5 percent (equivalent to an SWR of approximately 1.11) is preferred for most situations, a 50 percent reflection coefficient would not be suitable for most situations due to the large measurement uncertainty it causes. Some early waveguide sensors were specified at a reflection coefficient of 0.35.

The second cause of non-ideal behavior occurs inside the sensor when, RF power is dissipated in places other than in the power sensing element. Only the actual power dissipated in the sensor element gets metered. This effect is defined as the sensor's effective efficiency η_e. An effective efficiency of 1 (100%) means that all the power entering the sensor unit is absorbed by the sensing element and metered — no power is dissipated in conductors, sidewalls, or other components of the sensor.

The most frequently used specification of a power sensor is called the calibration factor, K_b. K_b is a combination of reflection coefficient and effective efficiency according to

$$K_b = \eta_e (1 - \rho \ell^2)$$

If a sensor has a K_b of 0.90 (90%) the power meter would normally indicate a power level that is 10 percent lower than the incident power P_i. Modern power sensors are calibrated at the factory and carry a calibration chart or have the correction data stored in EEPROM. Power meters then correct the lower-indicated reading by setting a calibration factor dial (or keyboard or GPIB on digital meters) on the power meter to correspond with the calibration factor of the sensor at the frequency of measurement. Calibration factor correction is not capable of correcting for the total effect of reflection coefficient, due to the unknown phase relation of source and sensor. There is still a mismatch uncertainty that is discussed in Chapter VII.

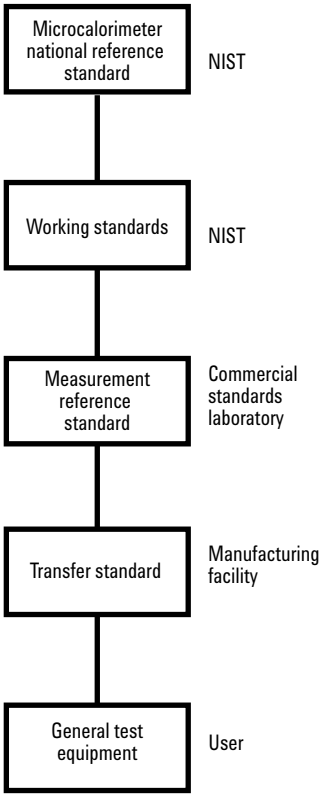

Figure 2-6. The traceability path of power references from the United States National Reference Standard.

The hierarchy of power measurements, national standards and traceability

Since power measurement has important commercial ramifications, it is important that power measurements can be duplicated at different times and at different places. This requires well-behaved equipment, good measurement technique, and common agreement as to what is the standard watt. The agreement in the United States is established by the National Institute of Standards and Technology (NIST) at Boulder, Colorado, which maintains a National Reference Standard in the form of various microwave microcalorimeters for different frequency bands.[3, 4] When a power sensor can be referenced back to that National Reference Standard, the measurement is said to be traceable to NIST.

The usual path of traceability for an ordinary power sensor is shown in figure 2-6. At each echelon, at least one power standard is maintained for the frequency band of interest. That power sensor is periodically sent to the next higher echelon for recalibration, then returned to its original level. Recalibration intervals are established by observing the stability of a device between successive recalibrations. The process might start with recalibration every few months. Then, when the calibration is seen not to change, the interval can be extended to a year or so.

Each echelon along the traceability path adds some measurement uncertainty. Rigorous measurement assurance procedures are used at NIST because any error at that level must be included in the total uncertainty at every lower level. As a result, the cost of calibration tends to be greatest at NIST and reduces at each lower level. The measurement comparison technique for calibrating a power sensor against one at a higher echelon is discussed in other documents, especially those dealing with round robin procedures.[5, 6]

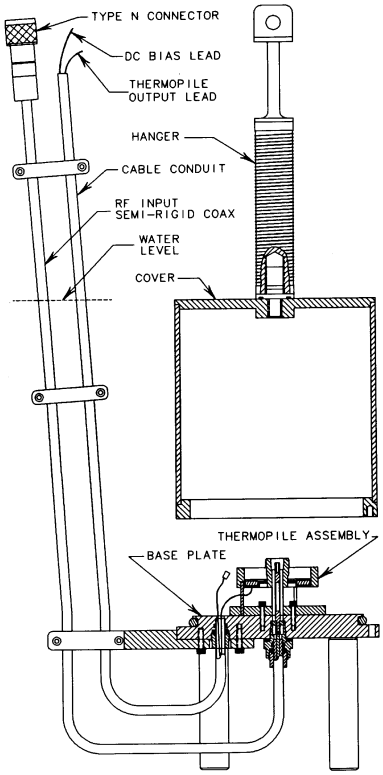

Figure 2-7. Schematic cross-section of the NIST coaxial microcalorimeter at Boulder, CO. The entire sensor configuration is maintained under a water bath with a highly-stable temperature so that RF to DC substitutions may be made precisely.

The National Power Reference Standard for the U.S. is a microcalorimeter maintained at the NIST in Boulder, CO, for the various coaxial and wave-guide frequency bands offered in their measurement services program. These measurement services are described in NIST SP-250, available from NIST on request.[7] They cover coaxial mounts from 10 MHz to 26.5 GHz and waveguide from 8.2 GHz to the high millimeter ranges of 96 GHz.

A microcalorimeter measures the effective efficiency of a DC substitution sensor which is then used as the transfer standard. Microcalorimeters operate on the principle that after applying an equivalence correction, both DC and absorbed microwave power generate the same heat. Comprehensive and exhaustive analysis is required to determine the equivalence correction and account for all possible thermal and RF errors, such as losses in the transmission lines and the effect of different thermal paths within the microcalorimeter and the transfer standard. The DC-substitution technique is used because the fundamental power measurement can then be based on DC voltage (or current) and resistance standards. The traceability path leads through the microcalorimeter (for effective efficiency, a unit-less correction factor) and finally back to the national DC standards.

In addition to national measurement services, other industrial organizations often participate in comparison processes known as round robins (RR). A round robin provides measurement reference data to a participating lab at very low cost compared to primary calibration processes. For example, the National Conference of Standards Laboratories (NCSL), a non-profit association of over 1400 world-wide organizations, maintains round robin projects for many measurement parameters, from dimensional to optical. The NCSL Measurement Comparison Committee oversees those programs.[5]

For RF power, a calibrated thermistor mount starts out at a "pivot lab," usually one with overall RR responsibility, then travels to many other reference labs to be measured, returning to the pivot lab for closure of measured data. Such mobile comparisons are also carried out between National Laboratories of various countries as a routine procedure to assure international measurements at the highest level.

Microwave power measurement services are available from many National Laboratories around the world, such as the NPL in the United Kingdom and PTB in Germany. Calibration service organizations are numerous too, with names like NAMAS in the United Kingdom.

---

1. IEEE STD 194-1977, "IEEE Standard Pulse Terms and Definitions," (July 26, 1977), IEEE, New York, NY.
2. ANSI/IEEE STD181-1977, "IEEE Standard on Pulse Measurement and Analysis by Objective Techniques," July 22, 1977. Revised from 181-1955, *Methods of Measurement of Pulse Qualities*, IEEE, New York, NY.
3. M.P. Weidman and P.A. Hudson, "WR-10 Millimeterwave Microcalorimeter," NIST Technical Note 1044, June, 1981.
4. F.R. Clague, "A Calibration Service for Coaxial Reference Standards for Microwave Power," NIST Technical Note 1374, May, 1995.
5. National Conference of Standards Laboratories, Measurement Comparison Committee, Suite 305B, 1800 30th St. Boulder, CO 80301.
6 M.P. Weidman, "Direct Comparison Transfer of Microwave Power Sensor Calibration," NIST Technical Note 1379, January, 1996.
7. Special Publication 250; NIST Calibration Services.

General references

R.W. Beatty, "Intrinsic Attenuation," IEEE Trans. on Microwave Theory and Techniques, Vol. I I, No. 3 (May, 1963) 179-182.
R.W. Beatty, "Insertion Loss Concepts," Proc. of the IEEE. Vol. 52, No. 6 (June, 1966) 663-671.
S.F. Adam, "Microwave Theory & Applications," Prentice-Hall, 1969.
C.G. Montgomery, "Technique of Microwave Measurements," Massachusetts Institute of Technology, Radiation Laboratory Series, Vol. 11. McGraw-Hill, Inc., 1948.
Mason and Zimmerman. "Electronic Circuits, Signals and Systems," John Wiley and Sons, Inc., 1960.

III. Thermistor Sensors and Instrumentation

Bolometer sensors, especially thermistors, have held an important historical position in RF/microwave power measurements. However, in recent years thermocouple and diode technologies have captured the bulk of those applications because of their increased sensitivities, wider dynamic ranges, and higher power capabilities. Yet, thermistors are still the sensor of choice for power transfer standards because of their DC power substitution capability. So, although this chapter is shortened from earlier editions, the remaining material should be adequate to understand the basic theory and operation of thermistor sensors and their associated dual-balanced bridge power meter instruments.

Bolometers are power sensors that operate by changing resistance due to a change in temperature. The change in temperature results from converting RF or microwave energy into heat within the bolometric element. There are two principle types of bolometers, barretters and thermistors. A barretter is a thin wire that has a positive temperature coefficient of resistance. Thermistors are semiconductors with a negative temperature coefficient.

To have a measurable change in resistance for a small amount of dissipated RF power, a barretter is constructed of a very thin and short piece of wire, for example, a 10 mA instrument fuse. The maximum power that can be measured is limited by the burnout level of the barretter, typically just over 10 mW, and they are seldom used anymore.

The thermistor sensor used for RF power measurement is a small bead of metallic oxides, typically 0.4 mm diameter with 0.03 mm diameter wire leads. Thermistor characteristics of resistance vs. power are highly non-linear, and vary considerably from one thermistor to the next. Thus the balanced-bridge technique always maintains the thermistor element at a constant resistance, R, by means of DC or low frequency AC bias. As RF power is dissipated in the thermistor, tending to lower R, the bias power is withdrawn by an equal amount to balance the bridge and keep R the same value. The decrease in bias power should be proportional to the increase in RF power. That decrease in bias power is then displayed on a meter to indicate RF power.

Thermistor sensors

Thermistor elements are mounted in either coaxial or waveguide structures so they are compatible with common transmission line systems used at microwave and RF frequencies. The thermistor and its mounting must be designed to satisfy several important requirements so that the thermistor element will absorb as much of the power incident on the mount as possible. First, the sensor must present a good impedance match to the transmission line over the specified frequency range. The sensor must also have low resistive and dielectric losses within the mounting structure because only power that is dissipated in the thermistor element can be registered on the meter. In addition, mechanical design must provide isolation from thermal and physical shock and must keep leakage small so that microwave power does not escape from the mount in a shunt path around the thermistor. Shielding is also important to prevent extraneous RF power from entering the mount.

Modern thermistor sensors have a second set of compensating thermistors to correct for ambient temperature variations. These compensating thermistors are matched in their temperature-resistance characteristics to the detecting thermistors. The thermistor mount is designed to maintain electrical isolation between the detecting and compensating thermistors yet keeping the thermistors in very close thermal contact.

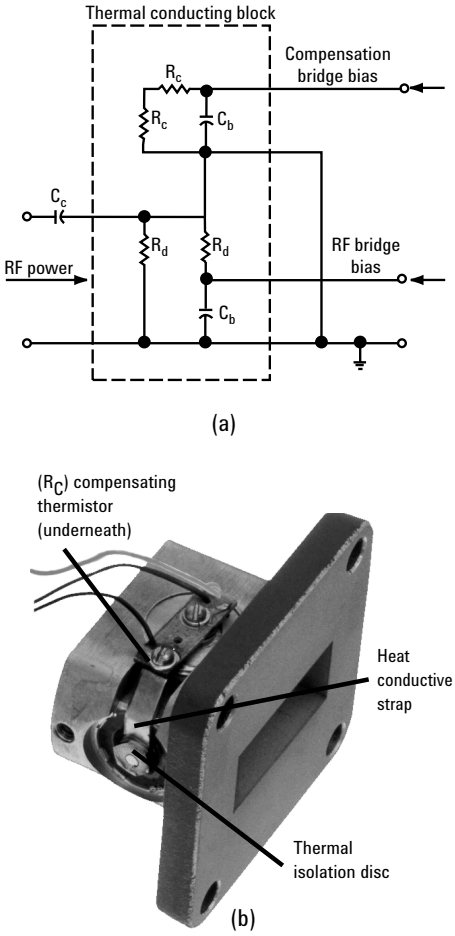

Figure 3-1.
(a) 478A coaxial sensor simplified diagram
(b) 486A waveguide sensor construction.

Coaxial thermistor sensors

The 478A and 8478B thermistor mounts (thermistor mount was the earlier name for sensor) contain four matched thermistors and measure power from 10 MHz to 10 and 18 GHz. The two RF-detecting thermistors, bridge-balanced to 100 Ω each, are connected in series (200 Ω) as far as the DC bridge circuits are concerned. For the RF circuit, the two thermistors appear to be connected in parallel, presenting a 50 Ω impedance to the test signal. The principle advantage of this connection scheme is that both RF thermistor leads to the bridge are at RF ground. See figure 3-1 (a).

Compensating thermistors, which monitor changes in ambient temperature but not changes in RF power, are also connected in series. These thermistors are also biased to a total of 200 Ω by a second bridge in the power meter, called the compensating bridge. The compensating thermistors are completely enclosed in a cavity for electrical isolation from the RF signal but they are mounted on the same thermal conducting block as the detecting thermistors. The thermal mass of the block is large enough to prevent sudden temperature gradients between the thermistors. This improves the isolation of the system from thermal inputs such as human hand effects.

There is a particular error, called dual element error, that is limited to coaxial thermistor mounts where the two thermistors are in parallel for the RF energy, but in series for DC. If the two thermistors are not quite identical in resistance, then more RF current will flow in the one of least resistance, but more DC power will be dissipated in the one of greater resistance. The lack of equivalence in the dissipated DC and RF power is a minor source of error that is proportional to power level. For thermistor sensors, this error is less than 0.1 percent at the high power end of their measurement range and is therefore considered as insignificant in the error analysis of Chapter VII.

Waveguide thermistor sensors

The 486A-series of waveguide thermistor mounts covers frequencies from 8 to 40 GHz. See figure 3-1 (b). Waveguide sensors up to 18 GHz utilize a post-and-bar mounting arrangement for the detecting thermistor. The 486A-series sensors covering the K and R waveguide band (18 to 26.5 GHz and 26.5 to 40 GHz) utilize smaller thermistor elements which are biased to an operating resistance of 200 Ω, rather than the 100 Ω used in lower frequency waveguide units. Power meters provide for selecting the proper 100 or 200 Ω bridge circuitry to match the thermistor sensor being used.

Bridges, from Wheatstone to dual-compensated DC types

Over the decades, power bridges for monitoring and regulating power sensing thermistors have gone through a major evolution. Early bridges such as the simple Wheatstone type were manually balanced. Automatically-balanced bridges, such as the 430C of 1952, provided great improvements in convenience but still had limited dynamic range due to thermal drift on their 30 µW (full scale) range. In 1966, with the introduction of the first temperature-compensated meter, the 431A, drift was reduced so much that meaningful measurements could be made down to 1 µW.[1]

The 432A power meter uses DC and not audio frequency power to maintain balance in both bridges. This eliminates earlier problems pertaining to the 10 kHz bridge drive signal applied to the thermistors. The 432A has the further convenience of an automatic zero set, eliminating the need for the operator to precisely reset zero for each measurement.

The 432A features an instrumentation accuracy of 1 percent. It also provides the ability to externally measure the internal bridge voltages with higher accuracy DC voltmeters, thus permitting a higher accuracy level for power transfer techniques to be used. In earlier bridges, small, thermo-electric voltages were present within the bridge circuits which ideally should have cancelled in the overall measurement. In practice, however, cancellation was not complete. In certain kinds of measurements this could cause an error of 0.3 µW. In the 432A, the thermo-electric voltages are so small, compared to the metered voltages, as to be insignificant.

The principal parts of the 432A (figure 3-2) are two self-balancing bridges, the meter-logic section, and the auto-zero circuit. The RF bridge, which contains the detecting thermistor, is kept in balance by automatically varying the DC voltage V_{rf}, which drives that bridge. The compensating bridge, which contains the compensating thermistor, is kept in balance by automatically varying the DC voltage V_c, which drives that bridge.

The power meter is initially zero-set (by pushing the zero-set button) with no applied RF power by making V_c equal to V_{rfo} (V_{rfo} means V_{rf} with zero RF power). After zero-setting, if ambient temperature variations change thermistor resistance, both bridge circuits respond by applying the same new voltage to maintain balance.

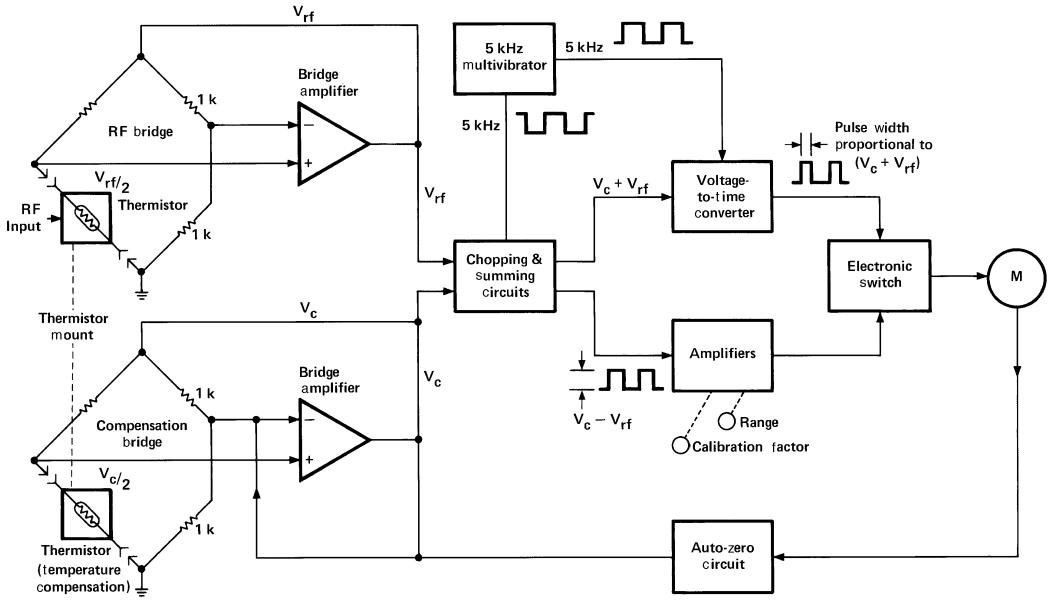

Figure 3-2. Simplified diagram of the 432A power meter.

If RF power is applied to the detecting thermistor, V_{rf} decreases so that

$$P_{rf} = \frac{V_{rfo}^2}{4R} - \frac{V_{rf}^2}{4R} \qquad (3\text{-}1)$$

where P_{rf} is the RF power applied and R is the value of the thermistor resistance at balance, but from zero-setting, $V_{rfo} = V_c$ so that

$$P_{rf} = \frac{1}{4R} (V_c^2 - V_{rf}^2) \qquad (3\text{-}2)$$

which can be written

$$P_{rf} = \frac{1}{4R} (V_c - V_{rf}) (V_c + V_{rf}) \qquad (3\text{-}3)$$

The meter logic circuitry is designed to meter the voltage product shown in equation (3-3). Ambient temperature changes cause V_c and V_{rf} to change so there is zero change to $V_c^2 - V_{rf}^2$ and therefore no change to the indicated P_{rf}.

As seen in figure 3-2, some clever analog circuitry is used to accomplish the multiplication of voltages proportional to (V_c -V_{rf}) and (V_c + V_{rf}) by use of a voltage-to-time converter. In these days, such simple arithmetic would be performed by the ubiquitous microprocessor, but the 432A predated that technology and performs well without it.

The principal sources of instrumentation uncertainty of the 432A lie in the metering logic circuits. But V_{rf} and V_c are both available at the rear panel of the 432A. With precision digital voltmeters and proper procedure, those outputs allow the instrumentation uncertainty to be reduced to ±0.2 percent for many measurements. The procedure is described in the operating manual for the 432A.

Thermistors as power transfer standards

For special use as transfer standards, the U.S. National Institute for Standards and Technology (NIST), accepts thermistor mounts, both coaxial and waveguide, to transfer power parameters such as calibration factor, effective efficiency and reflection coefficient in their measurement services program. To provide those services below 100 MHz, NIST instructions require sensors specially designed for that performance.

One example of a special power calibration transfer is the one required to precisely calibrate the internal 50 MHz, 1 mW power standard in the Agilent power meters, which use a family of thermocouples or diode sensors. That internal power reference is needed since those sensors do not use the power substitution technique. For standardizing the 50 MHz power reference, a specially-modified 478A thermistor sensor with a larger RF coupling capacitor is available for operation from 1 MHz to 1 GHz. It is designated the H55 478A and features an SWR of 1.35 over its range. For an even lower transfer uncertainty at 50 MHz, the H55 478A can be selected for 1.05 SWR at 50 MHz. This selected model is designated the H75 478A.

H76 478A thermistor sensor is the H75 sensor that has been specially calibrated in the Microwave Standards Lab with a 50 MHz power reference traceable to NIST. Other coaxial and waveguide thermistor sensors are available for metrology use.

Other DC-substitution meters

Other self-balancing power meters can also be used to drive thermistor sensors for measurement of power. In particular, the NIST Type 4 power meter, designed by the NIST for high-accuracy measurement of microwave power is well suited for the purpose. The Type 4 meter uses automatic balancing, along with a four-terminal connection to the thermistor sensor and external high precision DC voltage instrumentation. This permits lower uncertainty than standard power meters are designed to accomplish.

Some measurement considerations for power sensor comparisons

For metrology users involved in the acquisition, routine calibration, or round-robin comparison processes for power sensors, an overview might be useful. Since thermistor sensors are most often used as the transfer reference, the processes will be discussed in this section.

Typical sensor comparison system

The most common setup for measuring the effective efficiency or calibration factor of a sensor under test (DUT) is known as the power ratio method, as shown in figure 3-3[2]. The setup consists of a 3-port power splitter that is usually a 2-resistor design. A reference detector is connected to port 3 of the power splitter, and the DUT and standard (STD) sensors are alternately connected to port 2 of the power splitter. Other types of 3-ports can also be used such as directional couplers and power dividers.

The signal source that is connected to port 1 must be stable with time. The effects of signal source power variations can be reduced by simultaneously measuring the power at the reference and the DUT or the reference and the STD. This equipment setup is a variation of that used by the Agilent 11760S power sensor calibration system, (circa 1990), now retired.

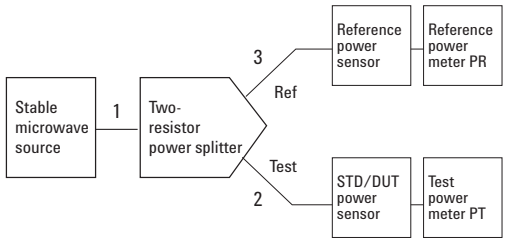

Figure 3-3. A two-resistor power splitter serves as a very broadband method for calibrating power sensors.

For coaxial sensors, the 2-resistor power splitters are typically very broadband and can be used down to DC. Because the internal signal-split common point is effectively maintained at zero impedance by the action of the power split ratio computation, Γ_g for a well balanced 2-resistor power splitter is approximately zero. Unfortunately, at the higher frequencies, 2-resistor power splitters are typically not as well balanced and Γ_g can be 0.1 or larger. The classic article describing coaxial splitter theory and practice is, "Understanding Microwave Power Splitters."[3] For waveguide sensors, similar signal splitters are built up, usually with waveguide directional couplers.

In the calibration process, both the DUT and STD sensors are first measured for their complex input reflection coefficients with a network analyzer. The reference sensor is usually a sensor similar to the type of sensor under calibration, although any sensor/meter will suffice if it covers the desired frequency range.

The equivalent source mismatch of the coaxial splitter (port 2) is determined by measuring the splitter's scattering parameters with a network analyzer and using that data in equation 3-4. That impedance data now represents the Γ_g. Measurement of scattering parameters is described in Chapter VII.

$$\Gamma_g = S_{22} - \frac{S_{21}\ S_{32}}{S_{31}} \qquad (3\text{-}4)$$

There is also a direct-calibration method for determining Γ_g, that is used at NIST.[4] Although this method requires some external software to set it up, it is easy to use once it is up and running.

Next, the power meter data for the standard sensor and reference sensor are measured across the frequency range, followed by the DUT and reference sensor. It should be noted that there might be two different power meters used for the "test" meter, since a 432 meter would be used if the STD sensor was a thermistor, while an EPM meter would be used to read the power data for a thermocouple DUT sensor. Then these test power meter data are combined with the appropriate reflection coefficients according to the equation:

$$K_b = K_s \frac{PT_{dut}}{PT_{std}} \frac{PR_{std}}{PR_{dut}} \frac{|1 - \Gamma_g \Gamma_d|^2}{|1 - \Gamma_g \Gamma_s|^2} \qquad (3\text{-}5)$$

Where:

K_b = cal factor of DUT sensor
K_s = cal factor of STD sensor
PT_{dut} = reading of test power meter with DUT sensor
PT_{std} = reading of test power meter with STD sensor
PR_{std} = reading of reference power meter when STD measured
PR_{dut} = reading of reference power meter when DUT measured
Γ_g = equivalent generator reflection coefficient $\rho_g = |\Gamma_g|$
Γ_d = reflection coefficient of DUT sensor $\rho_d = |\Gamma_d|$
Γ_s = reflection coefficient of STD sensor $\rho_s = |\Gamma_s|$

A 75 Ω splitter might be substituted for the more common 50 Ω splitter if the DUT sensor is a 75 Ω unit.

Finally, it should also be remembered that the effective efficiency and calibration factor of thermocouple and diode sensors do not have any absolute power reference, compared to a thermistor sensor. Instead, they depend on their 50 MHz reference source to set the calibration level. This is reflected by the equation 3-5, which is simply a ratio.

Network analyzer source method

For production situations, it is possible to modify an automatic RF/microwave network analyzer to serve as the test signal source, in addition to its primary duty measuring impedance. The modification is not a trivial process, however, due to the fact that the signal paths inside the analyzer test set sometimes do not provide adequate power output to the test sensor because of directional coupler roll off.

NIST 6-Port calibration system

For its calibration services of coaxial, waveguide, and power detectors, the NIST uses a number of different methods to calibrate power detectors. The primary standards are calibrated in either coaxial or waveguide calorimeters.[5,6] However, these measurements are slow and require specially built detectors that have the proper thermal characteristics for calorimetric measurements. For that reason the NIST calorimeters have historically been used to calibrate standards only for internal NIST use.

The calibration of detectors for NIST's customers is usually done on either the dual six-port network analyzer or with a 2-resistor power splitter setup such as the one described above.[7] While different in appearance, both of these methods basically use the same principles and therefore provide similar results and similar accuracies. The advantage of the dual six-ports is that they can measure Γ_g, Γ_s, and Γ_d, and the power ratios in equation 3-5 at the same time. The 2-resistor power splitter setup requires two independent measurement steps since Γ_g, Γ_s, and Γ_d are measured on a vector network analyzer prior to the measurement of the power ratios. The disadvantage of the dual six-ports is that the NIST systems typically use four different systems to cover the 10 MHz to 50 GHz frequency band. The advantage of the 2-resistor power splitter is its wide bandwidth and dc-50 GHz power splitters are currently commercially available.

1. Pramann, R.F. "A Microwave Power Meter with a Hundredfold Reduction in Thermal Drift," Hewlett-Packard Journal, Vol. 12, No. 10 (June, 1961).
2. Weidman, M.P., "Direct comparison transfer of microwave power sensor calibration," NIST Technical Note 1379, U.S. Dept. Of Commerce, January 1996.
3. Russell A. Johnson, "Understanding Microwave Power Splitters," *Microwave Journal*, Dec 1975.
4. R.F. Juroshek, John R., "A direct calibration method for measuring equivalent source mismatch,",*Microwave Journal*, October 1997, pp 106-118.
5. Clague, F. R. , and P. G. Voris, "Coaxial reference standard for microwave power," NIST Technical Note 1357, U. S. Department of Commerce, April 1993.
6. Allen, J.W., F.R. Clague, N.T. Larsen, and W. P Weidman, "NIST microwave power standards in waveguide," NIST Technical Note 1511, U. S. Department of Commerce, February 1999.
7. Engen, G.F., "Application of an arbitrary 6-port junction to power-measurement problems," IEEE Transactions on Instrumentation and Measurement, Vol IM-21, November 1972, pp 470-474.

General references

Fantom, A, "Radio Frequency & Microwave Power Measurements," Peter Peregrinus Ltd, 1990
"IEEE Standard Application Guide for Bolometric Power Meters," IEEE Std. 470-1972.
"IEEE Standard for Electrothermic Power Meters," IEEE Std. 544-1976.20

IV. Thermocouple Sensors and Instrumentation

Thermocouple sensors have been the detection technology of choice for sensing RF and microwave power since their introduction in 1974. The two main reasons for this evolution are: 1) they exhibit higher sensitivity than previous thermistor technology, and 2) they feature an inherent square-law detection characteristic (input RF power is proportional to DC voltage out).

Since thermocouples are heat-based sensors, they are true "averaging detectors." This recommends them for all types of signal formats from continuous wave (CW) to complex digital phase modulations. In addition, they are more rugged than thermistors, make useable power measurements down to 0.3 µW (–30 dBm, full scale), and have lower measurement uncertainty because of better voltage standing wave radio (SWR).

The evolution to thermocouple technology is the result of combining thin-film and semiconductor technologies to give a thoroughly understood, accurate, rugged, and reproducible power sensor. This chapter briefly describes the principles of thermocouples, the construction and design of modern thermocouple sensors, and the instrumentation used to measure their rather tiny sensor DC-output levels.

Principles of thermocouples

Thermocouples are based on the fact that dissimilar metals generate a voltage due to temperature differences at a hot and a cold junction of the two metals. As a simple example of the physics involved, imagine a long metal rod that is heated at the left end as in figure 4-1. Because of the increased thermal agitation at the left end, many additional electrons become free from their parent atoms. The increased density of free electrons at the left causes diffusion toward the right. There is also a force attempting to diffuse the positive ions to the right but the ions are locked into the metallic structure and cannot migrate. So far, this explanation has not depended on Coulomb forces. The migration of electrons toward the right is by diffusion, the same physical phenomenon that tends to equalize the partial pressure of a gas throughout a space.

Each electron that migrates to the right leaves behind a positive ion. That ion tends to attract the electron back to the left with a force given by Coulomb's law. The rod reaches equilibrium when the rightward force of heat-induced diffusion is exactly balanced by the leftward force of Coulomb's law. The leftward force can be represented by an electric field pointing toward the right. The electric field, summed up along the length of the rod, gives rise to a voltage source called the Thomson electromotive force (emf). This explanation is greatly simplified but indicates the principle.

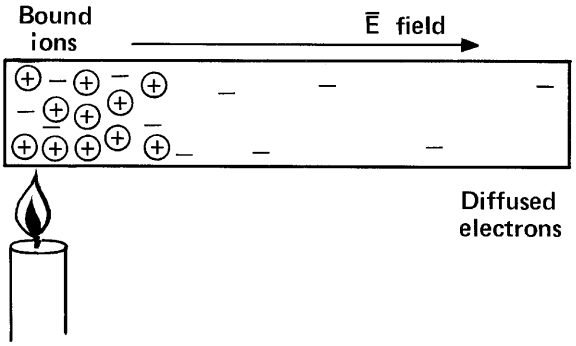

Figure 4-1. Heat at one end of a metal rod gives rise to an electric field.

The same principles apply at a junction of dissimilar metals where different free electron densities in the two different metals give rise to diffusion and an emf. The name of this phenomenon is the Peltier effect.

A thermocouple is usually a loop or circuit of two different materials as shown in figure 4-2. One junction of the metals is exposed to heat, the other is not. If the loop remains closed, current will flow in the loop as long as the two junctions remain at different temperatures. If the loop is broken to insert a sensitive volt-meter, it will measure the net emf. The thermocouple loop uses both the Thomson emf and the Peltier emf to produce the net thermoelectric voltage. The total effect is also known as the Seebeck emf.

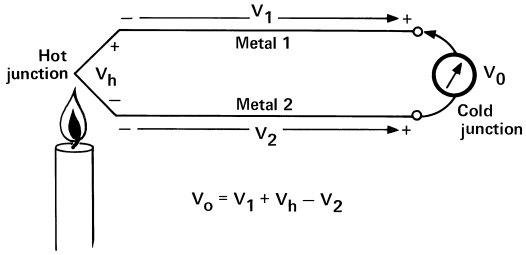

Figure 4-2. Total thermocouple output is the resultant of several thermoelectrical voltages generated along the two-metal circuit.

Sometimes many pairs of junctions or thermocouples are connected in series and fabricated in such a way that the first junction of each pair is exposed to heat and the second is not. In this way the net emf produced by one thermocouple adds to that of the next, and the next, etc., yielding a larger thermoelectric output. Such a series connection of thermocouples is called a thermopile. Early thermocouples for sensing RF power were frequently constructed of the metals bismuth and antimony. To heat one junction in the presence of RF energy, the energy was dissipated in a resistor constructed of the metals making up the junction. The metallic resistor needed to be small in length and cross section to form a resistance high enough to be a suitable termination for a transmission line. Yet, the junction needed to produce a measurable change in temperature for the minimum power to be detected and measured. Thin-film techniques were normally used to build metallic thermocouples. These small metallic thermocouples tended to have parasitic reactances and low burnout levels. Further, larger thermopiles, which did have better sensitivity, tended to be plagued by reactive effects at microwave frequencies because the device dimensions became too large for good impedance match at higher microwave frequencies.

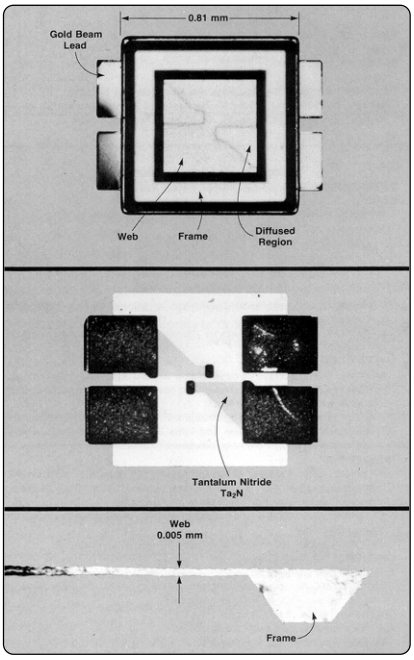

Figure 4-3. Photo-micrograph of the structure of the 8481A thermocouple chip on a thin silicon web.

The thermocouple sensor

The modern thermocouple sensor was introduced in 1974[1] and is exemplified by the 8481A power sensor. It was designed to take advantage of both semiconductor and microwave thin-film technologies. The device, shown in figure 4-3, consists of two thermocouples on a single integrated-circuit chip. The main mass of material is silicon.

The principal structural element is the frame made of p-type silicon, which supports a thin web of n-type silicon. The smoothly sloped sides of the frame result from an anisotropic etch acting on the silicon crystal planes. The thin web is produced by epitaxially growing it on the p-type substrate and then suitably controlling the etch, which also reveals the surface of the diffused regions in the web.

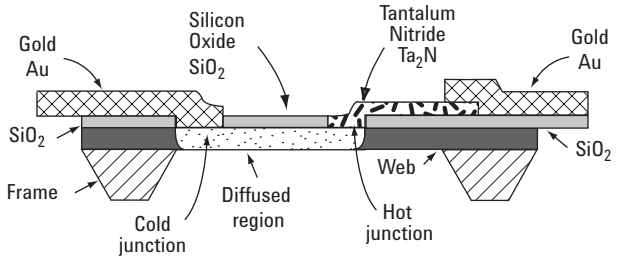

Figure 4-4. Cross section of one thermocouple. Power dissipated in the tantalum-nitride resistor heats the hot junction.

Figure 4-4 is a cross section through one of the thermocouples. One gold beam lead terminal penetrates the insulating silicon oxide surface layer to contact the web over the edge of the frame. This portion of the web has been more heavily doped by diffusing impurities into it. The connection between the gold lead and the diffused region is the cold junction of the thermocouple and the diffused silicon region is one leg of the thermocouple.

At the end of the diffused region near the center of the web, a second metal penetration to the web is made by a tantalum nitride film. This contact is the hot junction of the thermocouple. The tantalum nitride, which is deposited on the silicon oxide surface, continues to the edge of the frame where it contacts the opposite beam lead terminal. This tantalum nitride forms the other leg of the thermocouple.

The other edge of the resistor and the far edge of the silicon chip have gold beam-lead contacts. The beam leads not only make electrical contact to the external circuits, but also provide mounting surfaces for attaching the chip to a substrate, and serve as good thermal paths for conducting heat away from the chip. This tantalum-nitride resistor is not at all fragile in contrast to similar terminations constructed of highly conductive metals like bismuth/antimony.

As the resistor converts the RF energy into heat, the center of the chip, which is very thin, gets hotter than the outside edge for two reasons. First, the shape of the resistor causes the current density and the heat generated to be largest at the chip center. Second, the outside edges of the chip are thick and well cooled by conduction through the beam leads. Thus, there is a thermal gradient across the chip which gives rise to the thermoelectric emf. The hot junction is the resistor-silicon connection at the center of the chip. The cold junction is formed by the outside edges of the silicon chip between the gold and diffused silicon region.

The thin web is very important, because the thermocouple output is proportional to the temperature difference between the hot and cold junctions. In this case the web is fabricated to be 0.005 mm thick. Silicon is quite a good thermal conductor, so the web must be very thin if reasonable temperature differences are to be obtained from low power inputs.

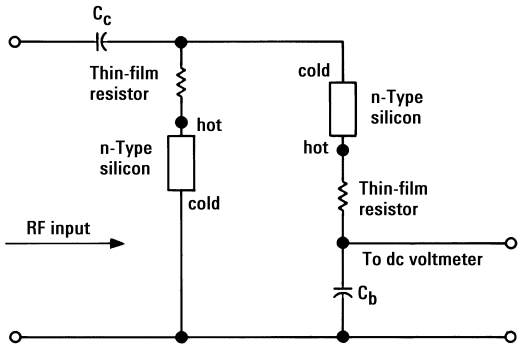

Figure 4-5. Schematic diagram of the 8481A thermocouple power sensor.

The 8481A power sensor contains two identical thermocouples on one chip, electrically connected as in figure 4-5. The thermocouples are connected in series as far as the DC voltmeter is concerned. For the RF input frequencies, the two thermocouples are in parallel, being driven through coupling capacitor C_c. Half the RF current flows through each thermocouple. Each thin-film resistor and the silicon in series with it has a total resistance of 100 Ω. The two thermocouples in parallel form a 50 Ω termination to the RF transmission line.

The lower node of the left thermocouple is directly connected to ground and the lower node of the right thermocouple is at RF ground through bypass capacitor C_b. The DC voltages generated by the separate thermocouples add in series to form a higher DC output voltage. The principal advantage, however, of the two-thermocouple scheme is that both leads to the voltmeter are at RF ground; there is no need for an RF choke in the upper lead. If a choke were needed it would limit the frequency range of the sensor.

The thermocouple chip is attached to a transmission line deposited on a sapphire substrate as shown in figure 4-6. A coplanar transmission line structure allows the typical 50 Ω line dimensions to taper down to the chip size, while still maintaining the same characteristic impedance in every cross-sectional plane. This structure contributes to the very low reflection coefficient of the 8480-series sensors, its biggest contribution, over the entire 100 kHz to 50 GHz frequency range.

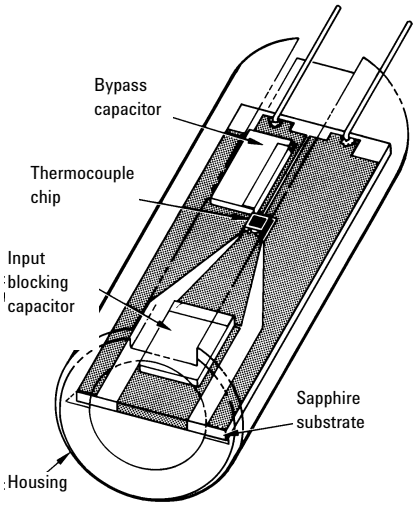

Figure 4-6. Sketch of the thermocouple assembly for the 8481A.

The principal characteristic of a thermocouple sensor for high frequency power measurement is its sensitivity in microvolts output per milliwatt of RF power input. The sensitivity is equal to the product of two other parameters of the thermocouple, the thermoelectric power and the thermal resistance.

The thermoelectric power (not really a power but physics texts use that term) is the thermocouple output in microvolts per degree Celsius of temperature difference between the hot and cold junction. In the 8481A thermocouple sensor, the thermoelectric power is designed to be 250μV/° C. This is managed by controlling the density of n-type impurities in the silicon chip.

The thickness of the 8481A silicon chip was selected so the thermocouple has a thermal resistance 0.4° C/mW. Thus, the overall sensitivity of each thermocouple is 100 μV/mW. Two thermocouples in series, however, yield a sensitivity of only 160 μV/mW because of thermal coupling between the thermocouples; the cold junction of one thermocouple is heated somewhat by the resistor of the other thermocouple giving a somewhat smaller temperature gradient.

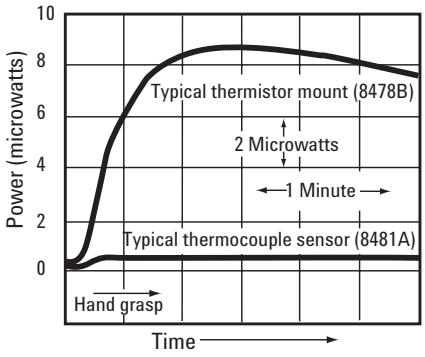

Figure 4-7. Zero drift of thermocouple and thermistor power sensors due to being grasped by a hand.

The thermoelectric voltage is almost constant with external temperature. It depends mainly on the temperature gradients and only slightly on the ambient temperature. Still, ambient temperature variations must be prevented from establishing gradients. The chip itself is only 0.8 mm long and is thermally short-circuited by the relatively massive sapphire substrate. The entire assembly is enclosed in a copper housing. Figure 4-7 depicts the superior thermal behavior of a thermocouple compared to a thermistor power sensor.

The thermoelectric output varies somewhat with temperature. At high powers, where the average thermocouple temperature is raised, the output voltage is larger than predicted by extrapolating data from low power levels. At a power level of 30 mW the output increases three percent, at 100 mW, it is about ten percent higher. The circuitry in the power meters used with thermocouples compensates for this effect. Circuitry in the sensor itself compensates for changes in its ambient temperature.

The thermal path resistance limits the maximum power that can be dissipated. If the hot junction rises to 500° C, differential thermal expansion causes the chip to fracture. Thus, the 8481A is limited to 300 mW maximum average power.

The thermal resistance combines with the thermal capacity to form the thermal time constant of 120 µs. This means that the thermocouple voltage falls to within 37 percent of its final value 120 µs after the RF power is removed. Response time for measurements, however, is usually much longer because it is limited by noise and filtering considerations in the voltmeter circuitry.

The only significant aging mechanism is thermal aging of the tantalum nitride resistors. A group of devices were stress tested, producing the results of figure 4-8. These curves predict that if a device is stressed at 300 mW for one year, the resistance should increase by about 3.5 percent. Nine days at a half watt would cause an increase in resistance of two percent. On the other hand, aging effects of the tantalum-nitride termination are compensated by use of the power calibration procedure, whereby a precision 1 mW, 50 MHz source is used to set a known level on the meter.

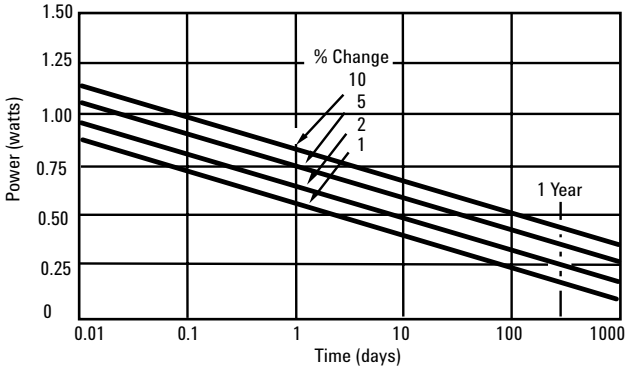

Figure 4-8. Results of a step stress aging test show percent change in thermocouple resistance when left at various power levels continuously for various periods of time.

It is relatively easy to adapt this sensor design for other requirements. For example, changing each tantalum-nitride resistor to a value of 150 Ω yields a 75 Ω system. To enhance low frequency RF performance, larger blocking and bypass capacitors extend input frequencies down to 100 kHz. This usually compromises high frequency performance due to increased loss and parasitic reactance of the capacitors. The 8482A power sensor is designed for 100 kHz to 4.2 GHz operation,while the standard 8481A operates from 10 MHz to 18 GHz.

Power meters for thermocouple sensors

Introduction of thermocouple sensor technology required design of a new power meter architecture that could take advantage of increased power sensitivity, yet be able to deal with the very low output voltages of the sensors. This led to a family of power meter instrumentation starting with the 435A analog power meter, to the 436A digital power meter.[2, 3, 4, 5] Some years later the dual-channel 438A was introduced, which provided for computation of power ratios of channels A and B as well as power differences of channels A and B. The most recent 437B power meter offered digital data manipulations with the ability to store and recall sensor calibration factor data for up to ten different power sensors. All of those models have been replaced.

To understand the principles of the instrument architecture, a very brief description will be given for the first-introduced thermocouple meter, the 435A analog power meter. This will be followed by an introduction of the newest power meters, E4418B (single channel) and E4419B (dual channel) power meters. They will be completely described in Chapter V, after a new wide-dynamic-range diode sensor is introduced. Two peak and average power meters are introduced in Chapter VI, the E4416/17A meters.

Thermocouple sensor DC output is very low-level (approximately 160 nV for 1 microwatt applied power), so it is difficult to transmit in an ordinary flexible connection cable. This problem is multiplied if the user wants a long cable (25 feet and more) between the sensor and power meter. For this reason it was decided to include some low-level AC amplification circuitry inside the power sensor, so only relatively high-level signals appear on the cable.

One practical way to handle such tiny DC voltages is to “chop” them to form a square wave, then amplify them with an AC-coupled system. After appropriate amplification (some gain in the sensor, some in the meter), the signal is synchronously detected at the high-level AC. This produces a high-level DC signal that is then further processed to provide the measurement result. Figure 4-9 shows a simplified block diagram of the sensor/meter architecture.

Cabling considerations led to the decision to include the chopper and part of the first AC amplifier inside the power sensor. The chopper itself (figure 4-10) uses field-effect transistor switches that are in intimate thermal contact. It is essential to keep the two FET’s at exactly the same temperature to minimize drift. To eliminate undesired thermocouple effects (in circuitry external to the RF sensor thermocouples), only one metal, gold, is used throughout the entire DC path. All these contributions were necessary to help achieve the low drift already shown in figure 4-7.

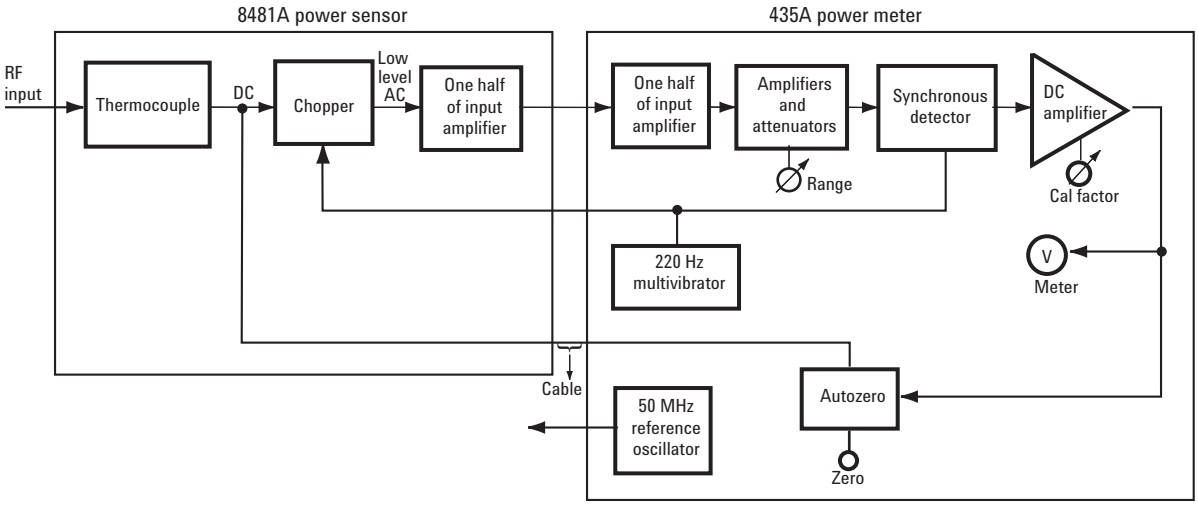

Figure 4-9. 435A/8481A architecture block diagram.

The chopping frequency of 220 Hz was chosen as a result of several factors. Factors that dictate a high chopping frequency include lower 1/f noise and a larger possible bandwidth, and thereby faster step response. Limiting the chopping to a low frequency is the fact that small transition spikes from chopping inevitably get included with the main signal. These spikes are at just the proper rate to be integrated by the synchronous detector and masquerade as valid signals. The fewer spikes per second, the smaller this masquerading signal. However, since the spikes are also present during the zero-setting operation, and remain the same value during the measurement of a signal, the spikes are essentially removed from the meter indication by zerosetting and cause no error. The spikes do, however, use up dynamic range of the amplifiers.

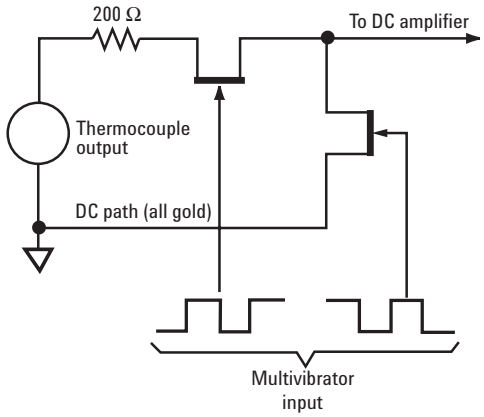

Figure 4-10. Simplified schematic of chopper amplifier.

One way to minimize noise while amplifying small signals is to limit the channel bandwidth. Since the noise generating mechanisms are broadband, limiting the amplifier bandwidth reduces the total noise power. The narrowest bandwidth is chosen for the weakest signals and the most sensitive range. As the power meter is switched to higher ranges, the bandwidth increases so that measurements can be made more rapidly. On the most sensitive range, the time constant is roughly two seconds, while on the higher ranges, the time constant is 0.1 seconds. A 2-second time constant corresponds to a 0 to 99 percent rise time of about ten seconds.

Reference oscillator

A frequent criticism of thermocouple power measurements is that such measurements are open-loop, and thus thermistor power measurements are inherently more accurate because of their DC-substitution, closed-loop process. The bridge feedback of substituted DC power compensates for differences between thermistor mounts and for drift in the thermistor resistance-power characteristic without recalibration.

With thermocouples, where there is no direct power substitution, sensitivity differences between sensors or drift in the sensitivity due to aging or temperature can result in a different DC output voltage for the same RF power. Because there is no feedback to correct for different sensitivities, measurements with thermocouple sensors are said to be open-loop.

Agilent thermocouple power meters solve this limitation by incorporating a 50 MHz power-reference oscillator whose output power is controlled with great precision (±0.7 %). To verify the accuracy of the system, or adjust for a sensor of different sensitivity, the user connects the thermocouple sensor to the power reference output and, using a calibration adjustment, sets the meter to read 1.00 mW. By applying the 1 mW reference oscillator to the sensor's input port just like the RF to be measured, the same capacitors, conductors and amplifier chain are used in the same way for measurement as for the reference calibration. This feature provides confidence in a traceability back to company and NIST standards.

EPM series power meters

Figure 4-11. E4418B features many user-conveniences and a 90 dB dynamic measurement range. The 50 MHz, 1 mW reference output connector is at the top-right.

The two-decade industry acceptance of thermocouple (and diode) sensor technology for RF power measurements has resulted in tens of thousands of units in the installed base around the world. Yet new technologies now allow for design of diode sensors with far larger dynamic range and new power meters with dramatically-expanded user features.

The E4418B (single channel) and E4419B (dual channel) power meters offer some significant user features:

- Menu-driven user interface, with softkeys for flexibility
- Large LCD display for ease of reading
- Sensor EEPROM which stores sensor calibration factors and other correction data (E series wide-dynamic-range CW sensors)
- Dedicated hardkeys for frequently-used functions
- Faster measurement speed, faster throughput
- Backward compatibility with all previous 8480-series sensors
- Form, fit, function replacement with 437B and 438A power meters (preserves automation software code)
- Built for wide-dynamic-range CW sensors from –70 to +20 dBm. See Chapter V.

Since the meters provide more powerful measurement capability when teamed with the E-series wide-dynamic range diode sensors, the detailed description of the meters will be presented in Chapter V. This will first allow for a presentation of the technology for the new diode sensors with the range from –70 to +20 dBm, and then the meters that take advantage of this increased capability.

Conclusion

Because of their inherent ability to sense power with true square-law characteristics, thermocouple sensors will always be best for handling signals with complex modulations or multiple tones. They always respond to the true average power of a signal, modulation, and multiple signals. They are rugged, stable, and reliable.

The large installed worldwide base of Agilent thermocouple and diode sensors and their compatible power meters argues that any new power meters be designed to be backward compatible with older sensors. All old 8480-series sensors will work with new EPM series meters, with the only limitation being the performance of the old sensors. The new E-series sensors are not backwards-compatible with Agilent's older meters due to a modified interface design, which allows for down-load of EEPROM-stored constants.

Thermocouple sensors are based on a stable technology that will be used to measure RF power in many applications for a long time in the future.

---

1. W.H. Jackson, "A Thin-Film Semiconductor Thermocouple for Microwave Power Measurements," Hewlett-Packard Journal, Vol. 26, No. 1 (Sept., 1974).
2. A.P. Edwards, "Digital Power Meter Offers Improved Accuracy, Hands-Off Operation, Systems Capability," Hewlett-Packard Journal, Vol. 27 No. 2 (Oct. 1975).
3. J.C. Lamy, "Microelectronics Enhance Thermocouple Power Measurements," Hewlett-Packard Journal, Vol. 26, No. 1 (Sept., 1974).
4. "Power Meter-New Designs Add Accuracy and Convenience." *Microwaves*, Vol. 13, No. 11 (Nov., 1974).
5. R.E. Pratt, "Very-Low-Level Microwave Power Measurements," Hewlett-Packard Journal, Vol. 27, No. 2 (Oct., 1975).

V. Diode Sensors and Instrumentation

Rectifying diodes have long been used as detectors and for relative power measurements at microwave frequencies. The earliest diodes were used mostly for envelope detection and as nonlinear mixer components in super-heterodyne receivers. For absolute power measurement, however, diode technology had been limited mainly to RF and low microwave frequencies.

High-frequency diodes began with point-contact technology which evolved from the galena crystal and cat-whisker types of early radio and found application as early as 1904.[1] Point-contact diodes were extremely fragile, not very repeatable, and subject to change with time. It was the low-barrier Schottky (LBS) diode technology which made it possible to construct diodes with metal-semiconductor junctions for microwave frequencies that were very rugged and consistent from diode to diode. These diodes, introduced as power sensors in 1974, were able to detect and measure power as low as –70 dBm (100 pW) at frequencies up to 18 GHz.[2]

This chapter will review the semiconductor principles as they apply to microwave detection, briefly review LBS technology and then describe the latest planar-doped-barrier (PDB) diode technology. It will describe how such devices are designed into power sensor configurations and introduce a new CW-diode sensor with an impressive 90 dB dynamic power range using digital-detection-curve correction techniques. Then, a novel two-path diode sensor with wide dynamic range is discussed. Signal and waveform effects for non-CW signals operating above the square-law range will also be examined.

The EPM-series power meters will be described, which exploit the advantages of the new 90-dB-range sensors and offer major user-conveniences as well.

Diode detector principles

Diodes convert AC signals to DC by way of their rectification proper-ties, which arise from their nonlinear current-voltage (i-v) characteristic. It might seem that an ordinary silicon p-n junction diode would, when suitably packaged, be a sensitive RF detector. However, stored charge effects limit the bandwidth of the p-n junction. The Schottky barrier diode does not store charge in its junction but most of them have extremely high impedance at low signal levels. A RF signal in the rage of –20 dBm is required to overcome the 0.3-volt junction voltage of a conventional Schottky diode. One alternative is to bias the diode to 0.3 volts and is a usable approach if the detected output can be AC coupled with eliminates the drift introduced by the bias. With AC coupling, the minimum power that can be metered by a biased diode may be improved by about 10 dB due to the drift and noise introduced by bias current. A typical application for this technique would be the diode detectors used for scalar network analyzers.

Metal-semiconductor junctions, exemplified by point-contact technology, exhibit a low potential barrier across their junction, with a forward voltage of about 0.3 volts. They have superior RF and microwave performance, and were popular in earlier decades. LBS diodes, which are metal-semiconductor junctions, succeeded point-contacts and vastly improved the repeatability and reliability. Figure 5-1 shows a typical diode i-v characteristic of an LBS junction, expanded around the zero-axis to show the square-law (see below) region.

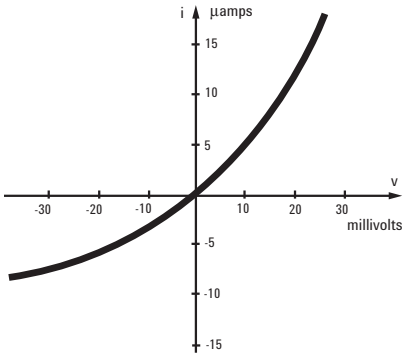

Figure 5-1. The junction rectifying characteristic of a low-barrier Schottky diode, showing the small-signal, square-law characteristic around the origin.

Mathematically, a detecting diode obeys the diode equation

$$i = I_S (e^{av} - 1) \qquad (5\text{-}1)$$

where a = q/nKT, and i is the diode current, v is the net voltage across the diode, I_S is the saturation current and is constant at a given temperature. K is Boltzmann's constant, T is absolute temperature, q is the charge of an electron and n is a correction constant to fit experimental data (n equals approximately 1.1 for the devices used here for sensing power). The value of a is typically a little under 40 $(volts)^{-1}$, in this case approximately 36 $volts^{-1}$.

Equation (5-1) is often written as a power series to better analyze the rectifying action,

$$i = I_s \left(av + \frac{(av)^2}{2!} + \frac{(av)^3}{3!} + \cdots\right) \qquad (5\text{-}2)$$

It is the second and other even-order terms of this series which provide the rectification. For small signals, only the second-order term is significant so the diode is said to be operating in the square-law region. In that region, output i (and output v) is proportional to RF input voltage squared. When v is so high that the fourth and higher order terms become significant the diode response is no longer in the square law region. It then rectifies according to a quasi-square-law i-v region which is sometimes called the transition region. Above that range it moves into the linear detection region (output v proportional to input v).

For a typical packaged diode, the square-law detection region exists from the noise level up to approximately –20 dBm. The transition region ranges from approximately –20 to 0 dBm input power, while the linear detection region extends above approximately 0 dBm. Zero dBm RF input voltage is equivalent to approximately 220 mV (rms) in a 50 Ω system. For wide-dynamic-range power sensors, it is crucial to have a well-characterized expression of the transition and linear detection range.

Figure 5-2 shows a typical detection curve, starting near the noise level of –70 dBm and extending up to +20 dBm. It is divided up into the square law, transition and linear regions. (Noise is assumed to be zero to show the square-law curve extends theoretically to infinitely small power.) Detection diodes can now be fabricated which exhibit transfer characteristics that are highly stable with time and temperature. Building on those stable features, data correction and compensation techniques can take advantage of the entire 90 dB of power detection range.

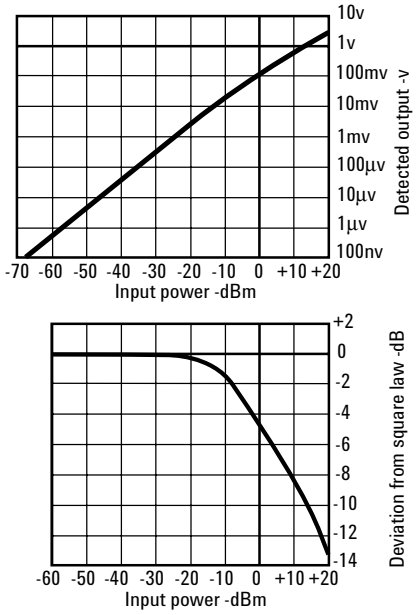

Figure 5-2. The diode detection characteristic ranges from square law through a transition region to linear detection.

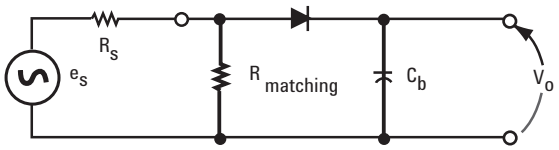

Figure 5-3. Circuit diagram of a source and a diode detector with matching resistor.

The simplified circuit of figure 5-3 represents an unbiased diode device for detecting low level RF signals. Detection occurs because the diode has a nonlinear i-v characteristic; the RF voltage across the diode is rectified and a DC output voltage results.

If the diode resistance for RF signals were matched to the generator source resistance, maximum RF power would be delivered to the diode. However, as long as the RF voltage is impressed across the diode, it will detect RF voltage efficiently. For reasons explained below, diode resistance for small RF signals is typically much larger than 50 Ω and a separate matching resistor is used to set the power sensor's input termination impedance. Maximum power is transferred to the diode when the diode resistance for small RF voltages is matched to the source resistance. The diode resistance at the origin, found by differentiating (5-1), is:

$$R_o = \frac{1}{\alpha I_s} \qquad (5\text{-}3)$$

Resistance R_o is a strong function of temperature which means the diode sensitivity and the reflection coefficient are also strong functions of temperature. To achieve less temperature dependence, R_o is much larger than the source resistance and a 50 Ω matching resistor serves as the primary termination of the generator. If R_o of the diode of figure 5-3 were made too large, however, there would be poor power conversion from RF to DC; thus, a larger R_o decreases sensitivity. An origin resistance of 1–2 kΩ will be obtained with diodes having a reverse saturation current (I_s) of between 27.5 to 13.8 μA. A compromise between good sensitivity to small signals and good temperature performance results from making I_s about 10 microamps and R_o approximately 2.75 kΩ.

The desired value of saturation current, I_s, can be achieved by constructing the diode of suitable materials that have a low potential barrier across the junction. Schottky metal-semiconductor junctions can be designed for such a low-barrier potential.

The origin resistance R_o is a very useful concept in understanding how a detector diode will operate under a wide variety of conditions. It forms the real part of the source impedance of the detected output, so the effect of finite load resistance can be estimated. If the value of the RF bypass capacitor, C_b, is known, the overall risetime may be accurately estimated. If the variation in Is vs temperature (Silicon LBSD's double every 10° C rise) is considered, the temperature coefficient of the loaded detector can also be estimated.

Of course, R_o is also sensitive to the input power into the device, and can only be considered to be constant for junction voltages which are lower than the "thermal voltage" V_t=nKT/q, or about 28 mV peak. This limit correlates well with the power level where the output departs from square law response in a 50 Ω system.

Using diodes for sensing power

Precision semiconductor fabrication processes for silicon allowed the Schottky diodes to achieve excellent repeatability and, because the junction area was larger, they were more rugged. Agilent's first use of such a low-barrier Schottky diode (LBSD) for power sensing was introduced in 1975 as the 8484A power sensor.[2] It achieved an exceptional power range from –70 dBm (100 pW) to –20 dBm (10 μW) from 10 MHz to 18 GHz.

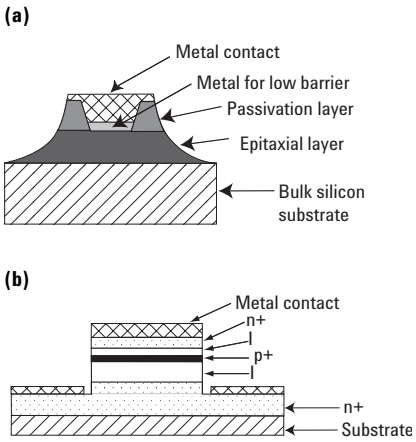

Figure 5-4. Idealized cross sections of two diode configurations. (a) low-barrier Schottky. (b) planar-doped-barrier.

As Gallium-Arsenide (GaAs) semiconductor material technology advanced in the 1980s, such devices exhibited superior performance over silicon in the microwave frequencies. A sophisticated diode fabrication process known as planar-doped-barrier (PDB) technology offered real advantages for power detection.[3] It relied on a materials preparation process called molecular beam epitaxy for growing very thin epitaxial layers. Figure 5-4 shows the device cross sections of the two types of diode junctions, low-barrier Schottky (figure 5-4a) and planar-doped barrier (figure 5-4b) diodes. The doping profile of the PDB device is n^+ –I–p^+–I–n^+, with intrinsic layers spaced between the n^+ and p^+ regions. The i/v characteristic has a high degree of symmetry which is related to the symmetry of the dopants.

The p^+ region is fabricated between the two intrinsic layers of unequal thickness. This asymmetry is necessary to give the PDB device the characteristics of a rectifying diode. An important feature of the PDB diode is that the device can be designed to give a junction capacitance, C_o, that is both extremely small (20 fF or less) (femto Farad) and nearly independent of the bias voltage. C_o is also independent of the size of the metal contact pad.

As a result of the very stable C_o versus bias voltage, the square-law characteristics of this device versus frequency are significantly more constant than those of metal-to-semiconductor devices. Low capacitance coupled with low junction resistance allows excellent microwave signal performance since the low junction resistance lowers the radio correction (RC) time constant of the junction and raises the diode cutoff frequency.

A PDB diode is far less frequency-sensitive than a normal p-n junction diode because of the intrinsic layer at the junction.[4] In a p-n junction diode the equivalent capacitance of the junction changes with power level, but in the planar-doped-barrier diode, junction capacitance is determined by the intrinsic layer, which remains almost constant as a function of power.

Agilent uses a specialized integrated circuit process that allows custom tailoring of the doping to control the height of the Schottky barrier. This controlled doping makes it practical to operate the detector diode in the current mode, while keeping the video resistance low enough to maintain high sensitivity.

The first power sensor application for PDB diodes was the 8481/85/87D-series power sensors, introduced in 1987.[4] The 8481D functionally replaced the low-barrier-Schottky 8484A sensor. The new PDB sensor employed two diodes, fabricated on the same chip using microwave monolithic integrated circuit (MMIC) chip technology. The two diodes were deposited symmetrically about the center of a coplanar transmission line and driven in a push-pull manner for improved signal detection and cancellation of common-mode noise and thermal effects. This configuration features several advantages:

- Thermoelectric voltages resulting from the joining of dissimilar metals, a serious problem below –60 dBm, are cancelled.
- Measurement errors caused by even-order harmonics in the input signal are suppressed due to the balanced configuration.
- A signal-to-noise improvement of 1 to 2 dB is realized by having two diodes. The detected output signal is doubled in voltage (quadrupled in power) while the noise output is doubled in power since the dominant noise sources are uncorrelated.
- PDB devices also have higher resistance to electrostatic discharge and are more rugged than Schottky's.
- Common-mode noise or interference riding on the ground plane is cancelled at the detector output. This is not RF noise but metallic connection noises on the meter side.

PDB diode technology provides some 3000 times (35 dB) more efficient RF-to-DC conversion compared to the thermocouple sensors of Chapter IV.

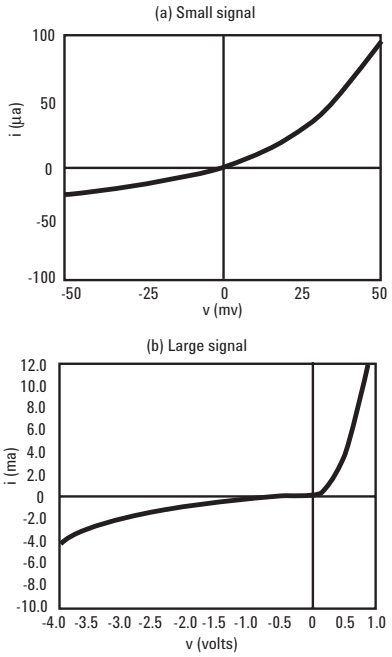

Figure 5-5. The i-v characteristics of a PDB diode are shown for two different drive voltage regions. The assymetry of the p^+ layer can be used to modify the shape of the i-v curve, while not affecting some of the other diode parameters such as C_0 and R_0.

Figure 5-5 shows two regions of the i-v characteristic of a typical PDB diode. Figure 5-5 (a) shows the small signal region, while figure 5-5 (b) shows the larger signal characteristics to include the linear region as well as the breakdown region on the left.

They also provide accurate square-law performance from –70 to –20 dBm. Diode sensor technology excels in sensitivity, although realistically, thermocouple sensors maintain their one primary advantage as pure square-law detectors for the higher power ranges of –30 to +20 dBm. Hence neither technology replaces the other and the user's measuring application determines the choice of sensors.

In detecting power levels of 100 picowatts (70 dBm) the diode detector output is about 50 nanovolts. This low signal level requires sophisticated amplifier and chopper circuit design to prevent leakage signals and thermocouple effects from dominating the desired signal. Earlier diode power sensors required additional size and weight to achieve controlled thermal isolation of the diode. The dual-diode configuration balances many of the temperature effects of those highly-sensitive circuits and achieves superior drift characteristics in a smaller, lower-cost structure.

Wide-dynamic-range, CW-only power sensors

Digital signal processing and microwave semiconductor technology have now advanced to the point where dramatically improved performance and capabilities are available for diode power sensing and metering. New diode power sensors are now capable of measuring over a dynamic power range of –70 to +20 dBm, an impressive range of 90 dB. This permits the new sensors to be used for CW applications which previously required two separate sensors.

The E4412A power sensor features a frequency range from 10 MHz to 18 GHz. E4413A power sensor operates to 26.5 GHz. Both provide the same –70 to +20 dBm power range. A simplified schematic of the new sensors is shown in figure 5-6. The front end construction is based on MMIC technology and combines the matching input pad, balanced PDB diodes, FET choppers, integrated RF filter capacitors, and the line-driving pre-amplifier. All of those components operate at such low signal levels that it was necessary to integrate them into a single thermal space on a surface-mount-technology PC board.

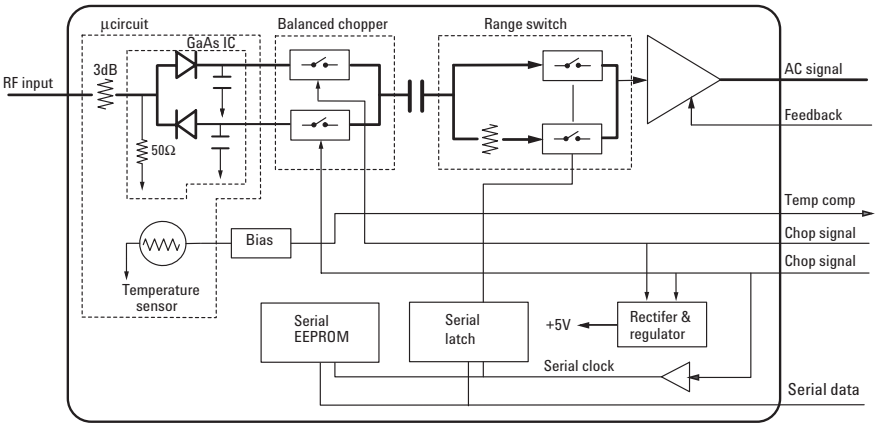

Figure 5-6. Simplified schematic for the E-series power sensors. The 90 dB power range is achieved using data stored in the individual sensor EEPROM which contains linearization, temperature compensation and calibration factor corrections.

To achieve the expanded dynamic range of 90 dB, the sensor/meter architecture depends on a data compensation algorithm that is calibrated and stored in an individual EEPROM in each sensor. The data algorithm stores information of three parameters, input power level vs frequency vs temperature for the range 10 MHz to 18 or 26.5 GHz and –70 to +20 dBm and 0 to 55° C.

At the time of sensor power-up, the power meter interrogates the attached sensor using an industry-standard serial bus format, and in turn the meter receives the upload of sensor calibration data. An internal temperature sensor supplies the diode's temperature data for the temperature-compensation algorithm in the power meter.

Since the calibration factor correction data will seldom be used manually, it is no longer listed on the sensor label of the E-series sensors. The data is always uploaded into the power meter on power-up or when a new sensor is connected. The new sensors store cal factor tables for two different input power levels to improve accuracy of the correction routines. If the cal factor changes upon repair or recalibration, the new values are re-loaded into the sensor EEPROM. For system users who need the cal factor for program writing, the data is furnished on a calibration certificate.

Wide-dynamic-range average power sensors

Today's average power measurement needs, as highlighted by complex digital modulation formats such as code division multiple access (CDMA), are for accurate measurements in the presence of high crest factors (peak-to-average ratio), and often require a dynamic range greater than 50 dB. As the E4412A and E4413A sensors are designed to measure the average power of CW signals, they cannot satisfy this requirement.

Agilent's approach to creating a wide-dynamic-range, average power sensor to meet this need is based on a dual sensor, diode pair/attenuator/diode pair topology as proposed by Szente et. al. in 1990.[5] This topology has the advantage of always maintaining the sensing diodes within their square law region and therefore will respond properly to complex modulation formats as long as the sensor's correct range is selected.

This approach was further refined by incorporating diode stacks in place of single diodes to extend square law operation to higher power levels at the expense of sensitivity. A series connection of m diodes results in a sensitivity degradation of 10 log(m) dB and an extension upwards in power limits of the square law region maximum power of 20 log(m) dB, yielding a net improvement in square law dynamic range of 10 log(m) dB compared to a single diode detector.

The new E-series E9300 power sensors are implemented as a modified barrier integrated diode (MBID)[6] with a two diode stack pair for the low power path (–60 to –10 dBm), a resistive divider attenuator and a five diode stack pair for the high power path (–10 to +20 dBm), as shown in figures 5-7a and 5-7b. Additionally, series FET switches are used off-chip to allow the low path diodes to self-bias off when not in use.

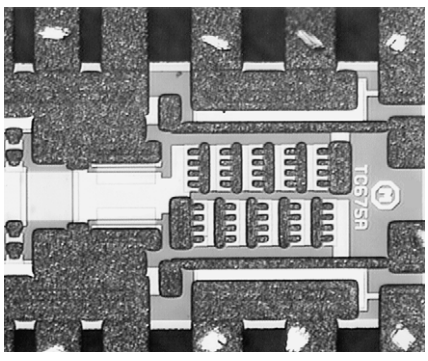

Figure 5-7a. Photograph of MBID.

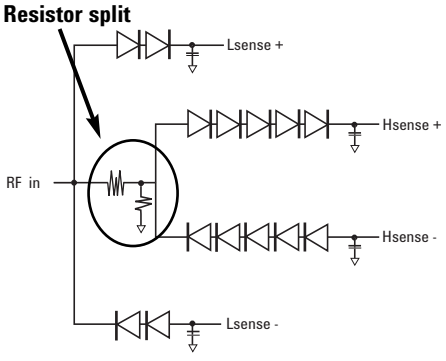

Figure 5-7b. Schematic of MBID.

Typical deviation from square law for the low power path (–60 to –10 dBm) and high power path (–10 to +20 dBm) for the new E-series E9300 power sensors is shown in figure 5-8.

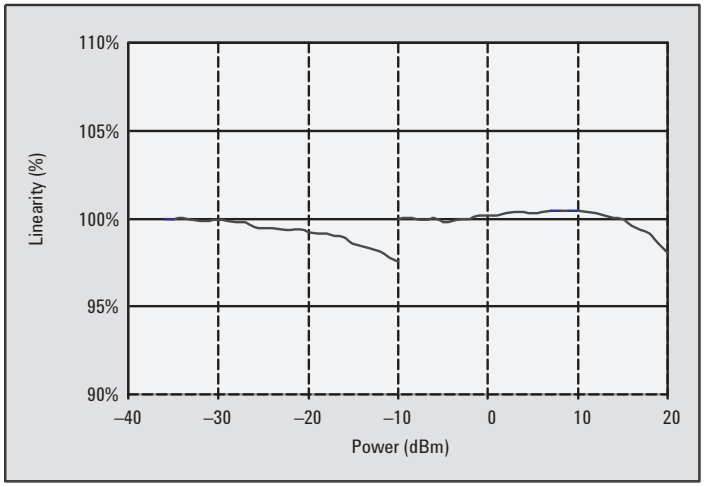

Figure 5-8. E9300 Power Sensor linearity. The linearity at the –10 dBm switching point is specified as being typically ≤ ± 0.5% (≤ ± 0.02 dB). The E9300 power sensors switch quickly and automatically between ranges, providing a transparent 80 dB dynamic range.

The decision for switching between the low and high power paths is made on the basis of the average power detected by the meter. For example, a –12 dBm average power signal with a high crest factor (peak-to-average ratio) would be measured by the low power path. For most CDMA signals, such as IS-95A, E9300 sensors will give better than ±0.05 dB accuracy up to –10 dBm average power using the low power path. However, for some 3G CDMA signals, with aligned symbols that have almost 20 dB maximum peak-to-average ratio, the accuracy of the measurement during the high power crests would be compromised. This is due to the sensor being in the low power path and the diodes being operated well outside the square law region of the low power path during the crests. A Range Hold function for the high power path deals with this situation as it allows both the peak and average powers to be measured in the square law region of the high power path.

To avoid unnecessary switching when the power level is near –10 dBm, switching point hysteresis has been added. This hysteresis causes the low power path to remain selected as the power level is increased up to approximately –9.5 dBm, above this power the high power path is selected. The high power path remains selected until approximately –10.5 dBm is reached as the signal level decreases. Below this level the low power path is selected.

To provide user-meaningful sensor information relevant to the numerous power measurement scenarios, from a temperature controlled manufacturing or R&D environment to field installation and maintenance applications, warranted specifications for E9300 sensors are provided over the temperature ranges 25 ±10 °C as well as 0 to 55 °C. Also, supplemental information is provided at 25 °C to illustrate the typical performance achievable, as shown in figure 5-9.

Power range	Linearity (25 ±10 °C)	Linearity (0 to 55 °C)
–60 to –10 dBm	± 3.0%	± 3.5%
–10 to 0 dBm	± 2.5%	± 3.0%
0 to +20 dBm	± 2.0%	± 2.5%

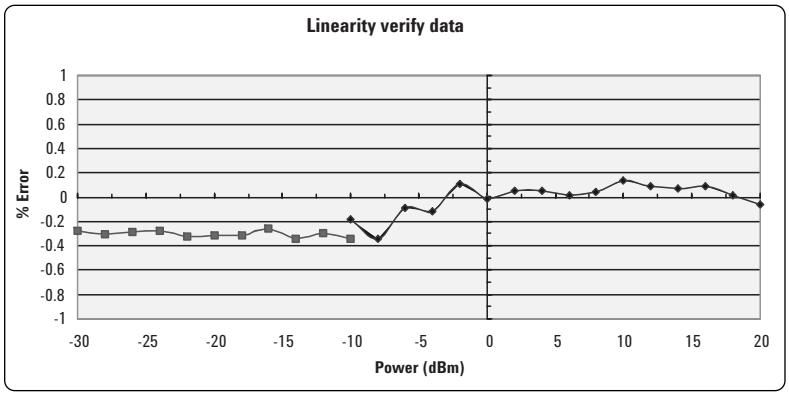

Power range	–30 to –20 dBm	–20 to –10 dBm	–10 to 0 dBm	0 to +10 dBm	+10 to +20 dBm
Measurement uncertainty	± 0.9%	± 0.8%	± 0.65%	± 0.55%	± 0.45%

Figure 5-9. Typical power linearity performance at 25° C, after a zero and calibration, (top chart) along with the measurement uncertainty for different power ranges is shown (lower plot). By providing this type of specification data, users can better understand how the power sensor will perform for their particular application and environment and so allow informed sensor selection.

A versatile power meter to exploit the E-series power sensors

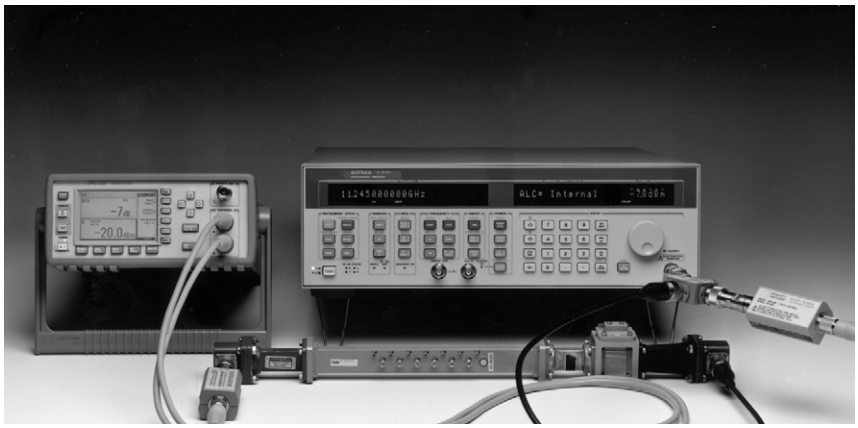

Figure 5-10. E4419B dual-channel power meter measures insertion loss of a 11.245 GHz waveguide bandpass filter, using the meter's power ratio mode, plus a sweeper and power splitter. Agilent's 90 dB dynamic-range sensors are ideal for such high-attenuation measurements.

Two power meters, E4418B (single channel) and E4419B (dual channel) take advantage of the sensor's 90 dB power measuring range. More importantly, advances in digital signal processing (DSP) technology now provide significant increases in measurement speeds. Digital processing permits functional conveniences resulting in a dramatically more versatile power meter.

The basic meter architecture is based on DSP technology which improves performance by removing meter range switching and their delays (except for a single range-switching transition point). It also provides faster signal detection. The DSP module performs several other functions, synchronous detection (de-chopping), matches up the two analog-to-digital converter (ADC) channels, and does the programmable filtering. It provides a 32-bit digital number that is proportional to the detected diode voltage over a 50 dB power range.

The power meter uses the uploaded calibration data from each connected sensor to compensate for the three critical sensor parameters, power from –70 to +20 dBm, frequency for its specified band, and operating temperature.

The calibration routine requiring connection to the 50 MHz power reference furnishes the power traceability path for the sensor connected. The operator then keys in the frequency of the RF signal under test so that the meter corrects for the sensor calibration factor. Mismatch uncertainty must still be externally calculated because the reflection coefficient of the unknown power source is usually not available.

Figure 5-11 shows a simplified schematic of the E4418B meter (see figure 5-6 for reference to the associated E-series sensors). The pre-amplified sensor output signal receives some early amplification, followed by some signal conditioning and filtering. The signal then splits, with one path receiving amplification. Both low and high-level chopped signals are applied to a dual ADC. A serial output from the ADC takes the sampled signals to the digital signal processor that is controlled by the main microprocessor. A differential drive signal, synchronized to the ADC sampling clock, is output to the sensor for its chopping function.

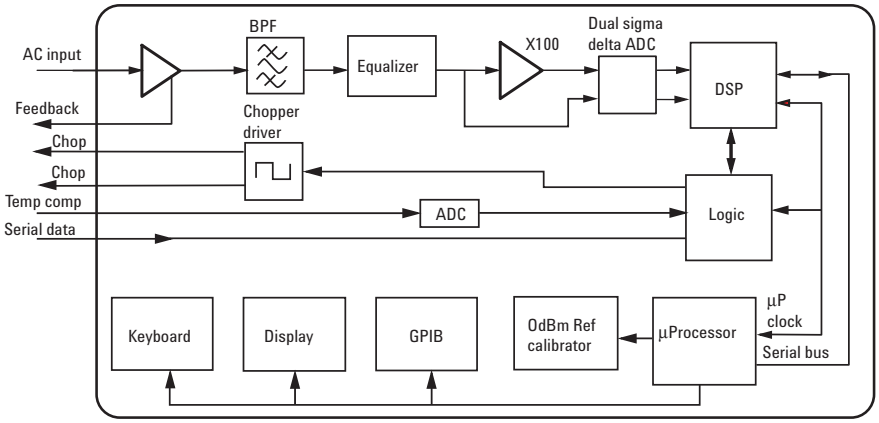

Figure 5-11. Simplified schematic of E4418B shows the transition to digital signal processing (DSP) architecture.

The dual-sigma-delta ADC provides a 20-bit data stream to the digital signal processor, which is under control of the main microprocessor. There is no range switching as in traditional power meters which maintain an analog signal path. Even the synchronous detection is performed by the ADC and DSP rather than use of a traditional synchronous detector.

Computation power permits the user to manipulate the basic measurement data to get desired units or format. Power reads out in watts or dBm, and inputs may be keyed in to compensate for attenuators or directional coupler losses to the unknown signal in front of the power sensor. Cabling losses can be compensated by entering the loss as a digital offset value.

For the E4419B two-channel power meter, either input power or both may be displayed, or for certain applications power ratios A/B or B/A might be useful. For example, if the two power sensors are sampling forward and reverse power in a transmission line using a dual directional coupler, these ratios would yield power reflection coefficient. The power difference, A–B or B–A, can be used for other applications. For example, using a dual directional coupler to sample forward and reverse power in a line, the power difference is a measure of net forward power being absorbed by a device under test. This is quite important in testing devices with very high reflections, such as mixer diodes, which are often deliberately mis-matched for better noise figure.

Power changes are displayed with the relative power function. And although the main display is all digital, a simple “peaking” display simulates an analog meter pointer and allows a user to adjust a unit under test for maximizing power output.

In system applications, the new single-channel power meter, when used with the wide-dynamic-range sensors can achieve 200 measurements per second. The programming code is also designed to be backward compatible with the previous 437B (the E4419B is code compatible with the 438A). Of course, the new meter offers far more versatile programming functions too, to handle modern complex test procedures. However, old software can be re-used to make programming projects more efficient.

When old sensors are utilized with the new meter, the calibration factor vs. frequency table printed on the label of the sensor must be keyed into the new power meters to take the fullest advantage of the measurement accuracy. A table of frequencies vs. cal factor is displayed and the routine prompted by the softkey display to ease editing.

Potential users of the new power meters will find that specification listings for this DSP-architecture meter without range switching will not follow traditional power meter range specifications, yet the meter meets the same range performance as the 43X-series meters.

Traceable power reference

All thermocouple and diode power sensors require a power reference to absolute power, traceable to the manufacturer or national standards. Power meters accomplish this power traceability by use of a highly stable, internal 50 MHz power reference oscillator. When used together, the 50 MHz reference and the sensor calibration factor data supplied with each sensor yields the lowest measurement uncertainty. All Agilent sensors are supplied with calibration factor versus frequency data. This includes both the value and uncertainty of each point.

The 1 mW reference power output is near the center of the dynamic range of thermocouple power sensors, but above the range of the sensitive diode sensor series. A special 30 dB calibration attenuator, designed for excellent precision at 50 MHz, is supplied with each HP 8481D-series diode power sensor. When that attenuator is attached to the power reference output on the power meter, the emerging power is 1 μW (–30 dBm). The attenuator design is such that a maximum error of one percent is added to the calibration step. Basic uncertainty of the reference output is factory adjusted to an accuracy of ±0.7 percent and is traceable to NIST. For one year, accuracy is ±1.2 percent worst case, ±0.9 percent rss.

Signal waveform effects on the measurement uncertainty of diode sensors

Along with the great increase in measurement flexibility of the E4412/3A and E9300-series power sensors, comes several new applications guidelines. These must be understood and followed to obtain valid measurement results when dealing with complex and non-CW signals. The EPM-P peak and average power meter and associated sensors are described in chapter VI.

These guidelines distinguish between earlier diode sensors of the 8481D vintage and the E-series CW-only diode sensors or the E9300-series dual-path sensors.

The power range from approximately –20 to +20 dBm is above the square-law region, and one in which the EPM (or EPM-P, Chapter VI) series power meters use digital-diode-curve correction to provide accurate power measurement for pure CW signals all the way from –70 to +20 dBm. The EPM meters and companion E-series sensors provide fully specified performance over that entire dynamic range of –70 to +20 dBm.

Since the unique design of the two-path E9300-series sensors always keeps the diodes in their square-law range, they can accept non-CW signals across their specified power range, if the peak value remains below the maximum specified power.

The following explanation reviews the effects of complex signals on existing 8481D-type diode sensors for non-CW or complex modulation signals.

Some examples of complex (non-CW) signals are as follows: 1) Pulsed RF such as radar or navigation formats, 2) Two-tone or multiple-tone signals such as those that might be present in a telecommunications channel with multiple sub-channels, 3) AM signals that have modulation frequencies higher than the bandwidth of the power meter detection filtering (in the kHz range for the E4418B), 4) Digital-phase-shift-keyed (PSK) modulations, 5) quadrature amplitude modulation (QAM) modulated signals, and 6) Pulse-burst formats.

Here is a summary of the measurement guidelines for diode sensors:

1) Using the 8481D type diode power sensors, any complex signal will yield highly-accurate measurement results as long as the peak power levels of the unknown signal are maintained below –20 dBm. In addition, the lowest-frequency-component of any modulation frequency must be above approximately 500 Hz. Since the power range of the 8481D-type diode sensors are automatically restricted by Agilent power meters to a top level of –20 dBm, the user need only assure that no peak power levels go above –20 dBm.

When peak power levels exceed approximately –20 dBm, accurate measurements can be accomplished by the simple expedient of attenuating the unknown signal through an external precise fixed or step attenuator, such that the complex signal peak power does not exceed –20 dBm. If pulse modulation frequencies are near the power meter chopping rate of 220 Hz or multiples thereof, some meter “beats” may be observed.

2) Using the E4412/3A power sensors, pure-CW signals will yield accurate results across their entire –70 to +20 dBm dynamic range. One reason E-series sensors may not be used for pulse power within their square-law range is that their output circuit filters are optimized for fast response to aid high data-rate automation.

3) Using the E9300-series sensors, pulsed and complex-modulated signals will yield accurate results if peak powers remain below the maximum specified input power.

4) For non-CW signals with average powers between –20 and +20 dBm, use the thermocouple sensors for true average power sensing.

5) Peak and average sensor/meter technology, which is specifically designed for peak and complex modulations, is introduced in the next Chapter VI.

It is quite easy to realize that thermal sensors such as the thermocouple are pure square law because they convert the unknown RF power to heat and detect that heat transfer. Conversely, it is less easy to understand how diode sensors can perform the square-law function without the heat transfer step in the middle. Diode detectors do deliver pure square-law performance in their lower power ranges below –20 dBm due to their mathematical detection transfer function as described by the power series equation of (5-2).

A two-tone example might clarify the measurement example. Consider two CW signals, f_1 and f_2 , of power level 0 dBm (1 mW) each, and separated by 1 MHz. In a 50 Ω system, each carrier would have voltage magnitudes of $v_1 = v_2 =$ 0.223 volts (rms). If the two-tone signal were measured by an 8481A thermocouple sensor, each carrier would convert the 1 mW into heat for a total of 2 mW.

Using a voltage vector analysis, these two-tone signals would be represented by a voltage minimum of zero and a voltage maximum of 0.446 volts, occurring at a frequency of 1 MHz. The problem then becomes evident when one realizes that two times voltage represents four times power. A shaped diode detector then interprets the 2V maximum as four times power, and averages it out to the wrong power reading.

Another example shows how subtle signal imperfections can cause errors. Consider a CW signal with a harmonic signal –20 dBc (20 dB below the carrier amplitude or with a voltage equal to 10% of the carrier). Figure 5-12 shows a mathematical model of the increasing maximum error caused by a –20 dBc harmonic signal, as the carrier power level ranges from –30 to +20 dBm. While actual deviation from true power is a function of the phase difference between the carrier and its harmonic, the error limits are shown to be as high as 0.9 dB. If the harmonic was measured in the true square-law region, a –20 dBc harmonic represents only $1/100^{th}$ of the power of the carrier or one percent added power to the carrier.

It might also be observed that the design architecture of the PDB sensors utilizes a balanced, push-pull-diode configuration. This structure inherently rejects even-number harmonics of the RF input signal, therefore will provide 15 to 20 dB rejection of even-number harmonics above the square-law region.

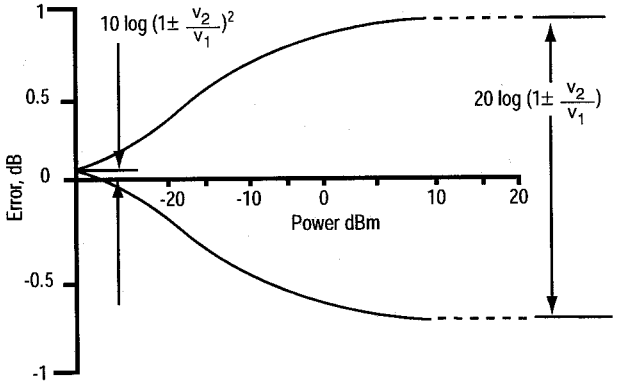

Figure 5-12. Estimated error limits for diode detectors operated above square-law range, for CW signal with –20 dBc harmonic.

Conclusion

Used with the EPM series of power meters, the E9300 wide-dynamic-range average power sensors provide accurate power measurements for digitally modulated signals, multi-tone, and CW signals over a wider range of power levels (80 dB) than is currently achieved with traditional thermocouple or diode based power sensors. This is because their two path architecture keeps the detection diodes below their square-law limits.

The EPM series of power meters, and E4412A and E4413A sensors, feature detector-shaping compensation to deliver dynamic range above square law (90 dB maximum), and should only be used for CW signals.

Average power measurements on pulsed and complex modulation signals can be measured using Agilent thermocouple sensors and EPM series power meters. The 8480D-type diode sensors can be used below –20 dBm.

Peak and average sensor and meter technology described in Chapter VI provide accurate measurement of pulsed and complex modulation signals.

---

1. S.M. Sze, *Physics of Semiconductor Devices*, Second Edition, Wiley, (1981).
2. P.A. Szente, S. Adam, and R.B. Riley, "Low-Barrier Schottky-Diode Detectors," *Microwave Journal*, Vol. 19 No. 2 (Feb., 1976).
3. R.J. Malik, T.R. Aucoin and R.L. Ross, "Planar-Doped Barriers in GaAs Molecular Beam Epitaxy," *Electronics Letters*, Vol 1G #22, (Oct., 1980).
4. A. A. Fraser, "A Planar-Doped-Barrier Detector for General Purpose Applications," *Microwave Journal*, (May, 1987).
5. US Patent #4943764, assigned to Hewlett-Packard Company
6. Zurakowski, M, et al, "Diode Integrated Circuits for MM Applications," Hewlett-Packard Journal, Nov. 1986.

VI. Peak and Average Diode Sensors and Instrumentation

Diode sensor technology is the natural solution for characterizing high performance pulsed-modulation envelopes or complex digital formats. Since diode elements respond to fast video modulation, they easily provide detected video signals for amplification and measurement of the envelope parameters.

Agilent's peak and average power sensors and meters are specifically designed for video bandwidths as wide as 5 MHz. Besides pulsed and digital formats, this recommends them for additional applications such as two-tone tests (if tone separation is less than the sensor bandwidth) or full-channel signal formats that can exhibit statistical spikes in signals which average-sensing diode detectors may not integrate correctly. This chapter will describe the theory and practice of power measurements on these types of signals.

Pulsed formats

Most early pulsed system applications from the late 1930's were simple, rectangular formats for radiolocation (radar and navigation). In the military/aerospace technology race of the 1960's, pulsed formats became much more sophisticated. Radar and EW (countermeasures) transmitters moved from traditional pulsed formats to exploit complex and pseudo-random pulse-rate configurations for immunity to jamming and to reveal more precise data on unknown target returns. Simple computations with an average power measurement and duty cycle didn't work anymore.

Navigation systems such as air-traffic control (ATC) or distance measuring equipment (DME) have non-traditional pulse configurations too, such as pulse pairs, triplets or Gaussian-shaped envelopes to conserve frequency spectrum and avoid spectrum overlap in multiple aircraft environments. (A Gaussian-shaped envelope exhibits the interesting property that its spectrum has no side lobes, compared to the much-wider $\frac{\sin x}{x}$ side-lobe spectrum of a rectangular pulse.)

The now-discontinued Agilent 8990A peak power analyzer served for a time in the 1990's as the leading instrument for characterizing these and many other complex modulation formats. However, as the new wireless communication technologies of the mid-1990's accelerated rapidly, users needed power measurement equipment for wideband data transmission formats. This led to the present power measuring instruments and sensors which handle average power, as well as time-gated and peak power or peak-to-average ratios, with all those measurements delivered at very high measurement-data rates.

It's important to understand that the 5 MHz video bandwidth of Agilent's peak and average sensors is not particularly well suited for modern radar or EW pulse formats, which feature rise and fall times in the nanosecond range. As will be shown in later descriptions, the time-gated function of the EPM-P meters is capable of averaging the power during the pulse-top period if the time-gate is set to bracket the radar pulse. It can also measure parameters such as the peak power, which in the case of a radar pulse, is usually the risetime overshoot. Other power spikes or parasitic oscillations would also qualify as a peak anomaly and be captured as peak power.

Complex modulation wireless signals

Digital vector modulation became the modulation of choice as the digital revolution swept over RF and microwave communication systems some 20 years ago. The need to pack the maximum amount of digital data into the limited spectrum made it an obvious choice. For example, some early migrations of microwave terrestrial links from traditional analog frequency-division-multiplex (FDM), used 64 QAM (quadrature-amplitude-modulation) formats.

The advent of wireless communications technology in the 1990's accelerated the migration from analog to digital modulation formats. Soon came an alphabet soup of digital modulation formats including, BPSK, QPSK, 8-PSK, 16 QAM, etc. Then came important variations such as π/4DQPSK and π/8-8PSK and others. But the breakthrough to successful cellular technology came with the sophisticated carrier switching of transmit signals. This permitted time-shared information to and from thousands of mobile subscribers, who were arrayed around in geographic regions (cells), communicating sequentially with one base station after another as the user's transceiver moved from cell to cell.

Some of those systems used data streams that featured time division multiple access (TDMA) technology, such as global system for mobile communication (GSM). Other system developers introduced a highly competitive code-division-multiple access (CDMA) format which includes IS-95.

TDMA is the technology for time-sharing the same base station channel. Encoded voice data and new high data rate wireless links are modulated onto the transmitted carrier in the phase plane. These modulation formats create "constellations" of bit symbol locations such as shown in the π/8 shifted-8PSK configuration of figure 6-1. This particular modulation format is used in the emerging Enhanced Data Rates for GSM Evolution (EDGE) systems which will offer high-speed data transfer over mobile wireless channels. By packing 3 bits per symbol, it increases data information rates, but thereby increases amplitude peak swings up to 16+ dB, making amplifier saturation more likely.

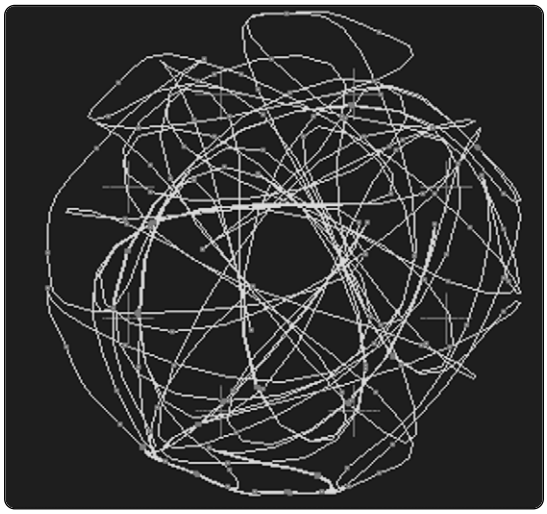

Figure 6-1. This pi/8 8PSK digital modulation format is emerging for wideband data transmission on wireless channels, such as the EDGE technology.

In GSM, each TDMA wireless subscriber's share of time allows a useful data burst of say 524.6 μS, during which it is crucial for the power amplifier to remain below its saturation region. Driving the output stage into non-linear amplification causes the outermost phase states to compress, thereby increasing demodulation bit errors and lowering system reliability.

The TDMA system feeds multiple carriers through a common output amplifier, which results in a transmitted power spectrum with almost white-noise-like characteristics. In contrast, CDMA encodes multiple data streams onto a single carrier using a pseudo-random code, with a similar transmitted power spectrum and similar power spikes.

Just like white noise, the average power of the transmitted signal is only one of the important parameters. Because of the statistical way that multiple carrier signal voltages can add randomly, instantaneous peak voltages can approach ratios of 10 to 30 times the carrier's rms voltage, depending on formats and filtering. This ratio, calculated with voltage parameters, is commonly called crest factor, and is functionally similar to the peak-to-average power ratio which is measured by Agilent peak and average power meters, described below.[i]

High peak-to-average power ratios imply dangers in saturation of the output power amplifiers. When saturation occurs, the outer bit-symbol locations compress, increasing bit errors and system unreliability. System designers handle this effect by "backing-off" the power amplifiers from their maximum peak ratings to assure that signal peak power operation is always within their linear range.

Wireless handsets also contain frequency-agile local oscillators that "hand-off" the mobile signal as it moves from ground cell to cell and links up to each new base-station frequency. Sometimes the transmitter power perturbations that occur during the frequency-switching transition also need to be characterized.

Other formats

Other application test signals cause problems for averaging diode sensors (above their square-law range) because of their spectrum content. For example, two-tone (or three-tone) test signals are often used for characterizing amplifiers for linearity of their amplification. If the amplification is non-linear, two pure input signals of $f_1$and f_2 result in intermodulation signals at the output, of the form $2f_1 - f_2$, $2f_2 - f_1$, and many more. The test is a very sensitive indicator of amplifier linearity.

Measuring power of such tones needs user analysis because the phase of the two carriers adds or cancels at the rate of the offset frequency. In a two-tone example, of V_1 and V_2, each with equal power, P, the constructive addition of tones results in a peak carrier of 2V, which is a peak power of 4P. An average-responding sensor would indicate 2P, but a peak-responding sensor would indicate 4P. It is the 2V effect that can saturate power amplifiers. When measuring peak power of such tone formats, the tone separation must be less than the sensor video bandwidth.

Other test signals, which contain high harmonic content, can also modify the carrier vector randomly and thus yield random power results. See the waveform analysis in Chapter V.

Still other formats are generated by frequency-agile synthesizers, which can simulate entire, full-channel communications traffic formats. Since their component signals also add statistically, their power envelope is random. If those power spikes fall within the sensor video bandwidth, they can be measured.

---

i Accepted definition of crest factor (pulsed carrier): The ratio of the pulse peak (voltage) amplitude to the root-mean-square (voltage) amplitude.

Peak and average power sensing

The Agilent E9320 family of peak and average sensors demonstrates the current art of power sensing. See Chapter VIII for product capability tables. They presently cover the 50 MHz to 6/18 GHz frequency ranges and –65 to +20 dBm power range. Ideal for comprehensive measurements on pulsed envelopes and signals with complex modulation, they also deliver accurate and reliable average power measurements. When teamed with the new Agilent EPM-P series power meters (E4416A/17A), the combination can handle test signal envelopes with up to 5 MHz video bandwidth.

The basic block diagram for the peak and average sensor is shown in figure 6-2. It features parallel amplification paths, one for CW (average-only) and one for video (normal). Both modes use the same micro-circuit diode-sensor (bulkhead) element at the RF input. Signal processing in the two amplification paths is optimized to their differing needs for selecting the video bandwidths, filtering, chopping and other data requirements. Amplification is distributed, with an optimum amount in the sensor unit and more in the meter.

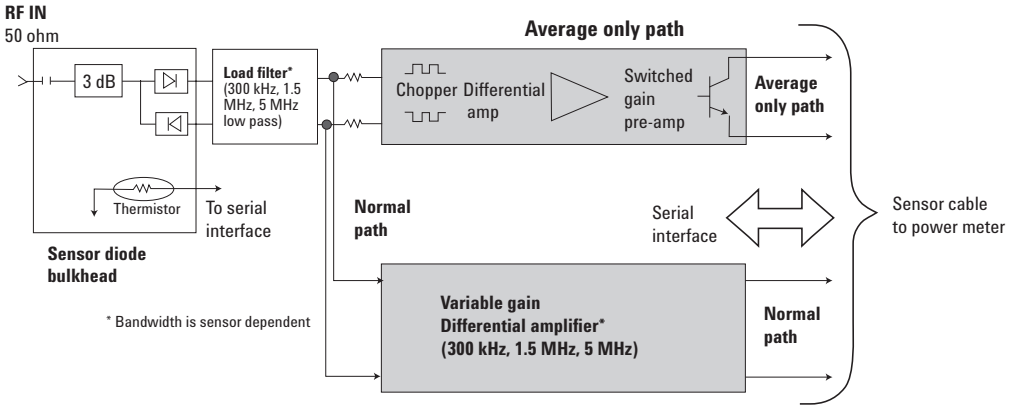

Figure 6-2. Simplified block diagram of a peak and average sensor, showing the parallel amplification paths, along with control lines and a temperature-sensing thermistor function, which corrects the diode's data.

In the average-only mode, amplification and chopping parameters are much the same as in previous Agilent averaging sensors, with typical dynamic power range of –65 to +20 dBm. In the normal mode, the separate-path dc coupled amplifier provides three sensor dependent maximum bandwidths of 300 kHz, 1.5 MHz or 5 MHz, allowing the user to match the test signal's modulation bandwidth to the sophisticated instrument data processing. These considerations will be discussed later in this chapter.

Several functions are included in these peak and average sensors that are not in most other diode sensors. First, all E-series sensors have temperature corrections to improve stability and accuracy, with the correction data stored in an on-board EEPROM. The temperature-sensing thermistor element is mounted inside the bulkhead unit on the same microcircuit as the RF diode sensing elements.

Secondly, the peak and average sensors communicate with the E4416/7A meters using the serial bus shown. It is bi-directional to allow calibration data to upload to the meter whenever a new sensor is connected. Sensor cal data can even flow further out the GPIB port for external computer purposes. In the other direction, the serial bus delivers control commands to the sensor, for example, to select which amplification path is to be activated.

Diode sensors used for peak pulse detection necessarily operate up into their linear detection regions and have various deviations from ideal. Power linearity is frequency dependent in the E9320 family, and the diodes also have some temperature dependence. Figure 6-3 shows how the EEPROM, resident in each sensor, stores the three-dimensional correction data that is derived from a special sensor calibration system at Agilent's factory and service facilities. The calibration process includes a run in a temperature oven, during which time the input power is ramped over the critical range at each calibration temperature.

Consider one axis of the temperature response in figure 6-3 to be the frequency response, and the other axis to be the response to the power dynamic range. The "warped" surface profile therefore represents a single temperature, so many such surfaces of data exist in the EEPROM.

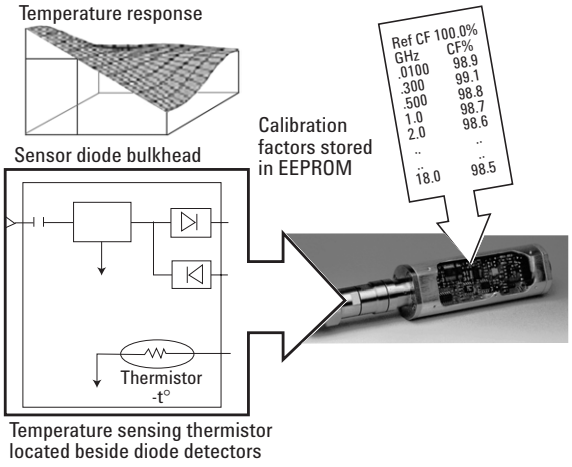

Figure 6-3. Temperature, power and frequency correction data, stored in each E9320-family peak and average sensor, uploads into the meter each time a new sensor is connected to the meter, improving measurement accuracy and confidence.

EPM-P series power meters

Figure 6-4 shows an overview block diagram for the E4416A (single channel) power meter. Under microprocessor control, all the various functional components from panel keyboard to the logic and digital signal processor (DSP) functions are coordinated. For the average-only mode, signal processing is similar to previous meters. In fact, the EPM-P series meters will accommodate all older Agilent thermocouple and diode sensors (but naturally won't read peak power). A 16-bit analog digital converter (ADC) processes the average power signal.

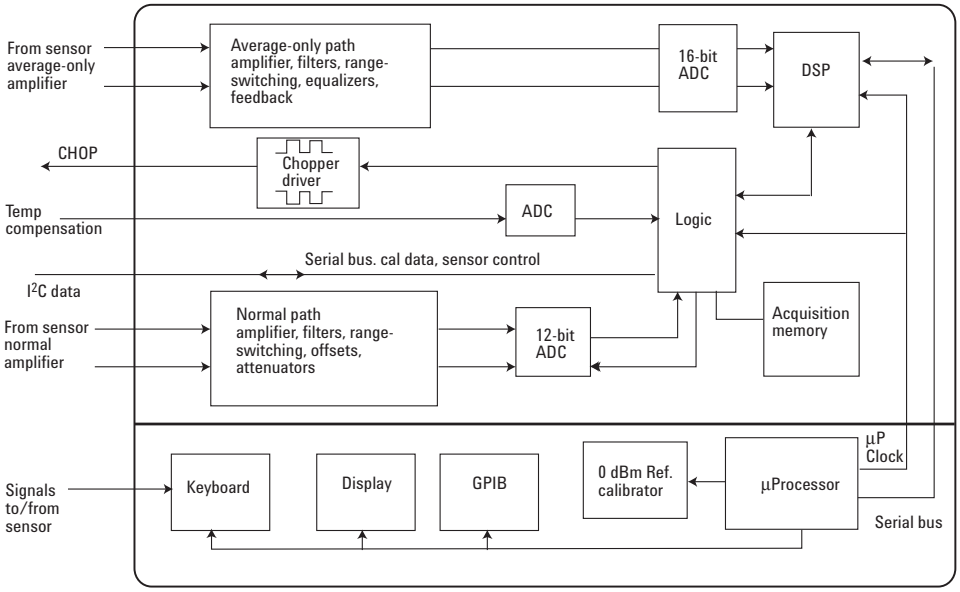

Figure 6-4. Simplified block diagram for E4416A shows extensive use of digital signal processing and control. Measurement confidence results from the comprehensive data correction routines.

A highly-sophisticated video amplifier design is implemented for the normal path to preserve envelope fidelity and accuracy. Innovative filtering and range-switching, as well as differential offset controls and zeroing functions are handled. A 12-bit ADC processes the amplified envelope into a data stream for the DSP.

Of particular importance for production testing is the 20 Msamples/second continuous sample rate in the pulsed ADC, which permits fast measurement speed, via the GPIB, of up to 1,000 corrected readings per second. This makes the meter ideal for use in automatic test system applications.

The central function for peak and average power meters is to provide reliable, accurate, and fast characterization of pulsed and complex modulation envelopes. The EPM-P meters excel in versatility featuring a technique called time-gated measurements. For a descriptive example, figure 6-5 shows 4 typical time-gated power measurements on a GSM signal.

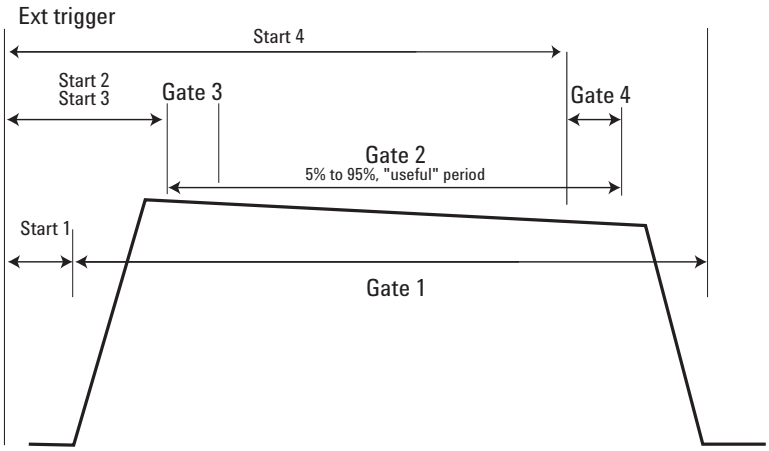

Figure 6-5. For this typical GSM pulse, time-gated measurement techniques permit the EPM-P meter user to configure four different measurement gate periods, each with its own delay time, measured from a "trigger-point" pulse.

In figure 6-5, Gate 2 provides the burst average power over the "useful" GSM time period, which is in essence the averaged power during the gate period, at the top of the pulse. It is therefore very similar to the Chapter II definition of pulse-top amplitude, although pulse-top is measured between the half-power points. Remember that each gate may be programmed to measure peak or average or ratio.

In this example, Gate 1 indicates the peak power over its complete Gate 1 period. In the E4416A, this definition of peak power is equivalent to the Chapter 2 definition of peak power, which is the highest instantaneous power spike to occur during the open measurement gate period. Functionally, the peak power data allows the user to measure the saturation effect that power spike overloads create in test amplifier performance.

The E4416/7A meters measure three different selectable parameters during each gate, peak power, average power and peak-to-average ratio. Thus, an industry-important peak-to-average ratio may be made during the same gate time, or conversely, the ratio of peak power in one gate time may be computed against the average power in another gate time.

A pulse droop measurement can be obtained by subtracting the two powers, Gate 3 – Gate 4. All three of these measurements can be simultaneously displayed on the 4-line numeric liquid-crystal display (LCD) screen, along with the peak power from Gate 1.

The trigger point may be selected from three sources, 1) an external pulse, 2) derived internally, digitally, from the measured pulse envelope, or 3) from the external GPIB source. The acquisition modes may be single, continuous or free-run. Other trigger manipulations are also featured, such as holdoff or delay. Once the trigger point is set, it may be output to other system instrumentation via a rear BNC connector.

Computation power

The signal processing in the E4416/7A meters has been designed to provide exceptional data computation and display versatility. Figure 6-6 shows the data paths for the four independent gate periods, each with its own delay time. Each gate can be set to measure average, peak, and peak-to-average power data.

Each gate can then manipulate those three parameters into two computed parameters (F-feeds) such as F1 minus F2 or F1/F2, to be displayed in one of the four window partitions. The block shown as the “measurement highway” takes care of moving data to the user-configured display line on the LCD. The highway also permits computation of shared data between the four gates.

This computational power is particularly valuable in TDMA wireless test scenarios such as GSM, GPRS, EDGE, and NADC, where various simultaneous combinations of computed parameters are required.

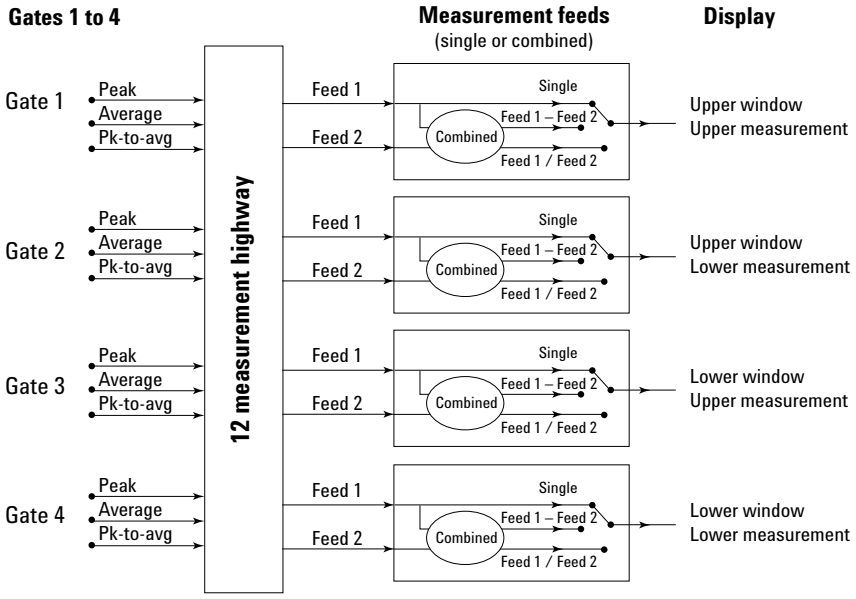

Figure 6-6. User-configured data manipulations are a major feature of the EPM-P series power meters.

The large LCD display partitions up to four-line formats to help interpret and compare measurement results, using the measurement highway. The user can also select large character readouts to permit viewing from a distance. For example, figure 6-7(b) shows how the four lines could be configured to display average power in dBm and W, peak power and peak-to-average ratio.
The user can also choose to show the analog power envelopes for two selected traces in the partitioned display. Figure 6-7(a) shows the user set-up display for four gate periods and delays.

It should be noted that all the above configurations for feeding actual data plus computed data, such as power ratios, through the measurement highway is for a single sensor. When using the E4417A dual-power meter, the second sensor provides a doubling of retrieved power data, all of which may be user-selected to create combined ratios or power differences between sensor A and sensor B channels.

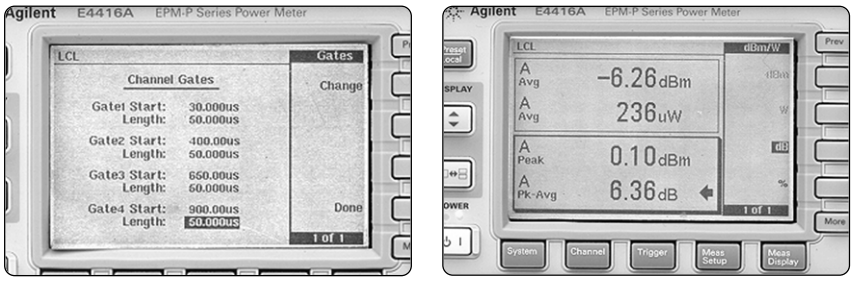

(a) (b)

Figure 6-7. The back-lighted LCD display delivers powerful readout versatility: (a) shows how the user sets the delay and measurement times for each of four gates, (b) shows a simultaneous display of four Gate A parameters; average power in dBm and µW, peak power, and peak to average ratio. The user could also choose a digitally-derived pulse envelope representation as well.

Bandwidth considerations

In the normal mode, the separate-path decoupled amplifier provides maximum bandwidths of 300 kHz, 1.5 MHz, or 5 MHz, defined by the sensor model number. This allows the user to match the test signal's modulation bandwidth to the sophisticated instrument data processing. For example, the three maximum bandwidth choices match up with these typical wireless system requirements:

300 kHz	TDMA, GSM
1.5 MHz	CDMA (IS-95)
5 MHz	W-CDMA, cdma2000

To further optimize the system's dynamic range, the video bandwidth can be user-selected in the meter (using DSP filtering) to high, medium, and low, as detailed in table 6-1. Thus, when users need to measure the power of multiple signal types within a single sensor by considering the dynamic range of the bandwidth settings shown in the table, they can determine if they require only one sensor or need multiple sensors for their application(s).

The filter video bandwidths stated in the table are not the traditional 3 dB bandwidths, since these video bandwidths are optimized and corrected for optimal flatness. Detailed response curves are shown in the product specifications (see reference literature in back of this publication), using a technique of applying a two-tone signal, programming the power meter for a peak to average measurement, then increasing the separation of the two-tones until a frequency response curve is generated. With such a procedure, the curve shape is not a traditional roll-off characteristic.

Table 6-1. E9320 sensor bandwidth versus peak power dynamic range (normal mode).

Sensor model	**Modulation bandwidth / Max. peak power dynamic range**			
6 GHz/18 GHz	**High**	**Medium**	**Low**	**Off**
E9321A/E9325A	300 kHz/–42 to +20 dBm	100 kHz/–43 to +20 dBm	30 kHz/–45 to +20 dBm	–40 dBm to +20 dBm
E9322A/E9326A	1.5 MHz/–37 to +20 dBm	300 kHz/–38 to +20 dBm	100 kHz/–39 to +20 dBm	–36 dBm to +20 dBm
E9323A/E9327A	5 MHz/–32 to +20 dBm	1.5 MHz/–34 to +20 dBm	300 kHz/–36 to +20 dBm	–32 dBm to +20 dBm

When instrumenting for peak power measurements, it is crucial to analyze the effect of the instrumentation video bandwidths on the accuracy of the resulting data. Agilent E4416/17A meters have been optimized to avoid degrading key specifications like linearity, mismatch, dynamic range and temperature stability. For further information on this matter, see the following article; “Power Measurements for the Communications Market.” [1]

Versatile user interface

The E4416A/17A meters feature a user-friendly interface and powerful display controls. Hardkeys control the most-frequently used functions such as sensor calibration and triggering, while softkey menus simplify configuring the meter for detailed measurement sequences. A save/recall menu stores up to ten instrument configurations for easy switching of test processes.

1. Anderson, Alan, “Power Measurements for the Communications Market,” *MW/RF Magazine*, October, 2000.

VII. Measurement Uncertainty

In RF and microwave measurements there are many sources of measurement uncertainty. In power measurements, the largest errors are almost always caused by sensor and source mismatch. Mismatch uncertainties, which have several aspects, are somewhat complicated and are seldom completely understood or properly evaluated. This chapter begins with a description of uncertainties associated with mismatch. The concept of signal flowgraphs is introduced to aid in the visualization needed for understanding the mismatch process. Other sensor uncertainties such as effective efficiency and calibration factor are then considered. This is followed by an analysis of the various instrumentation uncertainties of the power meter. Finally, the chapter treats the combining of all errors for a total uncertainty number.

An international guide to the expression of uncertainty in measurement

In recent years, the world's metrology and quality community has begun to accept and implement a new process for calculating and reporting the uncertainties of measurement. The process is based on a standard promulgated by the International Standards Organization, of Geneva, Switzerland, “ISO Guide to the Expression of Uncertainty in Measurement.”

The NCSL International (previously National Conference of Standards Laboratories), in Boulder, Colorado, cooperating with the American National Standards Institute, adopted the ISO document as a U.S. National Standard, and introduced it in the U.S. as an industry document, ANSI/NCSL Z540-2-1996, “U.S. Guide to the Expression of Uncertainty in Measurement.”[1,2]

Both of the uncertainty standards operate within a larger metrology context, specified by ISO Guide 25, “General Requirements for the Competence of Testing and Calibration Laboratories.” This document was adapted to a U.S. version with the identical title, ANSI/NCSL Z540-1-1994. Recently, ISO announced the replacement of ISO Guide 25 with ISO/IEC 17025.

In the U.S., the ANSI/NCSL industry committee determined that world metrology would be best served with a single standard for general laboratory requirements, and thus has begun the process of adopting the ISO/IEC 17025 document as a US National Standard in cooperation with the American Society of Testing Materials (ASTM) and the American Society for Quality (ASQ).

However, the ANSI/NCSL Z540-1-1994 Standard will be maintained at this time to meet the needs of some elements of U.S. industry which are not covered in ISO/IEC 17025. In the future the continued existence of Z540-1-1994 may depend on the extent to which the ISO/IEC 17025 is strengthened through revision.

A detailed example of uncertainty calculations using the Z540-2-1996 is given later in this chapter.

Power transfer, generators and loads

The goal of an absolute power measurement is to characterize the unknown power output from some source (generator). Sometimes the generator is an actual signal generator or oscillator where the power sensor can be attached directly to that generator. On other occasions, however, the generator is actually an equivalent generator. For example, if the power source is separated from the measurement point by such components as transmission lines, directional couplers, amplifiers, mixers, etc, then all those components may be considered as parts of the generator. The port that the power sensor connects to, would be considered the output port of the equivalent generator.

To analyze the effects of impedance mismatch, this chapter explains mathematical models which describe loads, including power sensors and generators, which apply to the RF and microwave frequency ranges. The microwave descriptions begin by relating back to the equivalent low-frequency concepts for those familiar with those frequencies. Signal flowgraph concepts aid in analyzing power flow between an arbitrary generator and load. From that analysis, the terms mismatch loss and mismatch uncertainty are defined.

RF circuit descriptions

At low frequencies, methods for describing a generator include the Thevenin and Norton equivalent circuits. The Thevenin equivalent circuit of a generator, for example, has a voltage generator, e_s, in series with an impedance, Z_g, as shown in figure 7-1. For a generator, even if composed of many components, e_s is defined as the voltage across the output port when the load is an open circuit. Z_g is defined as the impedance seen looking back into the generator when all the sources inside the generator are reduced to zero.

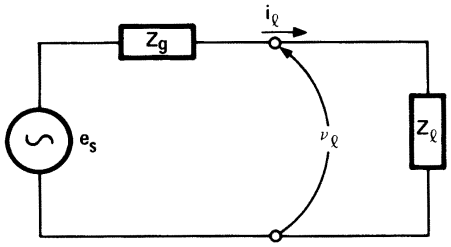

Figure 7-1. A Thevenin equivalent generator connected to an arbitrary load.

The power delivered by a generator to a load is a function of the load impedance. If the load is a perfect open or short circuit, the power delivered is zero. Analysis of figure 7-1 would show that the power delivered to the load is a maximum when load impedance, Z_ℓ, is the complex conjugate of the generator impedance, Z_g. This power level is called the "power available from a generator," or "maximum available power," or "available power." When $Z_\ell = (R_\ell + jX_\ell)$ and $Z_g = (R_g + jX_g)$ are complex conjugates of each other, their resistive parts are equal and their imaginary parts are identical in magnitude but of opposite sign; thus $R_\ell = R_g$ and $X_\ell = -X_g$. Complex conjugate is written with an "*" so that $Z_\ell = Z_g^*$ is the required relationship for maximum power transfer.

The Thevenin equivalent circuit is not very useful at microwave frequencies for a number of reasons. First, the open circuit voltage is difficult to measure because of fringing capacitance and the loading effect of a voltmeter probe. Further, the concept of voltage loses usefulness at microwave frequencies where it is desired to define the voltage between two points along a transmission path, separated by a significant fraction of a wavelength. Also, there are problems involved in discussing voltage in rectangular waveguide. As a result, the concept of power is much more frequently used than voltage for characterizing generators at RF and microwave frequencies.

The open circuit that defines the Thevenin equivalent voltage generator is useless for measuring power because the power dissipated in an open termination is always zero. The reference impedance used for characterizing RF generators is almost always 50 Ω. The reason for this is that 50 Ω is easy to realize over the entire frequency range of interest with a transmission line of 50 Ω characteristic impedance and with a reflection-less termination.

The standard symbol for characteristic impedance, Z_o, is also the standard symbol for reference impedance. In some cases, for example, where 75 Ω transmission lines are used in systems with a 50 Ω reference impedance, another symbol, such as Z_r, should be used for reference impedance. Z_o will be used in this application note to mean reference impedance. A generator is characterized, therefore, by the power it delivers to a reference load Z_o = 50 Ω. In general, that power is not equal to the maximum available power from the generator; they are equal only if $Z_g = Z_o$.

As frequencies exceed 300 MHz, the concept of impedance loses usefulness and is replaced by the concept of reflection coefficient. The impedance seen looking down a transmission line toward a mismatched load, varies continuously with the position along the line. The magnitude and the phase of impedance are functions of line position. Reflection coefficient is well-behaved; it has a magnitude that is constant and a phase angle that varies linearly with distance from the load.

Reflection coefficient

At microwave frequencies where power typically is delivered to a load by a transmission line that is many wavelengths long, it is very convenient to replace the impedance description of the load, involving voltage and current and their ratio (Ohm's law), with a reflection coefficient description involving incident and reflected traveling waves, and their ratio. To characterize a passive load, Ohm's law is replaced by:

$$\frac{b_\ell}{a_\ell} = \Gamma_\ell \qquad (7\text{-}1)$$

where a_ℓ is proportional to the voltage of the incident wave, b_ℓ is proportional to the voltage of the reflected wave, and is defined to be the reflection coefficient of the load. All three quantities are, in general, complex numbers and change with frequency. The quantities a_ℓ and b_ℓ are normalized[ii] in such a way that the following equations hold:

$$a_\ell^{\,2} = P_i \qquad (7\text{-}2)$$

$$b_\ell^{\,2} = P_r \qquad (7\text{-}3)$$

where P_i is power incident on the load and P_r is power reflected by it. The net power dissipated by the load, P_d , is given by:

$$P_d = P_i - P_r = a_\ell^{\,2} - b_\ell^{\,2} \qquad (7\text{-}4)$$

This power is the total power obtained from the source; it includes not only power converted to heat, but also power radiated to space and power that leaks through accessory cables to other pieces of equipment.

Transmission line theory relates the reflection coefficient, Γ_ℓ of a load to its impedance, Z_ℓ, as follows:

$$\Gamma_\ell = \frac{Z_\ell - Z_o}{Z_\ell + Z_o} \qquad (7\text{-}5)$$

where Z_o is the characteristic impedance of the system. Further, the load voltage, v_ℓ, and load current, i_ℓ, are given by

$$V_\ell = \text{Incident voltage} + \text{reflected voltage} = \sqrt{Z_o}\,(a_\ell + b_\ell) \qquad (7\text{-}6)$$

$$i_\ell = \text{Incident current} - \text{reflected current} = \frac{1}{\sqrt{Z_o}}\,(a_\ell - b_\ell) \qquad (7\text{-}7)$$

since current in a traveling wave is obtained from the voltage by dividing by Z_o. Solving for a_ℓ and b_ℓ results in:

$$a_\ell = \frac{1}{2\sqrt{Z_o}}\,(v_\ell + Z_o i_\ell) \qquad (7\text{-}8)$$

$$b_\ell = \frac{1}{2\sqrt{Z_o}}\,(v_\ell \leftarrow Z_o i_\ell) \qquad (7\text{-}9)$$

ii. If the transmission line characteristic impedance is Z_0 the normalization factor is $\sqrt{Z_0}$; that is, a_ℓ is obtained from the voltage of the incident wave by dividing by $\sqrt{Z_0}$. Similarly, b_ℓ is obtained from the voltage of the reflected wave by dividing by $\sqrt{Z_0}$.

These equations are used in much of the literature to define a_ℓ and b_ℓ (see the reference by Kurakawa.)[3] The aim here, however, is to introduce a_ℓ and b_ℓ more intuitively. Although (7-8) and (7-9) appear complicated, the relationships to power (equations 7-2, 7-3, and 7-4) are very simple. The Superposition Theorem, used extensively for network analysis, applies to a_ℓ and b_ℓ; the Superposition Theorem does not apply to power.

Reflection coefficient, Γ_ℓ, is frequently expressed in terms of its magnitude, ρ_ℓ, and phase, ϕ_ℓ. Thus ρ_ℓ gives the magnitude of b_ℓ with respect to a_ℓ and ϕ_ℓ gives the phase of b_ℓ with respect to a_ℓ.

The most common methods of measuring reflection coefficient involve observing a_ℓ and b_ℓ separately and then taking the ratio. Sometimes it is difficult to observe a_ℓ and b_ℓ separately, but it is possible to observe the interference pattern of the counter-travelling waves formed by a and b on a transmission line. This pattern is called the standing wave pattern. The interference pattern has regions of maximum and of minimum signal strength. The maximums are formed by constructive interference between a_ℓ and b_ℓ and have amplitude $|a_\ell| + |b_\ell|$. The minimums are formed by destructive interference and have amplitude $|a_\ell| - |b_\ell|$. The ratio of the maximum to the minimum is called the standing-wave ratio (SWR, sometimes referred to as voltage-standing-wave-ratio, VSWR) and can be measured with a slotted line and moveable probe, or more commonly with network analyzers. SWR is related to the magnitude of reflection coefficient ρ_ℓ by:

$$\text{SWR} = \frac{a_\ell + b_\ell}{a_\ell - b_\ell} = \frac{1 \Leftrightarrow b_\ell/a_\ell}{1 - b_\ell/a_\ell} = \frac{1 \Leftrightarrow \rho_\ell}{1 - \rho_\ell} \qquad (7\text{-}10)$$

Signal flowgraph visualization

A popular method of visualizing the flow of power through a component or among various components is by means of a flow diagram called a signal flowgraph.[3,4] This method of signal flow analysis was popularized in the mid-1960's, at the time that network analyzers were introduced, as a means of describing wave travel in networks.

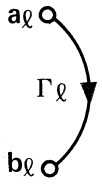

Figure 7-2. Signal flowgraph for a load.

The signal flowgraph for a load (figure 7-2) has two nodes, one to represent the incident wave, a_ℓ, and the other to represent the reflected wave, b_ℓ. They are connected by branch Γ_ℓ, which shows how a_ℓ gets changed to become b_ℓ.

Just as the Thevenin equivalent had two quantities for characterizing a generator, generator impedance, and open circuit voltage, the microwave equivalent has two quantities for characterizing a microwave or RF generator, Γ_g and b_s.

The equation for a generator is (see figure 7-3):

$$b_g = b_s + \Gamma_g a_g \qquad (7\text{-}11)$$

where:

b_g is the wave emerging from the generator
a_g is the wave incident upon the generator from other components
Γ_g is the reflection coefficient looking back into the generator
b_s is the internally generated wave

Γ_g is related to Z_g by:

$$\Gamma_g = \frac{Z_g - Z_o}{Z_g + Z_o} \qquad (7\text{-}12)$$

which is very similar to (7-5). The b_s is related to the power to a reference load from the generator, Pg_{zo}, by:

$$Pg_{zo} = b_s^{\ 2} \qquad (7\text{-}13)$$

b_S is related to the Thevenin voltage, e_s, by:

$$b_s = \frac{e_s \sqrt{Z_o}}{Z_o + Z_g} \qquad (7\text{-}14)$$

The signal flowgraph of a generator has two nodes representing the incident, wave a_g and reflected wave b_g. The generator also has an internal node, b_s, that represents the ability of the generator to produce power. It contributes to output wave, b_g, by means of a branch of value one. The other component of b_g is that portion of the incident wave, a_g, that is reflected off the generator.

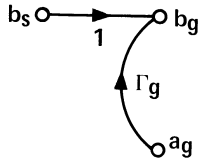

Figure 7-3. Signal flowgraph of a microwave generator.

Now that equivalent circuits for a load and generator have been covered, the flow of power from the generator to the load may be analyzed. When the load is connected to the generator, the emerging wave from the generator becomes the incident wave to the load and the reflected wave from the load becomes the incident wave to the generator. The complete signal flowgraph (figure 7-4) shows the identity of those waves by connecting node b_g to a_ℓ and node b_ℓ to a_g with branches of value one.

Figure 7-4 shows the effect of mismatch or reflection. First, power from the generator is reflected by the load. That reflected power is re-reflected from the generator and combines with the power then being created by the generator, generating a new incident wave. The new incident wave reflects and the process continues on and on. It does converge, however, to the same result that will now be found by algebra.

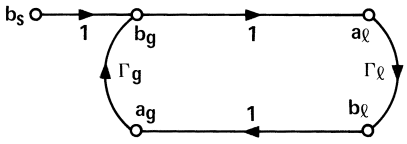

Figure 7-4. The complete signal flowgraph of a generator connected to a load.

The equation of the load (7-1) is rewritten with the identity of a_g to b_ℓ added as:

$$b_\ell = \Gamma_\ell \, a_\ell = a_g \qquad (7\text{-}15)$$

The equation of the generator (7-11) is also rewritten with the identity of a_ℓ to b_g added as:

$$b_g = b_g + \Gamma_g a_g = a_\ell \qquad (7\text{-}16)$$

Equations (7-15) and (7-16) may be solved for a_ℓ and b_ℓ in terms of b_s, Γ_ℓ and Γ_g:

$$a_\ell = \frac{b_s}{1 - \Gamma_g\Gamma_\ell} \tag{7-17}$$

$$b_\ell = \frac{b_s\Gamma_\ell}{1 - \Gamma_g\Gamma_\ell} \tag{7-18}$$

From these solutions the incident and reflected power can be calculated:

$$P_i = |a_\ell|^2 = |b_s|^2 \frac{1}{|1 - \Gamma_g\Gamma_\ell|^2} \tag{7-19}$$

$$P_r = |b_\ell|^2 = |b_s|^2 \frac{|\Gamma_\ell|^2}{|1 - \Gamma_g\Gamma_\ell|^2} \tag{7-20}$$

Equation (7-19) yields the somewhat surprising fact that power flowing toward the load depends on the load characteristics.

The power dissipated, P_d, is equal to the net power delivered by the generator to the load, $P_{g\ell}$:

$$P_d = P_{g\ell} = P_i - P_r = |b_s|^2 \frac{|1 - \Gamma_\ell|^2}{|1 - \Gamma_g\Gamma_\ell|^2} \tag{7-21}$$

Two particular cases of equation (7-21) are of interest. First, if Γ_ℓ were zero, that is if the load impedance were Z_o, equation (7-21) would give the power delivered by the generator to a Z_o load:

$$P_{g\ell}\ _{Z_\ell = Z_o} = P_{gZo} = |b_s|^2 \tag{7-22}$$

This case is used to define b_s as the generated wave of the source.

The second case of interest occurs when:

$$\Gamma_g = \Gamma_\ell^* \tag{7-23}$$

where * indicates the complex conjugate. Interpreting (7-23) means that the reflection coefficient looking toward the load from the generator is the complex conjugate of the reflection coefficient looking back toward the generator. It is also true that the impedances looking in the two directions are complex conjugates of each other. The generator is said to be “conjugately matched.” If Γ_ℓ is somehow adjusted so that (7-23) holds, the generator puts out its “maximum available power,” P_{av}, which can be expressed as:

$$P_{av} = \frac{|b_s|^2}{1 - |\Gamma_g|^2} \tag{7-24}$$

Comparing (7-22) and (7-24) shows that $P_{av} \geq P_{gZo}$.

Unfortunately, the term “match” is popularly used to describe both conditions, $Z_\ell = Z_o$ and $Z_\ell = Z_g^*$. The use of the single word “match” should be dropped in favor of “Z_o match” to describe a load of zero reflection coefficient, and in favor of “ conjugate match” to describe the load that provides maximum power transfer.

Now the differences can be plainly seen. When a power sensor is attached to a generator, the measured power that results is Pg_{zo} of equation (7-21), but the proper power for characterizing the generator is Pg_{zo} of equation (7-22). The ratio of equations (7-22) to (7-21) is:

$$\frac{Pg_{zo}}{Pg_{\ell}} = \frac{1 - \Gamma_g\Gamma_{\ell}\ ^2}{1 - \ \Gamma_{\ell}\ ^2} \qquad (7\text{-}25)$$

or, in dB:

$$dB = 10 \log \frac{Pg_{zo}}{Pg_{\ell}} \qquad (7\text{-}26)$$

$$= 10 \log \ 1 - \Gamma_g\Gamma_{\ell}\ ^2 - 10 \log (1 - \ \Gamma_{\ell}\ ^2)$$

This ratio (in dB) is called the "Z_o mismatch loss." It is quite possible that (7-25) could yield a number less than one. Then (7-26) would yield a negative number of dB.

In that case more power would be transferred to the particular load being used than to a Z_o load, where the Z_o mismatch loss is actually a gain. An example of such a case occurs when the load and generator are conjugately matched.

A similar difference exists for the case of conjugate match; the measurement of $P_{g\ell}$ from (7-21) differs from P_{av} of (7-24). The ratio of those equations is:

$$\frac{P_{av}}{P_{g\ell}} = \frac{1 - \Gamma_g\Gamma_{\ell}\ ^2}{(1 - \ \Gamma_g\ ^2)(1 - \ \Gamma_{\ell}\ ^2)} \qquad (7\text{-}27)$$

or, in dB:

$$dB = 10 \log \frac{P_{av}}{P_{g\ell}}$$

$$= 10 \log \ 1 - \Gamma_{\ell}\Gamma_g\ ^2 - 10 \log (1 - \ \Gamma_g\ ^2) - 10 \log (1 - \ \Gamma_{\ell}\ ^2) \qquad (7\text{-}28)$$

This ratio in dB is called the conjugate mismatch loss.

If Γ_{ℓ} and Γ_g were completely known, there would be no difficulty. The power meter reading of Pg_{ℓ} would be combined with the proper values of Γ_{ℓ} and Γ_g in (7-25) or (7-27) to calculate Pg_{zo} or P_{av}. The mismatch would be corrected and there would be no uncertainty.

Mismatch uncertainty

Γ_ℓ and Γ_g are seldom completely known for both magnitude and phase. Only the magnitudes ρ_ℓ and ρ_g areusually measured or specified. In these cases, the first term of the right side ofequations (7-26) and (7-28) cannot be exactly calculated because of the lack ofphase information, but the maximum and minimum values can be found. The maximum and minimum values of $10 \log|1 - \Gamma_g \Gamma_\ell|^2$ are called "mismatch uncertainty limits" and are given the symbol M_u. The maximum occurs when $\Gamma_g \Gamma_\ell$ combines with "one" in phase to yield:

$$M_{u\ max} = 10 \log (1 + \rho_g \rho_\ell)^2 \qquad (7\text{-}29)$$

This maximum limit will always be a positive number but it cannot be larger than 6 dB (this occurs when $\rho_\ell = \rho_g = 1$). The minimum value of the mismatch uncertainty occurs when $\Gamma_g \Gamma_\ell$ combines with "one" exactly out of phase to yield:

$$M_{u\ min} = 10 \log (1 - \rho_g \rho_\ell)^2 \qquad (7\text{-}30)$$

The minimum limit will always be a negative number. It is also true that the magnitude of the minimum limit will be greater than the magnitude of the maximum limit, but usually by a very small amount.

Sometimes the mismatch uncertainty limits are given in percent deviation from "one" rather than in dB. In this case:

$$\%M_u = 100 [(1 \pm \rho_g \rho_\ell)^2 - 1] \qquad (7\text{-}31)$$

Mismatch uncertainty limits can be calculated by substituting the values of ρ_ℓ and ρ_g into equations (7-29), (7-30), and (7-31).

Modern engineering electronic calculators have a series of programs available especially suited for electrical engineering problems. One of the programs is intended for calculating mismatch uncertainty limits, either in terms of SWR or of ρ. Computer-aided engineering models often contain routines for such transmission line calculations.

Mismatch loss and mismatch gain

Traditionally, the transmission power loss due to signal reflection was termed mismatch loss. This was done in spite of the fact that occasionally the two reflection coefficient terms would align in a phase that produced a small "gain." More recent usage finds the term mismatch gain more popular because it is a more inclusive term and can mean either gain (positive number) or loss (negative number). Similarly, it is more difficult to think of a negative mismatch loss as a gain. In this note, we use the terms interchangeably, with due consideration to the algebraic sign.

The second term on the right side of equation (7-26), $-10 \log (1 - |\Gamma_\ell|^2)$, is called mismatch loss. It accounts for the power reflected from the load. In power measurements, mismatch loss is usually taken into account when correcting for the calibration factor of the sensor, to be covered below.

The conjugate mismatch loss of equation (7-28) can be calculated, if needed. The uncertainty term is the same as the Z_o mismatch loss uncertainty term and the remaining terms are mismatch loss terms, one at the generator and one at the load. The term conjugate mismatch loss is not used much anymore. It was used when reflections were tuned out by adjusting for maximum power (corresponding to conjugate match). Now the various mismatch errors have been reduced to the point where the tedious tuning at each frequency is not worth the effort. In fact, modern techniques without tuning might possibly be more accurate because the tuners used to introduce their own errors that could not always be accounted for accurately.

Mismatch in power measurements generally causes the indicated power to be different from that absorbed by a reflection-less power sensor. The reflection from the power sensor is partially accounted for by the calibration factor of the sensor which is considered in the next chapter. The interaction of the sensor with the generator (the re-reflected waves) could be corrected only by knowledge of phase and amplitude of both reflection coefficients, Γ_ℓ and Γ_g. If only the standing wave ratios or reflection coefficient magnitudes ρ_ℓ and ρ_g are known, then only the mismatch uncertainty limits can be calculated. The mismatch uncertainty is combined with all the other uncertainty terms later where an example for a typical measurement system is analyzed.

Other sensor uncertainties

After mismatch uncertainty, the second source of error is the imperfect efficiency of the power sensor. There are two parameters that define the design efficiency of a sensor, effective efficiency and calibration factor. Although Agilent now furnishes only calibration factor data with its sensors, since both parameters are still available as measurement services for thermistor sensors from the National Institute of Standards and Technology, they will be reviewed here.

For a power sensor, the power input is the net power delivered to the sensor; it is the incident power minus the reflected power (Pi - Pr). However, not all that net input power is dissipated in the sensing element. Some might be radiated outside the transmission system or leaked into the instrumentation, some dissipated in the conducting walls of the structure, or in a capacitor component of the sensor, or a number of other places that are not metered by the instrumentation. The metered power indicates only the power that is dissipated into the power sensing element itself.

For metering, the dissipated high frequency power must go through a conversion process to an equivalent DC or low frequency level. The DC or low frequency equivalent is called P_{sub}, for substituted power. There are errors associated with the substitution process. In thermistor sensors, for example, errors result from the fact that the spatial distributions of current, power, and resistance within the thermistor element are different for DC and RF power.

To accommodate both the usual parasitic losses as well as the DC or low frequency substitution problem mentioned, a special term, effective efficiency η_e, has been adopted for power sensors. Effective efficiency is defined by:

$$\eta_e = \frac{P_{sub}}{Pg_\ell} \tag{7-32}$$

$P_{g\ell}$ is the net power absorbed by the sensor during measurement. P_{sub} is the substituted low frequency equivalent for the RF power being measured. For thermistor sensors P_{sub} is the change in bias power required to bring the thermistor back to the same resistance as before the application of RF power. For thermocouple and diode sensors, P_{sub} is the amount of power from a reference power source, at a specified frequency, when it yields the same voltage to the metering circuits as Pg_ℓ. The η_e normally changes with frequency, but changes with power level are usually negligible.

Effective efficiency is sometimes measured by the manufacturer when calibrating the sensor and furnished in a calibration chart with the product. Sometimes the data is printed on the label of the sensor, or delineated with dots on a label plot of efficiency. It is expressed in percentage and that factor is entered into the power meter by adjusting the analog dial to the appropriate number or entered digitally into digital power meters.

Calibration factor

There is another more frequently used term that has been defined for power measurements. It combines effective efficiency and mismatch loss and is called the calibration factor K_b. The K_b is defined by:

$$K_b = \frac{P_{sub}}{P_i} \tag{7-33}$$

where P_i is the incident power to the sensor. The accurate measurement of calibration factor K_b is quite involved and performed mainly by standards laboratories and manufacturers.

The definitions of K_b and η_e can be combined to yield

$$K_b = \eta_e \quad \frac{Pg_\ell}{P_i} \quad = \eta_e (1 - \rho_\ell{}^2) \tag{7-34}$$

where ρ_ℓ is the magnitude of the sensor reflection coefficient. The relationship on the right, which is found by substituting for P_i and Pg_ℓ from equations (7-19) and (7-21), shows that K_b is a combination of effective efficiency and mismatch loss.

Most modern power meters have the ability to correct their meter reading by setting a dial or keying in a digital number to the proper value of K_b. Then P_i is actually read off the meter. Values of K_b for various frequencies are indicated on each Agilent Technologies power sensor (except for the E series sensors which have the data stored on EEPROM). When this feature is used, the indicated or metered power P_m is (using equation 7-19):

$$P_m = \frac{Pg_{zo}}{K_b} = P_i = \frac{b_s{}^2}{1 - \Gamma_g\Gamma_\ell{}^2} \qquad (7\text{-}35)$$

But the desired quantity is usually not P_i to the sensor but Pg_{zo}, the power that would be dissipated in a Z_o load. Since P_{gZo} is by definition $|bs|^2$, the ratio of P_{gZo} to the meter indication is:

$$\frac{Pg_{zo}}{P_m} = 1 - \Gamma_\ell\Gamma_g{}^2 \qquad (7\text{-}36)$$

The right side of (7-36) is the mismatch uncertainty. Since the use of K_b corrects for efficiency and mismatch loss, only the mismatch uncertainty remains. It should be pointed out that there is an additional, unavoidable uncertainty associated with K_b. That uncertainty is due to inaccuracies in the measurement of K_b by the manufacturer, NIST or standards laboratories and thus the uncertainty of K_b is specified by the calibration supplier.

Power meter instrumentation uncertainties (including sensor)
There are a number of uncertainties associated within the electronics of the power meter. The effect of these errors is to create a difference between P_m and P_{sub}/K_b.

Reference oscillator uncertainty
Open-loop power measurements, such as those that use thermocouples or semiconductor diode sensors, require a known source of power to verify and adjust for the sensitivity of the sensor. Many power meters, such as the EPM and EPM-P, have a stable power reference built in. No matter what power reference is used, if it deviates from the expected power output, the calibration adjustment is in error. The uncertainty in the power output from the reference oscillator is specified by the manufacturer. Thermistor power measurements, being closed-loop and having no need for a reference oscillator, are free of this error.

Reference oscillator mismatch uncertainty
The reference oscillator has its own reflection coefficient at the operating frequency. This source reflection coefficient, together with that from the power sensor, creates its own mismatch uncertainty. Because the reference oscillator frequency is low, where the reflection coefficients are small, this uncertainty is small (approximately ±0.01 dB or ±0.2%).

Instrumentation uncertainty
Instrumentation uncertainty is the combination of such factors as meter tracking errors, circuit nonlinearities, range-changing attenuator inaccuracy, and amplifier gain errors. The accumulated uncertainty is guaranteed by the instrument manufacturer to be within a certain limit.

There are other possible sources of uncertainty that are, by nature or design, so small as to be included within the instrumentation uncertainty.

An example of one such error is the thermoelectric voltage that may be introduced by temperature gradients within the electronic circuits and interconnecting cables. Proper design can minimize such effects by avoiding junctions of dissimilar metals at the most sensitive levels. Another example is the small uncertainty which might result from the operator's interpolation of the meter indication.

±1 Count

Almost all modern power meters now provide digital readouts. Meters with digital output, however, contain a minor ambiguity in the least significant digit of ± one-half count. On some power meters, such as the EPM and EPM-P, this uncertainty is so small that it is absorbed in the instrumentation uncertainty. In some applications, such as relative power measurements or the ratio of two power measurements where most of the causes of instrumentation uncertainty do not affect the final result, this uncertainty is still applicable. In the case of relative power measurements, the uncertainty applies twice, once during the measurement of each power, for a total uncertainty of ± one count. One way of expressing the error is $1/P_{mant}$ where P_{mant} is the mantissa only of the meter indication. Another way is to find the relative power value of the least significant digit (lsd); the uncertainty is $\pm P_{lsd} / P_{ind}$. This uncertainty can be reduced by using an external digital voltmeter of greater resolution.

Zero set

In any power measurement, the meter must initially be set to "0" with no RF power applied to the sensor. Zero setting is usually accomplished within the power meter by introducing an offset voltage that forces the meter to read zero, by either analog or digital means. The offset voltage is contaminated by several sources including sensor and circuit noise. The zero set error is specified by the manufacturer, especially for the most sensitive range. On higher power ranges, error in zero setting is small in comparison to the signal being measured.

Zero carryover

Most modern power meters, as a matter of convenience, have internal circuitry that eliminates the need to zero set the power meter every time the power measurement range is changed. If the user zero sets on the most sensitive range, they are then able to measure power on whatever range is of interest without re-zeroing. The circuitry that allows the zero set to "carryover" to the other ranges may have slight offsets.

The EPM and EPM-P series meters are designed to not need considering zero carryover. The zero carryover for these meters is typically much less than the data-sheet specification and the automatic zero setting circuits operate more satisfactorily on the most sensitive range.

Noise

Noise is also known as short-term stability and it arises from sources within both the power sensor and circuitry. One cause of noise is the random motion of free electrons due to the finite temperature of the components. The power observation might be made at a time when this random fluctuation produces a maximum indication, or perhaps a minimum. Noise is specified as the change in meter indication over a short time interval (usually one minute) for a constant input power, constant temperature, and constant line voltage.

Drift

This is also called long-term stability and is mostly sensor induced. It is the change in meter indication over a long time (usually one hour) for a constant input power, constant temperature, and constant line voltage. The manufacturer may state a required warm-up interval. In most cases the drift is actually a drift in the zero setting. This means that for measurements on the upper ranges, drift contributes a very small amount to the total uncertainty. On the more sensitive ranges, drift can be reduced to a negligible level by zero setting immediately prior to making a reading.

Power linearity

Power measurement linearity is mostly a characteristic of the sensor. Deviation from perfect linearity usually occurs in the higher power range of the sensor. For thermocouple sensors, linearity is negligible except for the top power range of +10 to +20 dBm, where the deviation is specified at ±3%.

For a typical 8481D-series diode sensor, the upper power range of –30 to –20 dBm exhibits a specified linearity deviation of ±1%.

With their much wider dynamic power range, the new E series sensors exhibit somewhat higher deviations from perfect linearity. It is mostly temperature-driven effect and specifications are given for several ranges of temperature. For example, in the 25 ±5° C temperature range and the –70 to –10 dBm power range, the typical deviation from linearity is ±2% RSS.

Calculating total uncertainty

So far, only the individual errors have been discussed; now a total uncertainty must be found. This first description will use the traditional analysis for considering the individual uncertainties. It will be shortened to allow for later presentation of the recommended method for expressing uncertainties according to the ISO-based and U.S.-adapted considerations.

In some measurement applications, certain sources of error do not enter into the final uncertainty. An example of this is relative power measurement where the ratio of two power measurements is to be found. With proper procedure, the reference oscillator uncertainty affects the numerator and denominator in exactly the same way and therefore cancels out in the final result. In this same application, however, other errors might accumulate such as the ± half-count error.

Power measurement equation

The purpose of this section is to develop an equation that shows how a power meter reading, P_m, is related to the power a generator would deliver to a Z_o load, Pg_{zo} (figure 7-5). The equation will show how the individual uncertainties contribute to the difference between P_m and Pg_{zo}.

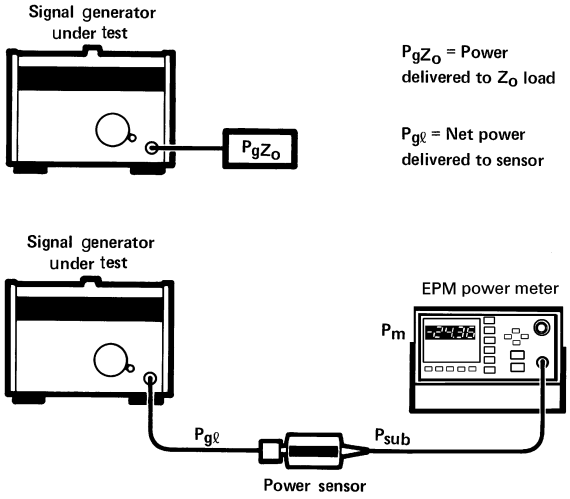

Figure 7-5. Desired power output to be measured is Pg_{zo} , but measurement results in the reading P_m.

Starting from the generator in lower part of figure 7-5, the first distinction is that the generator dissipates power Pg_ℓ in the power sensor instead of Pg_{zo} because of mismatch effects. That relationship, from (7-25) is:

$$Pg_{zo} = \frac{1 - \Gamma_\ell \Gamma_g \ ^2}{1 - \ \Gamma_\ell \ ^2} \ Pg_\ell \qquad (7\text{-}37)$$

The next distinction in figure 7-5 is that the power sensor converts $P_{g\ell}$ to the DC or low frequency equivalent, P sub, for eventual metering. However, this conversion is not perfect due to the fact that effective efficiency, η_e, is less than 100%. If Pg_ℓ is replaced by P_{sub} / η_e from equation (7-32), then (7-37) becomes:

$$Pg_{zo} = \ 1 - \Gamma_\ell \Gamma_g \ ^2 \quad \frac{}{\eta_e \ (1 - \rho_\ell^2 \ )} \ P_{sub} \qquad (7\text{-}38)$$

The first factor on the right is the mismatch uncertainty term, M_u, discussed previously. M_u is also referred to as “gain due to mismatch.” The denominator of the second factor is the calibration factor K_b from equation (7-34). Now (7-38) can be written:

$$Pg_{zo} = M_u \quad \frac{}{K_b} \ P_{sub} \qquad (7\text{-}39)$$

The last distinguishing feature of figure 7-5 is that the meter indication P_m, differs from P_{sub}. There are many possible sources of error in the power meter electronics that act like improper amplifier gain to the input signal P_{sub}. These include uncertainty in range changing attenuators and calibration-factor amplifiers, imperfections in the metering circuit and other sources totaled as instrumentation uncertainty. For open-loop power measurements this also includes those uncertainties associated with the calibration of amplifier gain with a power-reference oscillator. These errors are included in the symbol m for magnification.

There are other uncertainties associated with the electronics that cause deviation between P_m and P_{sub}. When P_{sub} is zero, then P_m should be zero. Improper zero setting, zero carryover, drift, and noise are likely contributors to P_m not being zero. The meter reading is offset or translated from mP_{sub} by a total amount t. A general linear equation gives P_m in terms of P_{sub}:

$$P_m = mP_{sub} + t \tag{7-40}$$

Substituting (7-40) into (7-39) gives the power measurement equation:

$$Pg_{zo} = \frac{M_u (P_m - t)}{K_b m} \tag{7-41}$$

In the ideal measurement situation, M_u has the value of one, the mK_b product is one, and t is zero. Under ideal conditions, meter reading P_m gives the proper value of Pg_{zo}.

Table 7-1. Chart of uncertainties for a typical absolute power measurement.

Measurement conditions:	**Pm = 50 µW** $\rho_\ell \leq 0.091$ ($SWR_\ell \leq 1.2$) K_b = 93% ± 3% (worst case), ±1.5% (RSS)	**Full scale (F.S.) = 100 µW** $\rho_g \leq 0.2$ ($SWR_g \leq 1.5$)		
Error	**Description**	**Worst case values**		**RSS component**
		P_{gZo} max	P_{gZo} min	$(\Delta X/X)^2$
M_u	$(1 \pm P_g P_\ell)^2$	1.0367	0.9639	$(0.0367)^2$
Kb uncertainty	±3% (w.c.), ±1.5% (RSS)	1.03	0.97	$(0.015)^2$
Components of m:				
Ref. Osc. Unc.	±1.2%	1.012	0.988	$(0.012)^2$
Ref. Osc. M_u	SWR_g = 1.05, SWR, = 1.1	1.002	0.998	$(0.002)^2$
Instrumentation	±0.5% of F.S.	1.01	0.99	$(0.01)^2$
Total m		1.0242	0.9762	
Components of t:				
Zero Set	±0.5% F.S. (low range)	+0.05 µW	-0.05 µW	$(0.001)^2$
Zero Carryover	±0.2% of F.S	+0.2 µW	-0.2 µW	$(0.004)^2$
Noise	±0.025 µW	+0.025 µW	-0.025 µW	$(0.0005)^2$
Total t		+0.275 µW	-0.275 µW	
Expressions of total uncertainty:				
P_{gZo} max	equation (7-44)	55.0421 µW		
P_{gZo} min	equation (7-45)		45.4344 µW	
ΔP_{gZo}		5.0421 µW	-4.5656 µW	
ΔP_{gZo} /Pm		+10.08%	-9.13%	$[0.001837)^{\frac{1}{2}}$ = ±4.3% +0.1823 dB
dB		0.4171 dB	-0.4159 dB	-0.1903 dB

Worst-case uncertainty

One method of combining uncertainties for power measurements in a worst-case manner is to add them linearly. This situation occurs if all the possible sources of error were at their extreme values and in such a direction as to add together constructively, and therefore achieve the maximum possible deviation between P_m and Pg_{zo}. Table 7-1 is a chart of the various error terms for the power measurement of figure 7-5. The measurement conditions listed at the top of table 7-1 are taken as an example. The conditions and uncertainties listed are typical and the calculations are for illustration only. The calculations do not indicate what is possible using the most accurate technique. The description of most of the errors is from a manufacturer's data sheet. Calculations are carried out to four decimal places because of calculation difficulties with several numbers of almost the same size.

Instrumentation uncertainty, i, is frequently specified in percent of full scale (full scale = P_{fs}). The contribution to magnification uncertainty is:

$$m_i = \frac{(1 + i)\, P_{fs}}{P_m} \tag{7-42}$$

The several uncertainties that contribute to the total magnification uncertainty, m, combine like the gain of amplifiers in cascade. The minimum possible value of m occurs when each of the contributions to m is a minimum. The minimum value of m (0.9762) is the product of the individual factors (0.988 * 0.998 * 0.99). The factors that contribute to the total offset uncertainty, t, combine like voltage generators in series; that is, they add. Once t is found, the contribution in dB is calculated from:

$$t_{dB} = 10 \log \left(1 \pm \frac{t}{P_m}\right) \tag{7-43}$$

The maximum possible value Pg_{zo} using (7-41) and substituting the values of table 7-1, is:

$$Pg_{zo\ max} = \frac{M_{u\ max}\,(P_m - t_{min})}{K_{b\ min}\, m_{min}} \tag{7-44}$$

$$= \frac{1.0367\ (50\ \mu W + 0.275\ \mu W)}{(0.97)\ (0.9762)}$$

$$= 55.0421\ \mu W = 1.1008\ P_m$$

In (7-44), the deviation of K_{bm} from the ideal value of one is used to calculate Pg_{zo} max. In the same way, the minimum value of Pg_{zo} is:

$$Pg_{zo\ min} = \frac{M_{u\ min}\,(P_m - t_{max})}{K_{b\ max}\, m_{max}} \tag{7-45}$$

$$= \frac{0.9639\ (50\ \mu W - 0.275\ \mu W)}{(1.03)\ (1.0242)}$$

$$= 45.4344\ \mu W = 0.9087\ P_m$$

The uncertainty in Pg_{zo} may be stated in several other ways:

(1) As an absolute differential in power:

$$\Delta Pg_{zo} = Pg_{zo}{}_{\substack{max \\ min}} - P_m = \begin{matrix} +5.0421 \\ -4.5656 \end{matrix} \mu W \qquad (7\text{-}46)$$

(2) As a fractional deviation:

$$\frac{\Delta Pg_{zo}}{P_m} = \frac{\begin{matrix} +5.0421 \\ -4.5656 \end{matrix}}{50} = \begin{matrix} +0.1008 \\ -0.0913 \end{matrix} \qquad (7\text{-}47)$$

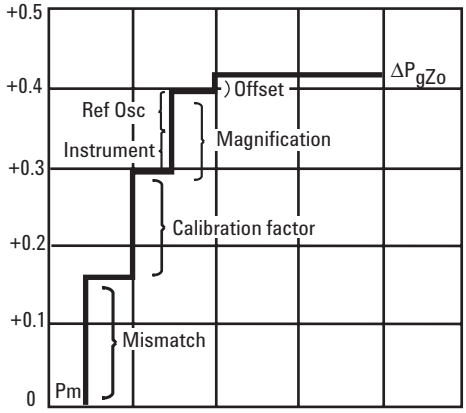

Figure 7-6. Graph of individual contributions to the total worst-case uncertainty.

(3) As a percent of the meter reading:

$$100 \quad \frac{\Delta Pg_{zo}}{P_m} = \begin{matrix} +10.08 \\ -9.13 \end{matrix} \% \qquad (7\text{-}48)$$

(4) As dB deviation from the meter reading:

$$dB = 10 \log \left(\begin{matrix} 1.1008 \\ 0.9087 \end{matrix} \right) = \begin{matrix} +0.4171 \\ -0.4159 \end{matrix} \ dB \qquad (7\text{-}49)$$

An advantage to this last method of expressing uncertainty is that this number can also be found by summing the individual error factors expressed in dB.

Figure 7-6 is a graph of contributions to worst-case uncertainty shows that mismatch uncertainty is the largest single component of total uncertainty. This is typical of most power measurements. Magnification and offset uncertainties, the easiest to evaluate from specifications and often the only uncertainties evaluated, contribute less than one-third of the total uncertainty.

RSS uncertainty

The worst-case uncertainty is a very conservative approach. A more realistic method of combining uncertainties is the root-sum-of-the-squares (RSS) method. The RSS uncertainty is based on the fact that most of the errors of power measurement, although systematic and not random, are independent of each other. Since they are independent, it is reasonable to combine the individual uncertainties in an RSS manner.

Finding the RSS uncertainty requires that each individual uncertainty be expressed in fractional form. The RSS uncertainty for the power measurement equation (7-41) is:

$$\frac{\Delta Pg_{zo}}{Pg_{zo}} = \left[\left(\frac{\Delta M_u}{M_u}\right)^2 + \left(\frac{\Delta K_b}{K_b}\right)^2 + \left(\frac{\Delta m}{m}\right)^2 + \left(\frac{\Delta t}{P_m}\right)^2 \right]^{1/2} \quad (7\text{-}50)$$

Each of the factors of (7-50), if not known directly, is also found by taking the RSS of its several components. Thus:

$$\frac{\Delta m}{m} = \left[\left(\frac{\Delta m_1}{m_1}\right)^2 + \left(\frac{\Delta m_2}{m_2}\right)^2 + \bullet \bullet \bullet \right]^{1/2} \quad (7\text{-}51)$$

Where m_1, m_2, and so forth are the reference oscillator uncertainty, the instrumentation uncertainty, and so forth of table 7-1. The extreme right hand column of table 7-1 shows the components used to find the total RSS uncertainty. The result is ±4.3%, which is much less than the worst case uncertainty of +10.1%, –9.1%. One characteristic of the RSS method is that the final result is always larger than the largest single component of uncertainty.

New method of combining power meter uncertainties

This section will describe a new method of combining uncertainties for power measurements. It is extended from the traditional uncertainty model, to follow a new guideline published by the American National Standards Institute and the NCSL International. The methods described in this document, ANSI/NCSL Z540-2-1996, *U.S. Guide to the Expression of Uncertainty in Measurement*, are now being implemented for many metrology applications in industry and government. This method is a derivative of the ISO uncertainty process described at the beginning of this chapter. Agilent has established a policy to transition to these new processes for determining measurement uncertainties for its product specifications.[4,5,6,7]

Generally, the impact of the ANSI\NCSL Z540-2-1996 is to inject a little more rigor and standardization into the metrology analysis. Traditionally, an uncertainty was viewed as having two components, namely, a random component and a systematic component. Random uncertainty presumably arises from unpredictable or stochastic temporal and spatial variations of influence quantities. Systematic uncertainty arises from a recognized effect or an influence which can be quantified.

The Z540-2-1996 groups uncertainty components into two categories based on their method of evaluation, Type “A” and Type “B.” These categories apply to uncertainty, and are not substitutes for the words “random” and “systematic.” Some systematic effects may be obtained by a Type A evaluation while in other cases by a Type B evaluation. Both types of evaluation are based on probability distributions. The uncertainty components resulting from either type are quantified by variances or standard deviations.

Briefly, the estimated variance characterizing an uncertainty component obtained from a Type A evaluation is calculated from a series of repeated measurements and is the familiar statistically estimated variance. Since standards laboratories regularly maintain histories of measured variables data on their standards, such data would usually conform to the Type A definition.

For an uncertainty component obtained from a Type B evaluation, the estimated variance, u^2, is evaluated using available knowledge. Type B evaluation is obtained from an assumed probability density function based on the belief that an event will occur, often called subjective probability, and is usually based on a pool of comparatively reliable information. Others might call it “measurement experience.” Published data sheet specifications from a manufacturer would commonly fit the Type B definition.

Power measurement model for ISO process

Beginning with the measurement equation of (7-41), and including power sensor linearity term P_ℓ,

$$Pg_{zo} = \frac{M_u\,(P_m - t)}{P_\ell K_b m} \tag{7-52}$$

The determination of m is through the calibration process. During calibration, Pg_{zo} is set to the known power, P_{cal}. Substituting P_{cal} for Pg_{zo} and rearranging equation (7-52), equation for m is:

$$m = \frac{M_{uc}\,(P_{mc} - t)}{K_c P_{cal}} \tag{7-53}$$

where:

m = power meter gain term
M_{uc} = gain due to the mismatch between the sensor and the internal calibration power source
P_{mc} = power level indicated by the power meter during calibration
t = power meter zero offset
K_c = power sensor calibration factor at the calibration frequency
P_{cal} = power delivered to a Z_o load by the power meter calibration output

In equations (7-52) and (7-53), t represents the power meter zero offset. In AN64-1, t is described as the sum of the zero set value, Z_s, zero carryover, Z_c, Noise, N, and Drift, D. However, assuming the zero procedure occurs just prior to calibration, D is zero during calibration, whereas D is non-zero during power meter measurements. To allow t to represent the same quantity in the equation for P_{gZo} and m, the equation for t is defined as:

$$t = Z_s + Z_c + N \tag{7-54}$$

where,
Z_s = power meter zero set value
Z_c = power meter zero carryover value
N = power meter noise

and the equation for P_{gZo} is redefined as

$$P_{gZo} = \frac{M_u\,(P_m - (t+D))}{P_\ell K_b m} \tag{7-55}$$

where D = power meter drift.

Equation (7-55) is the measurement equation for a power meter measurement. There are eleven input quantities that ultimately determine the estimated value of Pg_{zo}. These are M_u, P_m, D, K_b from equation (7-55); Z_s, Z_c, N from equation (7-54); and M_{uc}, P_{mc}, K_c, and P cal from equation (7-53). It is possible to combine equations in order to represent Pg_{zo} in terms of the eleven defined input quantities. This is a relatively complicated derivation, but the result is the uncertainty in terms of the eleven quantities:

$$u^2(Pg_{zo}) = Pg_{zo}^2 \left[\frac{u^2(M_u)}{M_u^2} + \frac{u^2(P_m)}{(P_m - (t + D))^2} + \frac{u^2(D)}{(P_m - (t + D))^2} + \frac{u^2(K_b)}{K_b^2} + \frac{u^2(M_{uc})}{M_{uc}^2} + \frac{u^2(P_{mc})}{(P_{mc} - t)^2} + \frac{u^2(K_c)}{K_c^2} + \frac{u^2(P_{cal})}{P_{cal}^2} + \left(\frac{1}{(P_m - (t+D))^2} + \frac{1}{(P_{mc} - t)^2} - \frac{2}{K_c P_{cal} m (P_m - (t+D))} \right) \left(u^2(Z_s) + u^2(Z_c) + u^2(N) \right) \right] \quad (7\text{-}56)$$

Solving with some nominal values of several input quantities simplifies equation (7-56),

$M_u = 1$
$M_{uc} = 1$
$P_{mc} = P_{cal}$
$Z_s = 0$
$Z_c = 0$
$N = 0$
$D = 0$
$t = 0$
$m = 1/K_c$

$$\frac{u^2(Pg_{zo})}{Pg_{zo}^2} = u^2(M_u) + \frac{u^2(P_m)}{P_m^2} + \frac{u^2(D)}{P_m^2} + \frac{u^2(K_b)}{K_b^2} + u^2(M_{uc}) + \frac{u^2(P_{mc})}{P_{mc}^2} + \frac{u^2(K_c)}{K_c^2} + \frac{u^2(P_l)}{P_l^2} + \frac{u^2(P_{cal})}{P_{cal}^2} + \left(\frac{1}{P_m} - \frac{1}{P_{cal}} \right)^2 (u^2(Z_s) + u^2(Z_c) + u^2(N)) \quad (7\text{-}57)$$

The following table 7-2 summarizes the various uncertainties shown in 7-57.

Table 7-2. Standard uncertainties for the Z540-2 process.

Standard uncertainty	Source
u(Mu)	Mismatch gain uncertainty between the sensor and the generator. The standard uncertainty is dependent upon the reflection coefficients of the sensor and the generator. Refer to the mismatch model. Reflection coefficients may have different distributions as shown in figure 7-9.
u(Muc)	Mismatch gain uncertainty between the sensor and the calibrator output of the power meter. The standard uncertainty is dependent upon the reflection coefficients of the sensor and the calibrator output. Refer to the mismatch model. Note: the calibrator output reflection coefficient is not a specified parameter of the E4418A power meter. AN64-1 suggests $\rho_g = 0.024$.
u(Pm)	Power meter instrumentation uncertainty.
u(Pmc)	Power meter instrumentation uncertainty (during calibration)
u(D)	Power meter drift uncertainty.
u(Kb)	Sensor calibration factor uncertainty. Typically, the value of the uncertainty is reported along with the calibration factor by the calibration laboratory or the manufacturer.
u(Kc)	Sensor calibration factor uncertainty at the frequency of the power meter calibrator output. If the sensor is calibrated relative to the associated calibrator output frequency, $K_c = 1$ and $u(K_c) = 0$.
$u(P_\ell)$	Power sensor linearity, which is related to power range. Generally negligible on lower ranges but has higher uncertainty at high power levels.
u(Pcal)	Calibrator output power level uncertainty.
u(Zs)	Power meter zero set uncertainty.
u(Zc)	Power meter zero carryover uncertainty.
u(N)	Power meter and sensor noise uncertainty.

Standard uncertainty of the mismatch model

The standard uncertainty of the mismatch expression, $u(M_u)$, assuming no knowledge of the phase, depends upon the statistical distribution that best represents the moduli of Γ_g and Γ_ℓ.

Combining equation (7-21) and (7-22), the power dissipated in a load when Γ_ℓ is not 0 is:

$$P_d = Pg_{zo} \quad \frac{1 - |\Gamma_\ell|^2}{|1 - \Gamma_g \Gamma_\ell|^2} \tag{7-58}$$

The numerator in (7-58) is known as mismatch loss, and the denominator represents the mismatch uncertainty:

$$M_u = |1 - \Gamma_g \Gamma_\ell|^2 \tag{7-59}$$

M_u is the gain or loss due to multiple reflections between the generator and the load. If both the moduli and phase angles of Γ_g and Γ_ℓ are known, M_u can be precisely determined from equation (7-59). Generally, an estimate of the moduli exists, but the phase angles of Γ_g and Γ_ℓ are not known.

Consider two cases:
Case (a): Uniform Γ, uniform phase distribution.
See figure 7-7 (a). The moduli of Γ_g and Γ_ℓ are each less than a specified value; Γ_g and Γ_ℓ each lie within a circle of radius, Γ. Assuming Γ_g and Γ_ℓ have equal probability of lying anywhere within the circle, the standard uncertainty of M_u is: (This results in uniform density.)

$$u(M\ u\ ) = \frac{1}{\sqrt{2}} \text{ x maximum } |\Gamma_g| \text{ x maximum } |\Gamma_\ell|$$

Case (b): Constant ρ, uniform phase distribution.
See figure 7-7 (b). An estimate of the moduli of Γ_g and Γ_ℓ are known; Γ_g and Γ_ℓ each lie on a circle of radius Γ. Assuming Γ_g and Γ_ℓ have equal probability of lying anywhere on the circle, (equal probability of any phase), the standard uncertainty of M_u is:[8]

$$u(M_u) = \sqrt{2} \text{ x } |\Gamma_g| \text{x} |\Gamma_\ell|$$

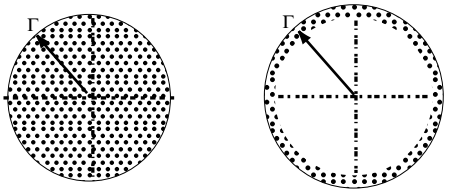

Figure 7-7. When the reflection coefficients of the generator and load are not known, the user may estimate probabilities of the mismatch uncertainty according to these two cases: (a) both Γ lie inside the circle with uniform density. (b) both Γ lie on the circle with uniform phase density.

Example of calculation of uncertainty using ISO model

Recognizing that each uncertainty calculation must meet a particular measuring requirement, the user will need to structure their calculations for appropriate conditions. This following measurement situation reflects some assumed and stated conditions for each of the parameters. The power meter is assumed to be the E4418B power meter, and the power sensor is assumed to be the E9300A power sensor.

Measurement conditions for calculation: Unknown CW power, 2 GHz, 50 microwatt level (–13 dBm).

Calculation comments for each parameter:

$u(M_u)$ Uncertainty of mismatch gain between sensor and generator at 2 GHz. Use case (a) and assume generator reflection coefficient specification (from data sheet) is $|\Gamma_g| = 0.1$ (uniform density distribution). Assume the E9300A sensor cal data shows a measured value of $|\Gamma_s| = 0.1$ (uniform distribution of phase).

Use mismatch gain equation of $M_u = |1 \pm \Gamma_g \Gamma_s|^2$
Since each Γ has a different distribution, use a Monte Carlo simulation.

$$\frac{u(M_u)}{M_u} = 0.1 \text{ x } 0.1 \text{ x } \frac{1}{\sqrt{2}} = 0.7\% \text{ (1–sigma)}$$

$u(M_{uc})$ Uncertainty of mismatch gain between sensor and 50 MHz calibrator source. Use case (a) and assume source reflection coefficient specification (from data sheet) is $|\Gamma_g| = 0.024$. E9300A sensor cal data shows a measured value of $|\Gamma_s| = 0.1$ (uniform distribution of phase). Use mismatch gain equation as above.

$$\frac{u(M_{uc})}{M_{uc}} = 0.024 \text{ x } 0.1 \text{ x } \frac{1}{\sqrt{2}} = 0.17\% \text{ (1–sigma)}$$

$u(P_m)$ E4418B power meter instrumentation uncertainty is specified at ± 0.5% (rectangular distribution). Use $\sqrt{3}$ for divisor.

$$\frac{u(P_m)}{P_m} = \frac{0.005}{\sqrt{3}} = 0.3\% \text{ (1–sigma)}$$

$u(P_{mc})$ E4418B power meter uncertainty during calibration. Specified at ±0.5% (rectangular distribution).

$$\frac{u(P_{mc})}{P_{mc}} = \frac{0.005}{\sqrt{3}} = 0.3\% \text{ (1–sigma)}$$

$u(D)$ E4418B power meter drift uncertainty due to sensor drift. Assume constant temperature, measurement taken one hour after calibration. From data sheet E9300A sensors are ±150pW (rectangular distribution).

$$\frac{u(D)}{P_m} = \frac{150 \times 10^{-12}}{50 \times 10^{-6}} \times \frac{1}{\sqrt{3}} = 0.017\% \text{ (1–sigma)}$$

$u(K_b)$ E9300A power sensor calibration factor uncertainty at 2 GHz. From the calibration certificate, specification is ±1.7% (Gaussian distribution, 2-sigma).

$$\frac{u(K_b)}{K_b} = \frac{0.017}{2} = 0.85\% \text{ (1–sigma)}$$

$u(K_c)$ E9300A power sensor cal factor uncertainty at 50 MHz is assumed to be 0 since it is referred to the internal calibration source.

$$\frac{u(K_c)}{K_c} = 0$$

$u(P_l)$ E9300A power sensor linearity uncertainty. For the 100 µW assumed range, this is specified for 25 ±10°C as ±3% (assume Gaussian distribution is 2←sigma).

$$\frac{u(P_1)}{P_1} = \frac{0.03}{2} = 1.5\% \text{ (1–sigma)}$$

$u(P_{cal})$ 50 MHz calibrator power reference output uncertainty is specified at 0.9%, RSS, for 1 year. Guassian distribution is 2←sigma.

$$\frac{u(P_{cal})}{P_{cal}} = \frac{0.009}{2} = 0.45\% \text{ (1–sigma)}$$

$u(Z_s)$ E4418B power meter zero set uncertainty is specified at ±500pW (rectangular distribution).

$$u(Z_s)\left(\frac{1}{P_m} - \frac{1}{P_{cal}}\right) = \left(\frac{1}{50 \times 10^{-6}} - \frac{1}{10^{-3}}\right) \times \frac{500 \times 10^{-12}}{\sqrt{3}} = 0.0005\% \text{ (1–sigma)}$$

$u(Z_c)$ E4418B power meter zero carryover is included in the overall instrument uncertainty specification, since there are no ranges as such in this meter. For other power meters this would need to be considered.

$$u(Z_c)\left(\frac{1}{P_m} - \frac{1}{P_{cal}}\right) = 0$$

u(N) E4418B power meter noise uncertainty is ±700 pW and negligible at the 50 mW power level.

$$u(N)\left(\frac{1}{P_m} - \frac{1}{P_{cal}}\right) = \left(\frac{1}{50 \times 10^{-6}} - \frac{1}{10^{-3}}\right) \times \frac{700 \times 10^{-12}}{\sqrt{3}} = 0.0007\% \text{ (1–sigma)}$$

Using the above comments, table 7-3 summarizes the various uncertainty factors. Each factor is normalized to a one sigma value. In the case of a data sheet specification, the divisor factor used to convert to one sigma is square root of three. These sigma values are added in RSS fashion and then multiplied with the coverage factor. The coverage factor is a guard band number, typically two is used, but experience and knowledge of the measurement process allows for the user to establish any other value.

Table 7-3. Worksheet for uncertainties calculation using ISO process.

Symbol	Source of uncertainty	Value ±%	Probability distribution	Divisor	D(Kx)
Mu	Mismatch gain between generator and sensor	$\|\Gamma_g\| = 0.1$ $\|\Gamma_s\| = 0.1$	$\|\Gamma_g\|$ - uniform density $\|\Gamma_s\|$ - uniform phase	(1)	0.7%
Muc	Mismatch gain between calibration source and sensor	$\|\Gamma_g\| = 0.024$ $\|\Gamma_s\| = 0.1$	$\|\Gamma_g\|$ - uniform density $\|\Gamma_s\|$ - uniform phase	(1)	0.17%
Pm	Power meter instrumentation	0.5%	rectangular	$\sqrt{3}$	0.29%
Pmc	Power meter instrumentation during calibration	0.5%	rectangular	$\sqrt{3}$	0.29%
D	Power meter drift	±150 pW	rectangular	$\sqrt{3}$	0.017%
Kb	Sensor calibration factor	1.7%	Gaussian	2	0.85%
Kc	Sensor calibration factor at 50 MHz	0	rectangular	—	0
Pl	Power sensor linearity	3.0%	Gaussian	2	1.5%
Pcal	Calibrator output power	0.9%	Gaussian	2	0.45%
Zs	Power meter zero set	±500 pW	rectangular	$\sqrt{3}$	0.0005%
Zc	Power meter zero carryover	0	rectangular	$\sqrt{3}$	0
N	Power meter and sensor noise	±700 pW	rectangular	$\sqrt{3}$	0.0007%
	Combined uncertainty—RSSed				1.94%
	Expanded uncertainty		Coverage factor K = 2		3.88%

(1) Monte Carlo simulation

1. "ISO Guide to the Expression of Uncertainty in Measurement," International Organization for Standardization, Geneva, Switzerland, ISBN 92-67-10188-9, 1995.
2. ANSI/NCSL Z540-2-1996, "U.S. Guide to the Expression of Uncertainty in Measurement," National Conference of Standards Laboratories, Boulder, CO 80301, 1996.
3. K. Kurakawa, "Power Waves and the Scattering Matrix," IEEE Trans. on Microwave Theory and Techniques, Vol. 13, No. 2, Mar 1965.
4. N.J. Kuhn, "Simplified Signal Flow Graph Analysis," *Microwave Journal*, Vol 6, No 10, Nov. 1963.
5. NAMAS NIS 3003, "The Expression of Uncertainty and confidence in Measurement for Calibrations," Edition 8, NAMAS Executive, National Physical Laboratory, Teddington, TW11 0LW, England, 1995.
6. B. N. Taylor and C. E. Kuyatt, "Guidelines for Evaluating and Expressing the Uncertainty of NIST Measurement Results," NIST Technical Note 1297, National Institute of Standards and Technology.
7. NCSL Recommended Practice RP-12, "Determining and Reporting Measurement Uncertainties," National Conference of Standards Laboratories.
8. I.A. Harris and F.L. Warner, "Re-examination of Mismatch Uncertainty when Measuring Microwave Power and Attenuation," Proceedings of the British IEE, Vol 128, pp 35-41, Feb 1981.

VIII. Power Measurement Instrumentation Compared

All the previous discussion about the theory and practice of power measurement equipment still leaves an important question for the user: which power meter and sensor technology should be used for a particular power measurement? As was seen earlier, each method of measuring average power has some advantages over the others, so the answer to that question becomes dependent on the particular measurement situation. Factors such as cost, frequency range, the range of power levels to be measured, the importance of processing and capturing data, accuracy, speed of measurement, and the skill of the personnel involved take on varying degrees of importance in different situations. This chapter compares the measurement systems from several aspects to aid in the decision-making process for any application. At the end, an applications chart profiles sensors best suited for particular modulation formats. Other charts briefly review the measurement capabilities of the sensor and power meter families now available from Agilent.

Accuracy vs. power level

The first comparison of power measuring systems demonstrates the measurement uncertainty and power range of several equipment selections. The EPM series power meters and E series sensors were emphasized, although several existing sensors were included. The EPM-P peak and average meters and sensors were not included in this comparison exercise since they require other considerations outlined in Chapter VI.

Figure 8-1 shows plots of the RSS uncertainty when measuring power at various levels from –70 to +20 dBm. The measurement conditions were assumed for a CW signal at 2 GHz and a source SWR of 1.15, and data sheet specifications.

The three parts of this figure are divided to show a comparison of three common combinations of power meter and sensor:

a) 432A analog power meter plus 8478B thermistor sensor.

b) E4418B digital power meter plus existing 8481A thermocouple and 8484D diode sensor.

c) E4418B digital power meter plus E4412A extended dynamic range power sensor.

The data for figure 8-1 was computed using a commercially-available mathematics simulation software product called MathCad. To present these operating performances under typical present-day conditions, the ISO uncertainty combining process of Chapter VII was used for the MathCad calculations. Results are approximate, although they are entirely suitable for these comparison purposes.

The reason for presenting these overall measurement uncertainties in this format is that, as far as the user is concerned, there is little need to know whether the sensor works on the diode principle or on the thermocouple principle. And, with the introduction of the new extended-range PDB diode sensors, a single E4412A sensor can achieve the 70 to +20 dBm power range, which previously required a combination of diode and thermocouple sensors.

The top graph of figure 8-1 describes the thermistor sensor/meter combination and is shown mostly for reference. With the decreasing applications of thermistor-type sensors, the primary need for understanding their theory and practice is that they are used as power transfer devices for metrology round robins or for transferring a power reference from a higher-accuracy echelon or national standards labs to operating labs. In the DC substitution process, 432 instrumentation error is substantially reduced because the substitution DC power is measured with precision digital voltmeters.

A comparison of the top two graphs of figure 8-1 (A) and (B), shows that the uncertainties of the thermocouple and diode-based systems (B) are somewhat less than the thermistor-based systems (A). At this 2 GHz calculation frequency, the thermocouple and diode sensors have the better SWR (see figure 8-2), but the thermistor system, being a DC substitution system, does not require a power reference oscillator and its small added uncertainty. These two effects tend to offset each other for this application. The significant advantage of the E4418B power meter measurement is the flexibility of being able to use the installed base of all the other Agilent family of thermocouple and diode sensors.

The third graph of figure 8-1 (C), for the E4418B power meter and E4412A extended dynamic range sensor, immediately shows that even with its wide dynamic measurement range from –70 to +20 dBm, it provides approximately equivalent uncertainties. The dashed portion of the E-series sensor curve (0 to +20 dBm) represents nominal high-power cal factor uncertainty limitations imposed by the sensor, meter, and the calibration system. Refer to the latest sensor technical specifications to determine actual uncertainties for your particular application.

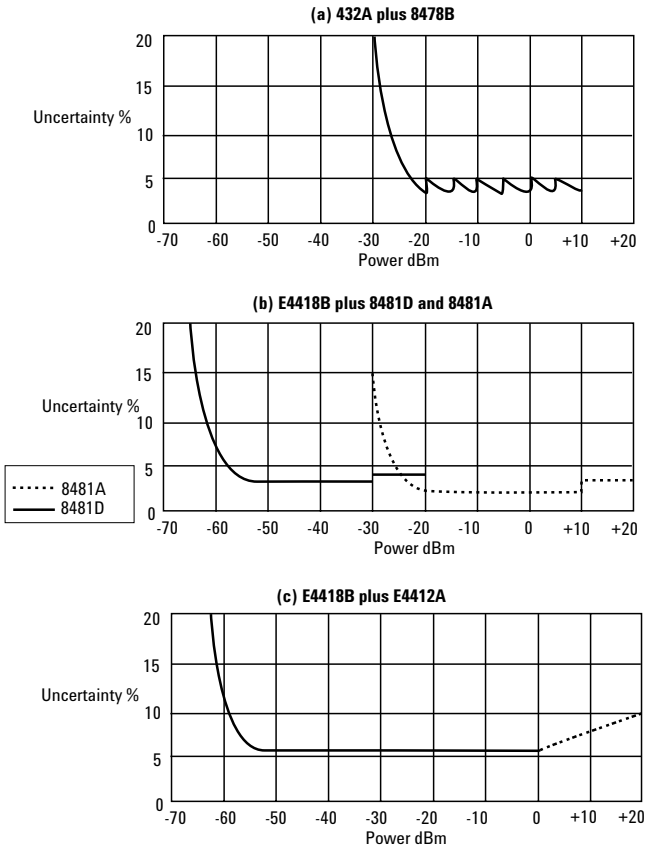

Figure 8-1. RSS uncertainty vs. dynamic power range from data sheet specs for source SWR = 1.15 (ρs =0.07) and f = 2 GHz: (a) Analog thermistor mount system. (b) E4418B digital power meter system using 8481D diode and 8481A thermocouple sensors. (c) E4418B digital power meter and E4412A PDB extended-range sensor. RSS-combining method is the same as used in Chapter VII.

While most modern power meter designs have utilized digital architectures, analog-based meters, such as the 432A, are still available. Analog meter measurements are limited by the mechanical meter movement of the instrument which requires uncertainty to be stated in percent of full scale. Thus, at the low end of each range, the uncertainty becomes quite large when expressed as a percent of the reading. Digital systems are free of those problems and, with proper design and an adequate digital display resolution, provide better accuracy.

The instrumentation accuracy for a digital meter is specified as a percent of the reading instead of as a percent of full scale. This means that at the point of each range change, there is not a big change in accuracy for the digital meter. This effect can be seen in the max-min excursions of the sawtooth-like curves of the analog meter shown in figure 8-1 (A). For this reason, the digital power meter does not need as many ranges; each digital range covers 10 dB with little change in accuracy across the range.

One application advantage attributed to analog meters is the "tweaking" functions where an operator must adjust some test component for optimum or maximum power. Digital displays are notoriously difficult to interpret for "maximum" readings, so modern digital meters usually contain a simple "peaker" analog meter. The display of the E4418B power meter features an analog scale in graphic display format, which provides that "virtual-peaking" function.

It should be recognized that the accuracy calculations of figure 8-1 (arc) are based on specification values. Such specifications are strongly dependent on the manufacturers' strategy for setting up their specification budget process. Some published specifications are conservative, some are less so. Manufacturers need to have a good production yield of instruments for the whole family of specifications, so this often leads to a policy of writing specifications that have generous "guard bands" and thus are more conservative.

Further, a particular measurement configuration is likely to be close to one specification limit, but easily meet another specification; a second system might reverse the roles. By using the new ISO RSS-uncertainty-combining method, this takes advantage of the random relationship among specifications and the uncertainties tend to be smaller, yet realistic.

A second reason to observe is that the figure 8-1 calculations are done for one particular frequency (2 GHz) and one particular source SWR (1.15). A different frequency and different source match would give a different overall uncertainty. Sources frequently have larger reflection coefficient values which would raise the overall uncertainty due to usually-dominant mismatch effects.

Frequency range and SWR (reflection coefficient)

All three types of power sensors have models that cover a frequency range from 10 MHz to 18 GHz, some higher, with coaxial inputs. A special version of the thermistor mount operates down to 1 MHz (see Chapter III) and the 8482A/H thermocouple power sensors operate down to 100 kHz. The effective efficiency at each frequency is correctable with the Calibration Factor dial or keyboard of the power meter, so that parameter is not particularly critical in deciding on a measurement system.

The sensor's SWR performance is most important because mismatch uncertainty is usually the largest source of error, as described in Chapter VII. Figure 8-2 shows a comparison of the specification limits for the SWR of a thermistor mount, a thermocouple power sensor, an 8481D PDB diode power sensor, as well as the E-series power sensors. It should be recognized that published SWR specifications are usually conservative and that actual performance is often substantially better, yielding lower uncertainty in practice. That fact argues for a measurement process that measures actual source SWR for situations where highest accuracy is important. These graphs indicate that over the bulk of the frequency range, the thermocouple and diode sensors have a considerably-lower SWR than the thermistor sensor. It also shows that the E4412A sensor, even with its superior dynamic range, still provides a satisfactory SWR.

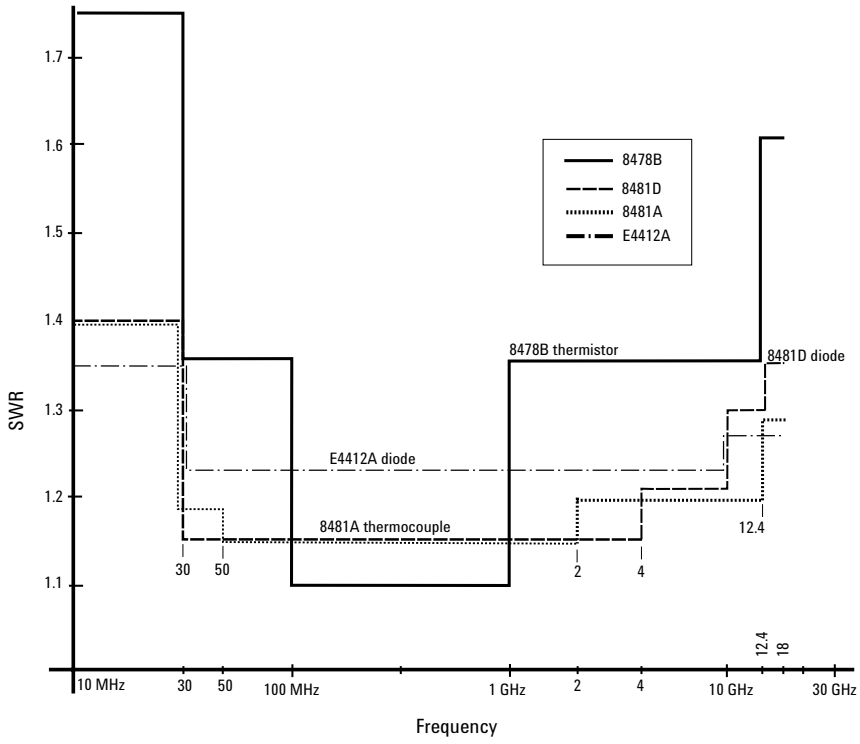

Figure 8-2. A comparison of specified SWR limits for the 8478B thermistor mount, 8481A thermocouple power sensor, 8481D PDB power sensor, and E4412A PDB sensor.

Waveguide sensor calibration

Power measurements in waveguide present several special considerations. Waveguide thermocouple and diode sensors must have the usual 50 MHz reference oscillator to adjust for calibration factor from one sensor to another. Such a low-frequency signal cannot propagate in a waveguide mode. Agilent waveguide thermocouple sensors (26.5 to 50.0 GHz) and waveguide diode sensors (26.5 to 50.0 GHz and 75 to 110 GHz) all utilize a special 50 MHz injection port that applies the reference oscillator output to the sensor element in parallel to the usual waveguide input. This permits the meter-sensor system to be calibrated at their waveguide operating frequencies.

Speed of response

To measure the lowest power ranges with optimum accuracy, power meters are designed with a highly-filtered, narrow bandwidth compared to most other electronic circuits. Narrow band circuits are necessary to pass the desired power-indicating signal but reject the noise that would obscure a weak signal. Narrow bandwidth leads to the long response time. For heat responding power sensors, like the thermistor and thermocouple, response time is also limited by the heating and cooling time constants of the heat sensing element. The typical thermistor power measurement has a 35 millisecond time constant and 0 to 99 percent response time of about five time constants or 0.175 seconds. The power meters for thermocouple and PDB sensors have 0 to 99 percent response times of 0.1 to 10 seconds, depending on the range of the power meter. The more sensitive ranges require more averaging and hence longer settling times.

For manual measurements, the speed of response is seldom a problem. By the time the observer turns on the RF power and is ready to take data, the power meter has almost always reached a steady reading.

For analog systems applications, where rapid data acquisition is required, or where the power meter output is being used to control other instruments, the power meter acts like a low pass filter. The equivalent cutoff frequency of the filter has a period roughly the same as the 0 to 99 percent response time. For signals where the power changes too rapidly for the power meter to respond, the power meter averages the changing power. When a power meter is being used to level the output of a signal generator whose frequency is being swept, the speed of the frequency sweep may have to be reduced to allow the power meter time to respond to the power level changes.

There is no clear-cut advantage with regard to speed of one power measurement system over another. In some power ranges one system is faster, and in other ranges another system is faster. If response time is important, manufacturers' data sheets should be compared for the particular application.

Automated power measurement

Recognizing that a large percentage of digital power meters are used in production test and in automated systems, it is reasonable to assume that digitizing measurement speed is critical in at least some of those applications. Digital power meters programmed for automatic operation gather data rapidly and with minimum errors. The data can be processed and analyzed according to programmed instructions, and the system can be operated with little process attention. Even in a manual mode, digital indications are less prone to the human error of misinterpreting the meter scale and using wrong range multipliers. In the case of power measurement, there are additional advantages to automatic systems. Successive data points can be compared mathematically to assure that the power measurement has reached steady state and multiple successive readings can be averaged to statistically reduce the effects of noise.

The EPM-series power meters have been optimized for maximum digitizing speed. Since its architecture is totally DSP-based, and it is married to a new E-series diode sensors, circuit decisions were made to increase the digitizing speed to maximum. For example, output filtering on the sensor is smaller, which provides faster response. On the lower power ranges, this smaller filtering might cause an increase in measurement noise, but the power meter itself provides for digital averaging up to 1,024 readings to minimize noise effects. The meter is specified to provide up to 20 readings per second and 40 per second in the X2 mode. 200 readings per second are specified for the FAST range in the free-run trigger mode, using the binary output format. For that function, circuit settling times are 5 mS for the top 70 dB power ranges.

The EPM-P power meters have advanced their measuring speed another step. Partly because their peak and average sensors have wider video bandwidth, and partly because of higher-speed DSP circuitry, they can provide measurements up to 1000 readings per second. Further, because they internally compute parameters like peak-to-average ratio, important production measurement requirements are easier to meet.

Susceptibility to overload

The maximum RF power that may be applied to any power sensor is limited in three ways. The first limit is an average power rating. Too much average power usually causes damage because of excessive accumulated heat. The second limit is the total energy in a pulse. If the pulse power is too high for even a very short time, in spite of the average power being low, the pulses cause a temporary hot spot somewhere in the sensor. Damage occurs before the heat has time to disperse to the rest of the sensor. The third limit is peak envelope power. This limit is usually determined by voltage breakdown phenomena that damages sensor components. The limits are usually stated on the manufacturer's data sheet. None of the three limits should be exceeded. The power limits of any sensor may be moved upward by adding an attenuator to pre-absorb the bulk of the power. Then the power limits are likely to be dictated by the attenuator characteristics, which, being a passive component, are often fairly rugged and forgiving.

Table 8-1 shows that the 8481H power sensor, which consists of a 20-dB attenuator integrated with a thermocouple sensor element, excels in all respects. One characteristic, which might be important but not obvious from the chart, is the ratio of maximum average power to the largest measurable power. The 8481D PDB sensor can absorb 100 mW (+20 dBm) of average power, while the high end of its measurement range is 10 µW (20 dBm). This means that the PDB is forgiving in situations where the power level is accidentally set too high. A mistake of 10 dB in setting a source output attenuator, during a measuring routine will merely cause an off-scale reading for the 8481D. The same mistake might damage the other sensors. Excessive power is, by far, the primary cause of power sensor failure.

Although intended for handling pulsed signals, peak and average sensors, typified by the E9320A sensor, are not necessarily more immune to overload limits. In fact, it might be argued that the user needs to exert even more caution when using pulsed power signals, especially if the actual peak power is unknown. One simple way to do this is to insert a step attenuator between the unknown pulsed power and the peak and average sensor and set in an appropriate amount of attenuation. Since peak and average sensors have an excellent dynamic range, the meter will indicate some peak power on the high sensitivity ranges. At that point, the user can determine whether the test signal peak power will do damage to the sensor.

Table 8-1. Overload characteristics for various types of power sensors.

	8478B Thermistor sensor	8481A Thermocouple sensor	8481H Thermocouple sensor	8481D Diode sensor	E4412A Extended-range diode sensor	E9320A Peak and average diode sensor
Maximum average power	30 mW	300 mW	3.5 W	100 mW	200 mW	200 mW
Maximum energy per pulse	10 W • µS	30 W • µS	100 W • µS	(1)	(1)	(1)
Peak envelope power	200 mW	15 W	100 W	100 mW	200 mW	1W <10 µS

1. Diode device response is so fast, device cannot average out high-energy pulses

Signal waveform effects

While the waveform considerations were fully covered in Chapter V, it is well to consider the waveform factor as a differentiator for the various meters and sensor technology. Briefly, the thermistor is a totally heat-based sensor and therefore the thermistor sensors handle any input waveform with any arbitrary crest factor, that is, they are true square law sensing elements. Thermocouple sensors are full square law sensing for the same reason, but thermocouples operate beyond the thermistor high limit of 10 mW, all the way to 100 mW and 3 watts for the 848X H-models, which have the integrated fixed pads. The 8481B features a 25-watt internal attenuator and operates from 10 MHz to 18 GHz for medium power applications.

PDB-diode-based sensors of the 8481D family feature full square-law performance because their operating power range is limited to a top level of –20 dBm, thus restricting their meter indications to the square-law range of diodes. The user should assure that peak power excursions do not exceed –20 dBm.

The E series diode sensors require simple attention to their input signal characteristics. CW signals may be applied all the way from –70 to +20 dBm with confidence and accuracy.

An applications overview of Agilent sensors

In general, power sensors are designed to match user signal formats and modulation types. Similarly, power meters are designed to match the user's testing configurations and measurement data requirements. Thus, it is the user's responsibility to understand the test signals in detail, the technology interaction with the sensor capabilities, and combine those results with the optimum power meter to match the data output needs of the test combination.

Table 8-2 presents an overview of the most common signal formats in various industry segments and suggests appropriate sensor technologies that can characterize them. Since Agilent thermistor sensor/meter technology is almost uniquely metrology-based, they are not included in the following charts.

Table 8-2. Agilent sensor applications chart.

		Signal characteristics						
		CW			Modulated			
		CW	Pulse/ averaged	Pulse/ profiled	AM/FM	Wireless standards		
Sensor technology	Typical application examples >	Metrology lab	Radar/ navigation	Radar/ navigation	Mobile radio	TDMA GSM EDGE IS-136 IDEN Bluetooth	CDMA IS-95	W-CDMA 3GPP CDMA-2000
Thermocouple sensors		•	•		•	• Avg. only	• Avg. only	• Avg. only
Diode sensors		•	•		•	• Avg. only	• Avg. only	• Avg. only
Diode sensors compensated for extended range		•			FM only	• Avg. only	• Avg. only	• Avg. only
Two-path diode-stack sensors		•	•		•	• Avg. only	• Avg. only	• Avg. only
Peak and average diode sensors (modulation BW)[1]		•	• (5 MHz)	• (5 MHz)	•	• (300 kHz) time-gated	• (1.5 MHz) peak, avg, peak/avg	• (5 MHz) peak, avg, peak/avg

1. The modulation bandwidth is sometimes referred to as the video bandwidth.

Once the power sensor decision is made, the power meter decision is straightforward. Generally, since the new Agilent EPM and EPM-P power meters are completely backward-compatible with diode and thermocouple sensors of several-decade vintage, the decision becomes mostly whether a single or dual channel meter is needed, except in the case of a VXI or MMS test system strategy. Remember that E9320A peak and average sensors only work with the EPM-P meter. Table 8-3 presents the compatibility chart for combining Agilent sensors and meters.

Table 8-3. A compatibility overview of Agilent power meters and sensors.

	Agilent power meters		
Agilent power sensors	EPM-P series peak, average and time gating E4416A single Ch E4417A dual Ch	EPM series averaging E4418B single Ch E4419B dual Ch	System power meters 70100A MMS E1416A VXI
Thermocouple 8480A/B/H-family (9 models)	●	●	●
Diode 8480D-family 8486-W/G-family (9 models)	●	●	●
Diode sensors with extended range E4412A/13A (2 models)	●	●	
Two-path-diode-stack E9300 family (7 models)	●	●	
Peak and average sensors E9320 family (6 models)	●		

And now, the final user step is to select the appropriate sensor to match the application, based on the technology presentations of chapters III-VI, using the following table 8-4.

Table 8-4. Agilent's family of power sensors.

Thermocouple sensors

Sensor family	Technology	Max. dynamic range	Frequency range[1]	Power range[1]	Signal type	Max. measurement speed (rdgs/sec)
8480 series	Thermocouple	50 dB	100 kHz to 50 GHz	-30 to +44 dBm	All signal types, unlimited bandwidth	40 (x2 mode)

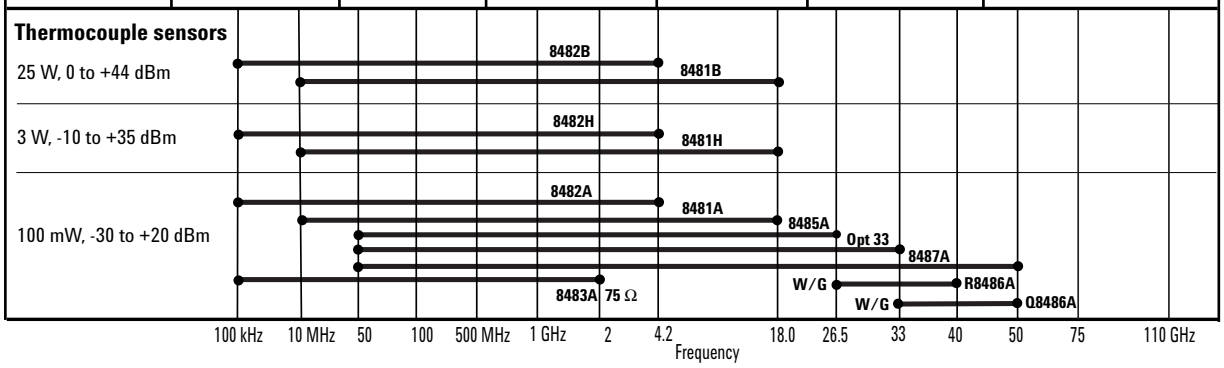

Diode sensors

Sensor family	Technology	Max. dynamic range	Frequency range[1]	Power range[1]	Signal type	Max. measurement speed (rdgs/sec)
8480 series	Diode	50 dB	10 MHz to 110 GHz	-70 to -20 dBm	All signal types, unlimited bandwidth	40 (x2 mode)

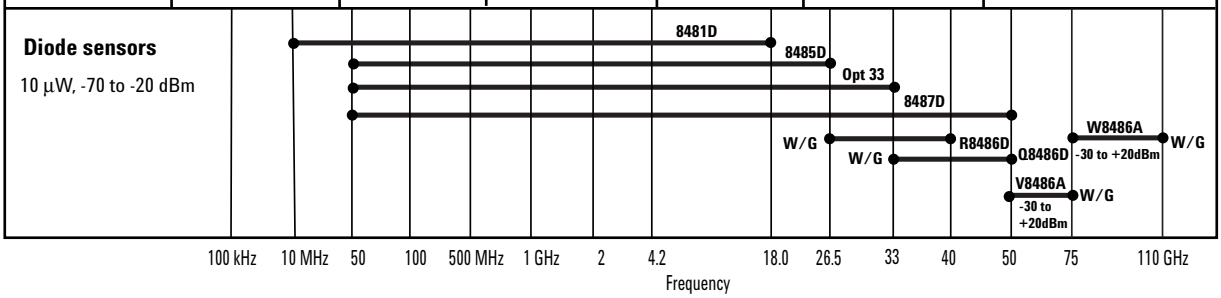

Extended range diode sensors

Sensor family	Technology	Max. dynamic range	Frequency range[1]	Power range[1]	Signal type	Max. measurement speed (rdgs/sec)
E-series: CW E4412A E4413A	Single diode pair	90 dB	10 MHz to 26.5 GHz	-70 to +20 dBm	CW only	200 (fast mode)

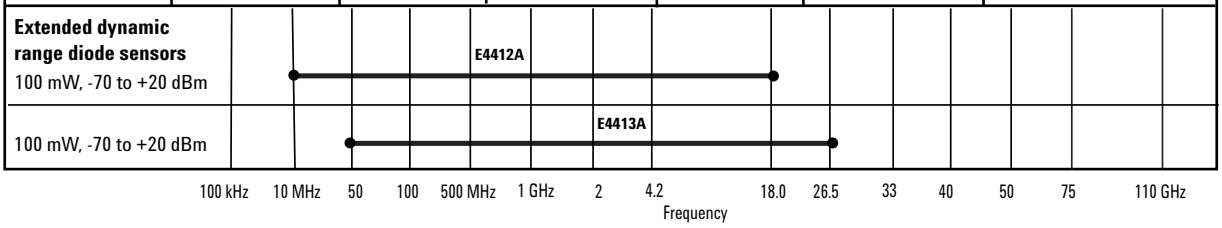

1. Sensor dependent

Two-path diode stack sensors

Sensor family	Technology	Max. dynamic range	Frequency range[1]	Power range[1]	Signal type	Max. measurement speed (rdgs/sec)
E-series: average power sensors E9300	Diode-attenuator-diode	80 dB	9 kHz to 18 GHz	-60 to +44 dBm	All signal types unlimited bandwidth	200 (fast mode)

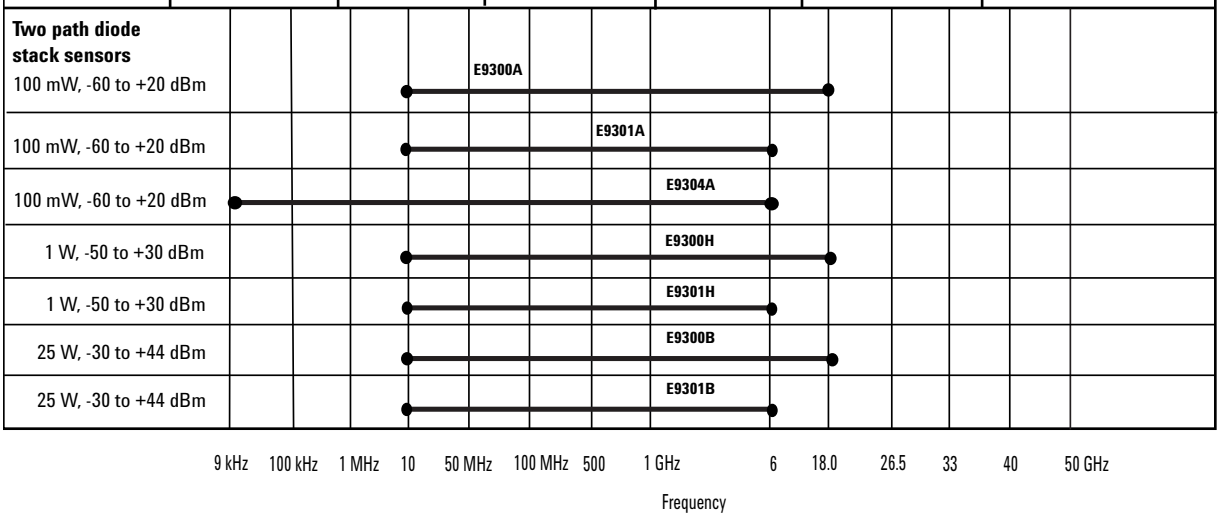

Peak and average sensors

Sensor family	Technology	Max. dynamic range	Frequency range[1]	Power range[1]	Signal type	Max. measurement speed (rdgs/sec)
E9320-series[2] peak and average E9321/22/23A E9325/26/27A	Single diode pair, two-path	85 dB	50 MHz to 18 GHz	–65 to +20 dBm	CW, avg, peak	Up to 1000

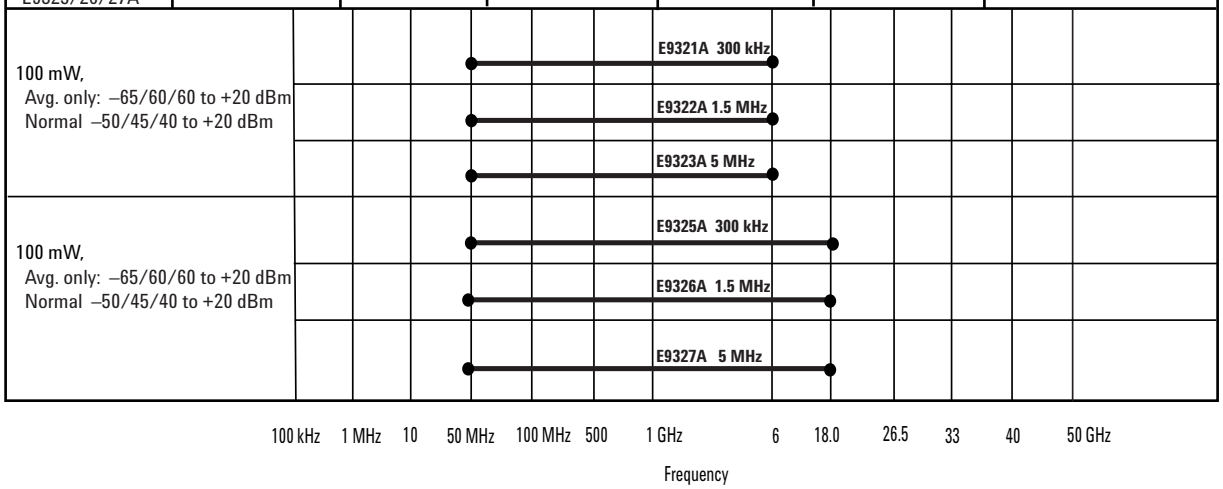

1. Sensor dependent
2. Peak and average sensors must be used with an E9288A, B, or C sensor cable, and only operate with the E4416A/17A power meters

Glossary and List of Symbols

ADC	analog-digital converter
a_g	incident wave upon a generator
ANSI	American National Standards Institute
AM	amplitude modulation
a_ℓ	incident wave upon a load
bg	emerging wave from a generator
b_ℓ	reflected wave from a load
BPSK	Binary Phase-Shift Keyed
b_s	generated wave of a source
C_b	bypass capacitance
C_c	coupling capacitance
CDMA	Code-Division-Multiple-Access
C_o	diode junction capacitance
CW	continuous wave
C, C1, C2	capacitors
dB	decibel
dBm	decibels referenced to 1 mW
D	power meter drift
DSP	digital signal processor
e	instantaneous voltage
EDGE	Enhanced Data rates for GSM Evolution (wireless standard)
emf	electromotive force
e_p	peak voltage
E_{rms}	root mean-square of a voltage waveform
e_s	source voltage
FDM	Frequency-Division-Multiplex
FET	field effect transistor
f_m	maximum modulation frequency component
f_r	repetition frequency
FM	frequency modulation
GaAs	Gallium arsenide
GPIB	General Purpose Interface Bus
GSM	Groupe Spêciale Mobile, a wireless standard sometimes read as Global System for Mobile communication
i	instantaneous current
i	instrumentation uncertainty
i_ℓ	load current
i_p	peak current
I_{rms}	root mean-square of a current waveform
I_s	diode saturation current
IS-95A	Wireless Communication Standard
ISO	International Standards Organization
K	Boltzmann's constant
K_b	calibration factor
K_c	sensor cal factor at cal frequency
L	inductance
L_w	wire lead inductance
m	power meter magnification (gain)
mi	instrument magnification uncertainty
MMIC	microwave monolithic integrated circuit
M_u	gain due to mismatch between unknown generator and sensor
M_{uc}	gain due to mismatch between sensor and cal source
n	a diode correction constant
N	power meter noise
NADC	North American Digital Cellular
NAMAS	National Measurement Accreditation Scheme (UK)
NBS	National Bureau of Standards (now NIST)
NCSLI	National Conference of Standards Laboratories International
NIST	U.S. National Institute of Standards & Technology (formerly NBS)
NPL	National Physics Laboratory (UK)
P	product of voltage and current
P	power
P_{av}	available generator power
P_{avg}	average power
P_{cal}	power delivered to Zo load by meter cal source
P_d	dissipated power
P_{fs}	power at full scale
$P_{g\ell}$	net power transferred to load from generator
Pg_{zo}	power delivered to Zo load from generator
P_i	incident power

P_m	meter indication of power
P_{mc}	power level indicated during calibration
P_p	pulse power
P_r	reflected power
P_{ref}	reference power
P_{rf}	radio frequency power
P_{sub}	substituted power, dc or low frequency equivalent of an RF power
PDB	planar-doped-barrier (diode)
PTB	Physikalisch-Technische Bundesanstalt (Germany)
P_l	power sensor linearity
q	charge of electron
QAM	Quadrature-Amplitude-Modulation
QPSK	Quadrature-Phase-Shift-Keyed (digital modulation)
R	resistance
RF	radio frequency
RSS	root-sum-of-the-squares
R_b	bulk resistance of silicon
R_c	resistance of compensating thermistor
R_d	resistance of detecting thermistor
R_o	diode origin resistance
R, R_1, R_2, R_L	resistor
RR	round robin
Rs	source resistance
R_t	thermistor resistance
t	time as a variable
t	power meter translation (offset) error
T	temperature in Kelvins
T	time lapse
TDMA	Time-Division-Multiple-Access
T_o	period of a waveform
T_ℓ	period of the lowest frequency
T_r	period of the repetition frequency
Time-gated	time window for power measurement
SWR*	voltage standing wave ratio
SI	International System of Units
u	standard uncertainty
U	expanded uncertainty (for example catalog spec)
v	instantaneous voltage
v	voltage across a load
v_o	output voltage
V_0, V_1, V_2, V_T	Voltages
V_c	Voltage driving the compensating bridge
V_h	Peltier emf at a hot junction
V_{rf}	voltage driving the rf thermistor bridge
V_{rfo}	voltage driving the rf thermistor bridge when no rf power is applied
W	watt
Z	load impedance
Zc	power meter zero carryover value
Z_g	generator impedance
Z_o	reference impedance
Zr	reference impedance
Zs	power meter zero set value
π/8 8PSK	π/8 shifted, 8-Phase-Shift-Keyed (digital modulation)
a	q/nKT
Γ_g	complex reflection coefficient looking back into a generator
Γ_ℓ	complex reflection coefficient of a load
η_e	effective efficiency
ρ_ℓ	reflection coefficient magnitude of a load
ρ_g	reflection coefficient magnitude of a generator
τ	pulse width
ϕ	phase angle between a sinusoidal waveform and a reference waveform
ϕ_g	reflection coefficient angle of a generator
ϕ_ℓ	reflection coefficient angle of a load
Ω	ohms
3G	Third-Generation Wireless Systems
8-PSK	8 Phase-Shift Keyed (digital modulation)
64-QAM	64 Quadrature-Amplitude-Modulation

* Due to infrequent use of the term power standing wave ratio, common usage in the U.S.A. has shortened VSWR to SWR. Some parts of the world continue to use VSWR to refer to voltage standing wave ratio.

Agilent Technologies' Test and Measurement Support, Services, and Assistance

Agilent Technologies aims to maximize the value you receive, while minimizing your risk and problems. We strive to ensure that you get the test and measurement capabilities you paid for and obtain the support you need. Our extensive support resources and services can help you choose the right Agilent products for your applications and apply them successfully. Every instrument and system we sell has a global warranty. Support is available for at least five years beyond the production life of the product. Two concepts underlie Agilent's overall support policy: "Our Promise" and "Your Advantage."

Our Promise

Our Promise means your Agilent test and measurement equipment will meet its advertised performance and functionality. When you are choosing new equipment, we will help you with product information, including realistic performance specifications and practical recommendations from experienced test engineers. When you use Agilent equipment, we can verify that it works properly, help with product operation, and provide basic measurement assistance for the use of specified capabilities, at no extra cost upon request. Many self-help tools are available.

Your Advantage

Your Advantage means that Agilent offers a wide range of additional expert test and measurement services, which you can purchase according to your unique technical and business needs. Solve problems efficiently and gain a competitive edge by contracting with us for calibration, extra-cost upgrades, out-of-warranty repairs, and on-site education and training, as well as design, system integration, project management, and other professional engineering services. Experienced Agilent engineers and technicians worldwide can help you maximize your productivity, optimize the return on investment of your Agilent instruments and systems, and obtain dependable measurement accuracy for the life of those products.

By internet, phone, or fax, get assistance with all your test and measurement needs.

Online assistance:

www.agilent.com/find/assist

Phone or Fax
United States:
(tel) 1 800 452 4844

Canada:
(tel) 1 877 894 4414
(fax) (905) 282-6495

Europe:
(tel) (31 20) 547 2323
(fax) (31 20) 547 2390

Japan:
(tel) (81) 426 56 7832
(fax) (81) 426 56 7840

Latin America:
(tel) (305) 269 7500
(fax) (305) 269 7599

Australia:
(tel) 1 800 629 485
(fax) (61 3) 9210 5947

New Zealand:
(tel) 0 800 738 378
(fax) 64 4 495 8950

Asia Pacific:
(tel) (852) 3197 7777
(fax) (852) 2506 9284

Product specifications and descriptions in this document subject to change without notice.

Printed in USA, April 16, 2001
5965-6630E

Agilent Technologies